Experimental and Simulation Analysis of the Jitter Response of a Single-Shot Oil Switch with a High-K Particle Suspension

---

A Dissertation

Presented to

The Faculty of the Graduate School

At the University of Missouri

In Partial Fulfillment

Of the Requirements for the Degree

Electrical and Computer Engineering

By

CHRISTOPHER YECKEL

Dr. Randy Curry, Dissertation Supervisor

December 2012

The undersigned, appointed by the Dean of the Graduate School, have examined the thesis entitled

Experimental and Simulation Analysis of the Jitter Response of a Single-Shot Oil Switch with a High-K Particle Suspension

Presented by Christopher Yeckel

A candidate for the degree of Doctor of Philosophy

and hereby certify that in their opinion it is worthy of acceptance.

_____

Dr. Randy Curry

_____

Dr. Thomas Clevenger

_____

Dr. Gregory Triplett

_____

Dr. Robert Druce

Acknowledgements

I would like to acknowledge the contributions of several members of our team at the Center for Physical and Power Electronics at the University of Missouri – Columbia for their indispensible contributions in reducing the self-break jitter of oil switches.

I would like to thank my advisor, Dr. Randy Curry, for his knowledge and support of my research effort. The idea to add high-K particles to an oil dielectric to reduce switch jitter was originally suggested by him. It is my hope that he will continue my research with the help of our new graduate student, Chris Lapp, until oil switches become a feasible option in future pulsed power systems.

I would like to thank Josh Leckbee and Dr. Peter Norgard, both of whom set the groundwork for my research. I would particularly like to thank Dr. Peter Norgard for being a great mentor when I was learning the basics of pulsed power systems as a young graduate student.

I would like to thank Dan Crosby, our resident chemist, for his valuable discussion and insight into the inner workings of the oil and particle molecules. Dan developed and implemented the drying methods utilized to determine particle concentrations and also helped develop particle suspension techniques.

I would like to thank my PhD committee: Dr. Randy Curry, Dr. Robert Druce, Dr. Gregory Triplett and Dr. Thomas Clevenger for their valuable discussion and suggestions.

I would like to thank our lab supervisor, Bill Carter, for always making sure I had the things I needed as soon as I need them.

I would like to thank my undergraduate assistants, Chris Lapp and Kelly Steinhaus, for getting their hands dirty in support of my research.

I would like to thank my family and friends for motivating me and providing a firm foundation from which to reach a higher level of education.

Most of all, I would like to thank my wife Amy, for putting up with me for the last seven years smelling of dirty transformer oil and listening patiently while I ranted about electrostatic simulation code and clogged filters. Her support and understanding was invaluable to my sanity.

Table of Contents

i. List of Figures

ii. List of Tables

CHAPTER 1

INTRODUCTION

High voltage closing switches have widespread application in directed energy technologies where large quantities of energy are transferred to nonlinear loads over short durations of time. The typical directed energy (DE) load has stringent voltage and current requirements, and often must be synchronized in time with other parallel systems that make up the complete DE package. The high voltage closing switch must exhibit reliable breakdown (e.g., closure) with a minimum statistical variation in time or amplitude. Proven present-day technologies for achieving voltage hold-off at a significant portion of a megavolt, while producing reliable breakdown at a particular voltage are almost entirely limited to high-pressure gas switches.

The Center for Physical and Power Electronics at the University of Missouri – Columbia is developing an alternative switch technology based on an earlier success in industry of a pressurized, flowing oil switch [1]. The University of Missouri – Columbia (UMC) high pressure oil switch was designed to provide high voltage hold-off capability to 300 kV, a service life to greater than 10^7 breakdowns between electrode replacements and repetition rates up to 100 Hz [2-3]. The high pressure is used as a means of controlling the post-pulse gaseous byproducts by driving hydrodynamic events at a greater rate (e.g., increased rate of cavity decay). Forced convection, or flow, is used to control the post-pulse solid byproducts. Utilizing an optimized geometry, UMC was able to achieve rep-rate breakdown electric fields on the order of 1 – 2 MV/cm with a 1-σ statistical error as low as 9 % of the average breakdown electric field at low pressure, and as low as 11 % of the average breakdown electric field at high pressure. The breakdown electric field strength is significantly improved with the use of high pressure, whereas the statistical error of a collection of breakdowns, known as jitter, is significantly degraded with high pressure.

This dissertation discusses investigations into oil switching systems to address and reduce the jitter observed in the breakdown electric field strength of a pressurized, oil dielectric. The work

is conducted in two phases, the first of which examines the effects of oil chemistry on breakdown statistics, and the second of which considers the effects of particle additions to the best-performing fluids identified during the first phase of the experiment. A single-shot high voltage advanced dielectric test stand (HVADTS) was designed and built to test these oils. The HVADTS is capable of applying a 250 kV pulse with a '1-cos' rise-time of 1.6 μs to a pressurized oil dielectric. Numerous oil chemistries were evaluated, including straight-chain hydrocarbons and branched olefins, silicone and ester fluids, alkylbenzene and two types of transformer oil. Following the oil chemistry evaluation, a high-K particle dielectric was added in concentrations up to 5 % (by weight) to the best-performing fluids.

Controlled breakdown tests yielded statistically significantly results corresponding to the importance of the fluid chemistry. The breakdown testing on the single-shot HVADTS system indicates that the straight-chain hydrocarbons and branched olefins tend to produce reduced jitter on-par with, or better than the UMC rep-rate test stand. The transformer oils both tend to produce greater jitter than the UMC rep-rate test stand. The jitter of alkylbenzene is observed to perform as well as the branched olefins. The ester-based fluids and silicon-based fluids demonstrated increased jitter, by comparison.

The selected fluids were then evaluated with high-K particle concentrations of up to 5% of barium-strontium-titanate (BST). The BST particle dispersion further reduces jitter in some of the test fluids. In no case does the BST particle dispersion significantly increase jitter [4]. Based on the research conducted to date, UMC has determined that oil chemistry is a significant factor in establishing low breakdown statistical error, or jitter, and a high-permittivity particle additive can, in some cases, produce a significant decrease in breakdown jitter.

The introduction of high-K BST particles into an oil dielectric has reduced the self-breakdown voltage jitter of our HVADTS system. The particles are thought to interact with the field enhancement defects on the surface of the electrode, potentially cancelling the effects of the surface field non-uniformity. A non-uniform surface electric field distribution increases the probability that a local field enhancement on an electrode surface maxima or minima will initiate a low or high voltage breakdown event, respectively. High and low voltage breakdown events occurring over the lifetime of the switch significantly increase the switch jitter. Most modern

pulsed circuits require switch jitter of 5% or less. The results show that switch jitter can be reduced by manipulating the oil chemistry.

An electrostatic simulation model of a dielectric system composed of a uniformly-distributed suspension of high-K particles is extensively evaluated. The simulations examine the effects of various concentrations of submicron-sized particles of BST in an oil dielectric subject to uniform electric fields. The model suggests the formation of localized, nonlinear electric field enhancements near the electrode surface, as well as in the bulk dielectric. It is believed that these localized enhancements are the result of the BST particles becoming highly polarized under the influence of the applied voltage gradient.

In an attempt to further optimize switch breakdown jitter, both rough and smooth electrode surface conditions are employed at variable gap spacing. It is found that a rough electrode surface produces lower jitter and more consistent breakdown values than the smooth electrode surface. This discovery prompted the use of preconditioned electrode surfaces in all subsequent testing. It is also apparent that electrode gap spacing has a significant effect on jitter performance. The data and simulations suggest that at smaller gap spacing the particle's effect on jitter is more significant than at larger gap spacings; with jitter performance improving with increasing gap spacing.

An extensive procedure was developed to suspend the High-K BST particles in the oil dielectric. The procedure is used with great success to produce an effective dielectric oil shelf-life of several months. It was found that the particle-infused oil dielectrics are prone to excessive water concentrations many times greater than those in the base oil. Water concentration is found to heavily influence switch jitter. Reducing the water concentration of the particle -infused oils has tended to improve jitter performance in nearly every case.

This dissertation is divided into this introduction and seven additional chapters. The theory behind electrical breakdown phenomenon in liquids as well as the significant experimental variables are investigated in chapter two. The physical and electrical characteristics of the BST dielectric particle are described with the aid of a scanning electron microscope (SEM) and energy dispersive x-ray spectrometry in chapter three. Also in chapter 3, the characteristics of the dielectric oils are analyzed with Photon Correlative Spectroscopy (PCS) and a drying method to

determine the mean particle size and concentration; as well as the procedure to produce the particle/oil colloid. The simulated electrostatic field interactions between the electrode and polarized high-K particles generated by CST EM Studio 3D electromagnetic PIC simulation software are analyzed in chapter four. The characteristics of rough and smooth electrode surfaces are analyzed with an optical profilometer in chapter five. The experimental single-shot test stand (HVADTS) and supporting components are outlined in chapter six. The experimental results and corresponding discussion are included in chapters seven and eight. Altogether, these chapters attempt to build an understanding of the effect that high-K particles and other variables have on the breakdown performance of an oil switch. Proposed future adjustments to the physical parameters of the switch to achieve the optimum jitter performance are also discussed.

CHAPTER 2

OIL BREAKDOWN THEORY

Oil is being considered as a dielectric switching medium for current and future pulsed power applications due to its high electrical breakdown strength and rapid recovery. The electrical breakdown of dielectric oil is the final stage of switch closure, which is preceded by several pre-breakdown stages. Breakdown is characterized by the formation of an arc; an electrical short circuit through the oil, which allows luminous currents to flow between two electrodes. This flow of electrons would otherwise be insulated by the liquid. This breakdown event is the fundamental purpose of the oil closing switch as it allows energy transfer between circuits; typically between a storage element and a load. The high voltage breakdown strength of the oil allows the electrodes to be spaced close together in millimeter gap spacing. Shorter gap spacing lowers the inductance of the arc, which is approximately $5\frac{nH}{cm}$, producing a faster current rise time [1]. A fast and reliable current rise is vital to directed energy loads.

2.1 Formation of a Breakdown Arc

The dielectric breakdown strength of oil is defined as its ability to withstand an applied electric field without breaking down and allowing current to flow. A breakdown event in oil begins when electrons obtain sufficient energy from the applied field to overcome the work function of the electrode/oil boundary. Once free from the electrode, the electrons interact with the neutral oil molecule chains and any foreign particulates [5]. At first, the electrons interact with the oil molecules through non-ionizing collisions causing the local oil temperature to increase (joule heating). The increased oil temperature results in local evaporation of the oil and subsequent formation of vapor cavities near the electrode surface. As the vapor 'bubble" forms and expands, the mean free path of the emitted electrons become long enough for ionizing collisions to begin to occur [6].

The current theory of breakdown in oil suggests that a vapor cavity, or bubble, grows off the electrode as the electrons impart energy to the system through vaporization and ionization. The growth of this bubble, or low density region, is suppressed by the pressure of the surrounding liquid. The bubble expands against this external pressure due to its increasing electron density. The expansion is a result of the repulsive force between electrons and subsequent space charge density in the area [5].

The plasma in the bubble is charged such that the bubble and electrode have a matching potential [5]. As the bubble expands due to localized current injection, charge density decreases within the bubble. This charge reduction leads to a redistribution of ions on the bubble/oil interface leading to breakdowns within the bubble fueled by electrons or holes seeded from the electrode, thus imparting more charge density to the system [6]. These breakdowns drive the bubble expansion. As the bubble's volume and surface area increase it becomes more difficult to resist the external fluid pressure and the surface of the bubble begins to oscillate. These surface oscillations increase in amplitude as the bubble continues to expand [7].

As the bubble expands, the surface of the bubble oscillates due to external pressure and develops finger-shaped protrusions commonly referred to as streamers. These streamers act as field enhancements emitting charge carriers and elongating across the gap. Once contact is made with the opposite electrode the resistance of the spark gap drops several orders of magnitude and an arc channel forms. The stored energy is transferred through the liquid in a luminous current pulse.

2.2 Electrode Field Enhancement

An electric field applied across the electrode gap results in emission of electrons from the electrode surface. These electrons are then free to collide and impart energy to the neutrally-charged oil molecules. As more electrons are emitted they begin to vaporize the oil through joule heating and microscopic vapor bubbles are formed. Once the bubble size is large enough that the mean free path of the electrons is long, they gain sufficient energy to begin ionizing the gas molecules through collision dynamics [8].

Ionization of the oil generates electron-ion pairs that are swept by the applied electric field. Charged ions are drawn to and strike the electrode surface, forming ion impurity layers on the surface of the electrodes as they attach. These layers lower the work function of the electrode allowing lower-energy electrons to emit. Charged ions continue to bombard these layers over the switch lifetime and form field enhancements on the electrode surface [5]. These layers are thought to limit the electron secondary emission by preventing ions from striking the electrode directly [8].

Field enhancements on the electrode surface increase electron emission potential. Breakdown discharges and bubble cavitations cause arc pits and erosion on the surface of the electrodes [3, 7]. These microscopic irregularities, or deformations, create points of higher electric fields which enhance the electron emission potential of that point; increasing the probability that a breakdown will initiate at the site [5]. Electron emission from the electrode consists of trains of nanosecond pulses corresponding to breakdown events within the expanding bubble [5]. This energy drives the vaporization of the oil and provides the electrostatic force for bubble expansion. Microbubbles are formed by the rapid, localized emission of electrons from the electrode into the oil dielectric from these high field enhancements resulting in a breakdown event.

2.3 Controllable and Uncontrollable Testing Variables

There are many variables to consider when assessing the self-break jitter observed in oil dielectric switches. These variables can be described as controllable and uncontrollable variables. Controllable aspects of the switch include: gap spacing, rate of voltage rise, external fluid pressure, ambient temperature, electrode material, electrode geometry, and oil chemistry.

Other variables are uncontrollable in rep-rate operation, such as: electrode erosion patterns, the shape, thickness, and rate of deposition of ion impurity layers on the electrode surface, and the randomness inherent in bubble formation and streamer propagation. These uncontrollable aspects are particularly bothersome as they change over the lifetime of the switch. The effects of the type of oil and any additives are appealing as they can be controlled and reproduced.

2.4 Effect of Particle Suspension

Experimental results indicate that suspending high-K particles in the oil dielectric reduces switch jitter. Electromagnetic theory and simulation suggest that the high dielectric constant of the particles is a result of their ability to polarize into dipoles in an applied field. A particle near the electrode surface increases the local electric field and draws electrons from the electrode and into collision with the neutrally charged oil molecules, stimulating the breakdown process at the site.

The simulations also suggest that the polarized particles affect the electric field profile within the bulk of the oil and act as a propagation path for the ionizing streamer. The local non-uniform electric fields generated by the polarized particles may guide the streamer between electrodes resulting in more predictable breakdown events, or provide an enhancement for the initial formation and subsequent propagation of the streamer.

By whichever mechanism, it is apparent from the experimental data that a suspension of high-K, BST, particles reduces the self-break jitter in our HVADTS switch. The jitter-reducing effect is more pronounced with specific oils and switch parameters. By optimizing switch parameters and particle concentration self-break jitter values of less that 5% PSD (percent standard deviation) are attainable.

References

[1] R. Curry, P. Champney and C. Eichenberger, "The development and testing of aubnanosecond-rise, kilohertz, oil switches for the generation of high-frequency impulses," *IEEE Transactions on Plasma Science*, vol 20, No.3, June 1992.

[2] P. Norgard and R. D. Curry, "An in-depth investigation into the effect of oil pressure on the complete statistical performance of a high pressure, flowing oil switch," *17th IEEE. International Pulsed Power Conference*, Washington D.C., U.S.A., 2009.

[3] P. Norgard and R. Curry, "Rep-rate jitter and electrode erosion of a high pressure flowing oil switch", *27th International Power Modulator Conference,* 2006.

[4] C. Yeckel and R. Curry, "Pulsed breakdown characterization of advanced liquid dielectrics for high-Power high-pressure rep-rate oil switching", *the 17th International Pulsed Power Conference*, 2009.

[5] P. K.Watson,W. G. Chadband and M. I. Qureshi, "The growth of pre-breakdown cavities in silicone fluids and the frequency of the accompanying discharge pulses,' *IEEE Transactions on Electrical Insulation*, Vol. 5, pp. 344-350, 1998.

[6] A. M. Sletten and T. J. Lewis, "The influence of dissolved gases on the electric strength of n-hexane," *Britain Journal of Applied Phys*ics, Vol. 14, pp. 883-888, 1963.

[7] P. K. Watson, W. G. Chadband and M. Sadeghzadeh-Araghi, "The role of electrostatic and hydrodynamic forces in the negative-point breakdown of liquid dielectrics," *IEEE Transactions on Electrical Insulation*, Vol. 26, pp. 543-559, 1991.

[8] M. Lieberman and A. Lichtenburg, Principles of Plasma Discharges and Materials Processing. New Jersey: Wiley, 2005.

CHAPTER 3

PHYSICAL AND ELECTRICAL CHARACTERISTICS OF THE HIGH-K PARTICLE-INFUSED OIL DIELECTRICS

3.1 High-K BST Particle Characteristics

The BST particles were purchased from TRS Technologies Incorporated in a powder form [9]. The quoted particle diameter is 70 nm. The dielectric constant of the particles varies significantly with temperature and electrical frequency. Figure 1 plots the dielectric constant and dielectric loss of BST as a function of temperature and frequency. At 25° C and 250 KHz the graph indicates that the BST particles have an approximate dielectric constant of 2000. Thus, a dielectric constant of 2000 is assumed in the electrostatic simulations. The rest of this section defines the electrical and physical characteristics of a BST particle as well as outlines the procedure to suspend the particles in the dielectric oil.

3.1.1 Electrical Characteristics of the BST Particle

An electric field affects a dielectric by disrupting the equilibrium charge distribution within its spatial matrix. Charges are bound within dielectrics and an electric field exerts a force on them. Positive charges are displaced toward the field and negative charges shift in the opposite direction. Oil molecules are dielectrics composed of long carbon chains that are neutral in charge and resistant to ionization. An electric field polarizes the charge and any free charge drifts in the electric field. The equilibrium charge structure of an oil molecule is only slightly disrupted by an electric field. This results in a low polarization charge magnitude and a relatively low dielectric constant of 2.3.

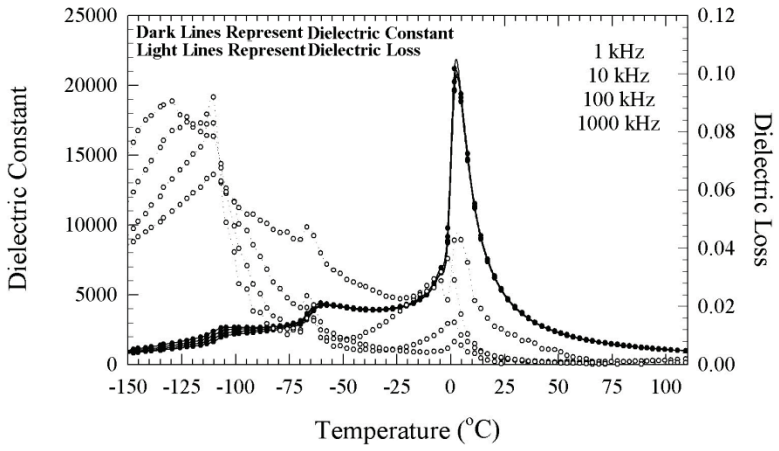

Figure 3.1**:** This graph from TRS Technologies Inc. plots the dependency of dielectric constant and loss on the temperature of the BST particle. At 25°C and 250 KHz the dielectric constant is approximately 2000. The dark circles/lines represent the dielectric constant while the light circles/lines represent the dielectric loss.

Under the influence of an electric field the net charges on the dielectric remains zero, preventing them from drifting, however equal and opposite charges develop on the dielectric extremes aligned with the field. This creates an internal electric field that partly compensates the external field around the dielectric. The magnitude of this polarization charge scales with the dielectric constant as shown in equation 1. A barium strontium titanate (BST) particle has a large polarization charge potential resulting in a dielectric constant of ~2000. The polarization charge generated is a result of the electric field forcing the dielectric's internal charges out of their equilibrium configuration [8]. Figure 3.2 shows how dielectric particles align and polarize in an electric field.

$$\vec{P} = \varepsilon \vec{E} \qquad \textbf{(1)}$$

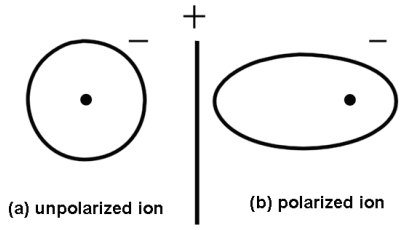

Figure 3.2: The application of an electric field to a dielectric forces the molecules in the material to polarize and align. The electric field points away from the center positive line.

The electrical breakdown of oil in a switch is initiated and highly influenced by electric fields in the gap near the electrode surface [10]. When an electron is emitted from the electrode it travels along an electric field vector, a mean free path, until it encounters a collision. The polarized edge of the particle bends the electric field lines towards it, increasing the probability that an electron will collide with it. Electrons will attach to and neutralize the polarized particle until the polarization charge is completely neutralized as in figure 3.3. As the mean-free-path of the electron increases and the energy of the electron approaches 3-eV, a probability exists that a collision will result in the emission of an electron through ionization and secondary emission processes [10].

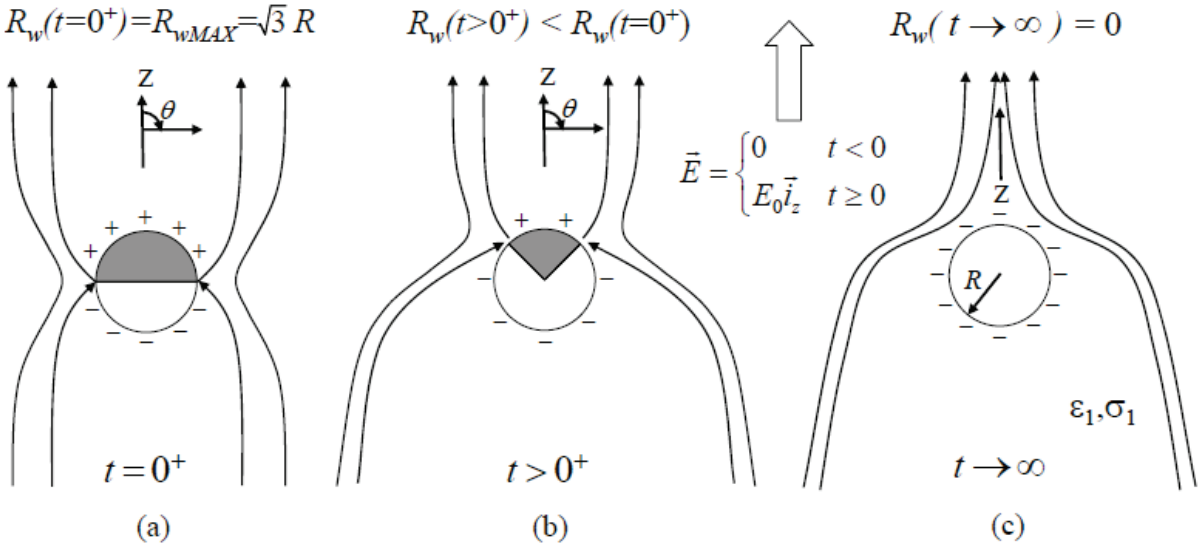

Figure 3.3: Particle with a radius R surrounded by transformer oil with a permittivity of ϵ_1 and conductivity σ_1 stressed by a uniform z-directed electric field is pictured. (a) At time t= 0+ the particle is polarized and all the electric field lines which pass through the cross sectional area of radius $\sqrt{3}$R will terminate on the particle such that the electron charging window is at a maximum, $R_w(t = 0+) = R_{wMAX} = \sqrt{3}R$. The particle is polarized with positive surface charge for $0<\theta<\frac{\pi}{2}$ and negative surface charge for $\frac{\pi}{2}<\theta<\pi$. (b) At later times t > 0+, the electron charge deposited on the particle modifies the surrounding electric field distribution and the charging window is $0<R_w(t)<R_{wMAX}$. (c) As $t\to\infty$, the electric field distribution is modified until a point where no field lines terminate on the particle and $R_w(t\to\infty) = 0$. In this situation, a particle is fully charged with a total charge of $Q_s=-12\pi\epsilon_1 R^2 E_0$ [10,11].

The presence of particles in the breakdown regime has a significant effect on breakdown streamer velocity. The polarized particles attract electrons. Using the generalized analysis of the charging dynamics for finitely conducting particles, a complete electrodynamic model is developed. The simulation study shows that the significant dynamics in the electric field and thermal enhancement in highly electrically stressed particle-infused fluids are due to molecular ionization just as in transformer oil. However, streamer propagation is hindered because the charging of slow particles by electrons in the ionization zone changes fast electrons into slow negatively charged particles that modifies the electrodynamics in the oil and slows the propagation of negative streamers [12]. The field enhancement factor regulated by the particle size and shape may also alter the surface charge and electric fields at the particle surface.

3.1.2 Physical Characteristics of the BST Particle

Utilizing a SEM (scanning electron microscope) to determine the particle size has previously proven ineffective when dealing with the particles suspended in oil. However, after the oil is evaporated, a SEM image, such as the images of figures 3.4, 3.5, 3.6 and 3.7, allows the particle size to be measured directly. The images were generated by the FEI Quanta 600F with EDS [13] located on the the UMC campus. Figure 3.4 shows the BST particles with a 10 μm reference point. The particle sizes look very uniform across the sample. Figure 3.5 shows the BST particles with a 3 μm reference point. The image clearly shows that the particle size ranges from 200 to 400 nm in diameter. This size range conforms to what is expected with the sonication techniques utilized [14]. Figure 3.6 shows the BST particles with a 1 μm reference point demonstrating with even more clarity the 200 to 400 nm particles. Figure 3.7 utilizes a 400 nm reference point and is at such a high magnification that clear resolution is difficult to establish, however the 50 to 70 nm particles within the 200 to 400 nm agglomeration can be identified in the image. The agglomerations are undesirable as they gradually fall out of suspension; however, simulations suggest that larger particles generate greater local electric fields on the electrode surface.

The SEM-EDS (energy dispersive spectroscopy) is employed to confirm that the sample is BST and not a separate byproduct of the high voltage testing. Figure 3.8 shows the results of that analysis. It clearly shows evidence of barium, titanium, strontium and aluminum.

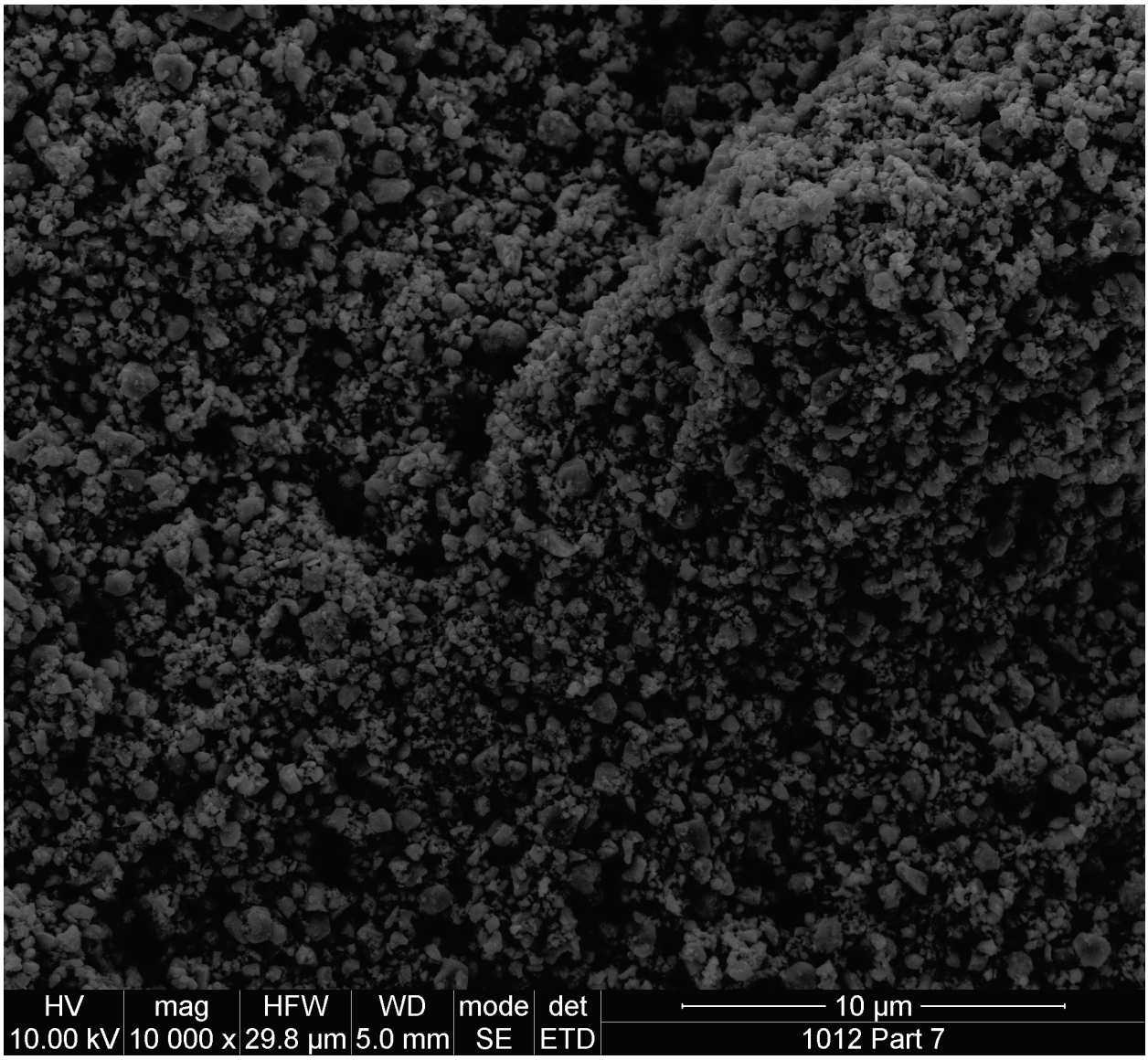

Figure 3.4: This SEM image has a resolution of 10 µm. The BST particles are clearly visible across the sample. The absence of larger sized particles is evidence that they settled out of the oil or are removed by the filtration.

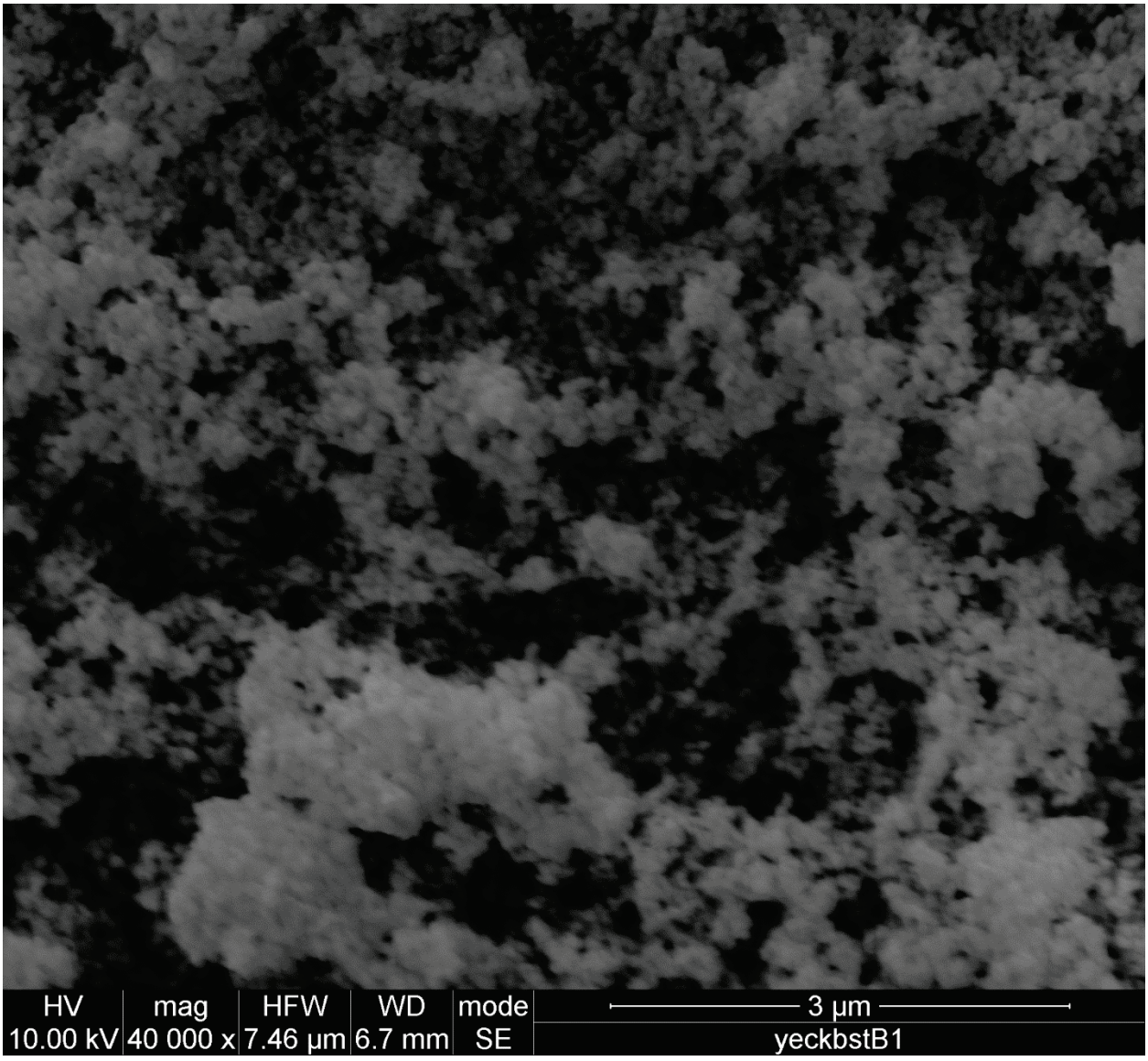

Figure 3.5: This SEM image has a resolution of 3 µm. The BST particles are clearly visible across the sample. The absence of larger sized particles is evidence that they are removed by filtration or settling.

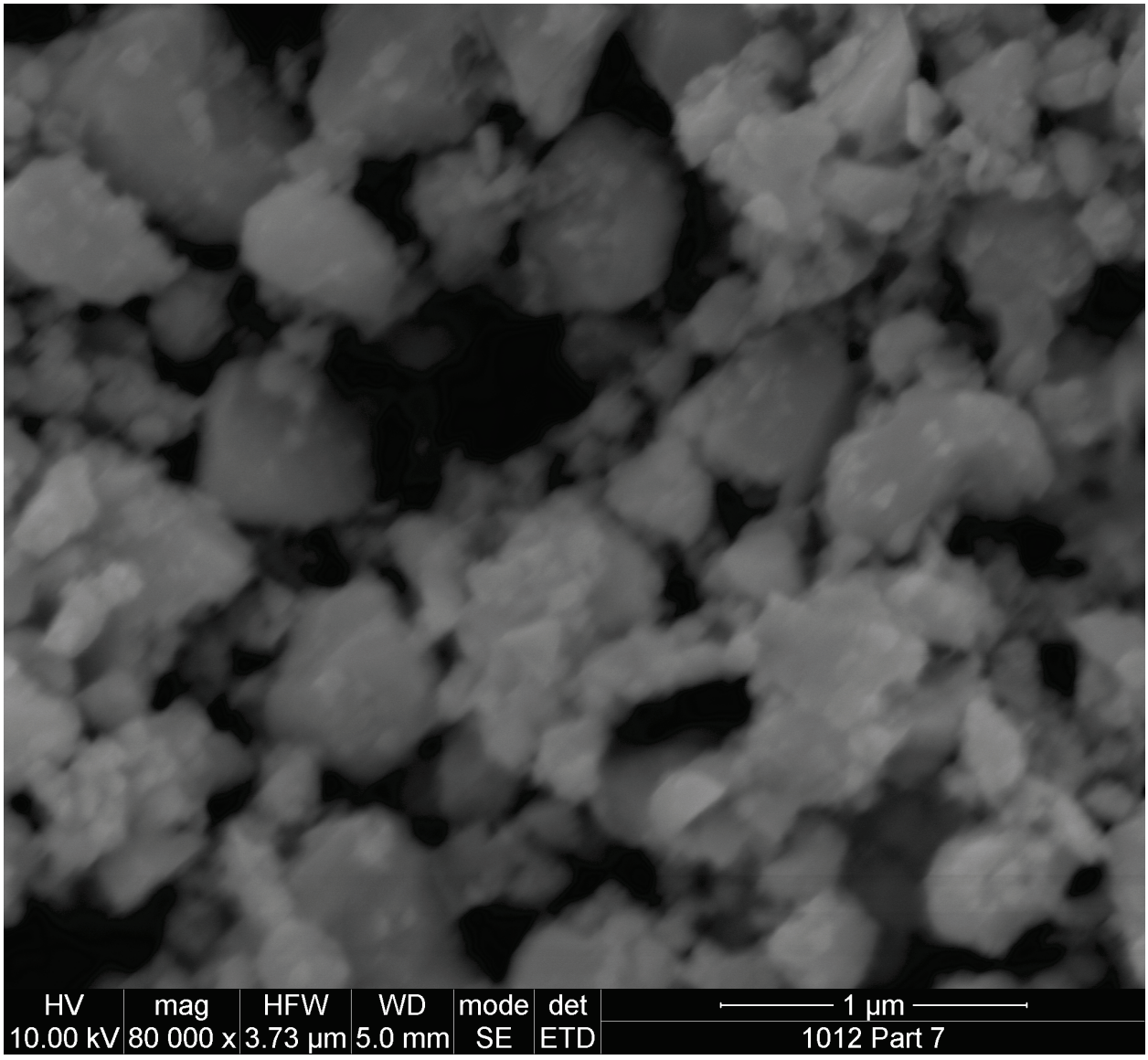

Figure 3.6: This SEM image has a resolution of 1 µm. While the image focus is poor at this resolution, the particles can be distinguished from each other and measured. The results of the PCS analysis indicate that the mean particle/agglomeration size for this sample is between 200 and 400 nm.

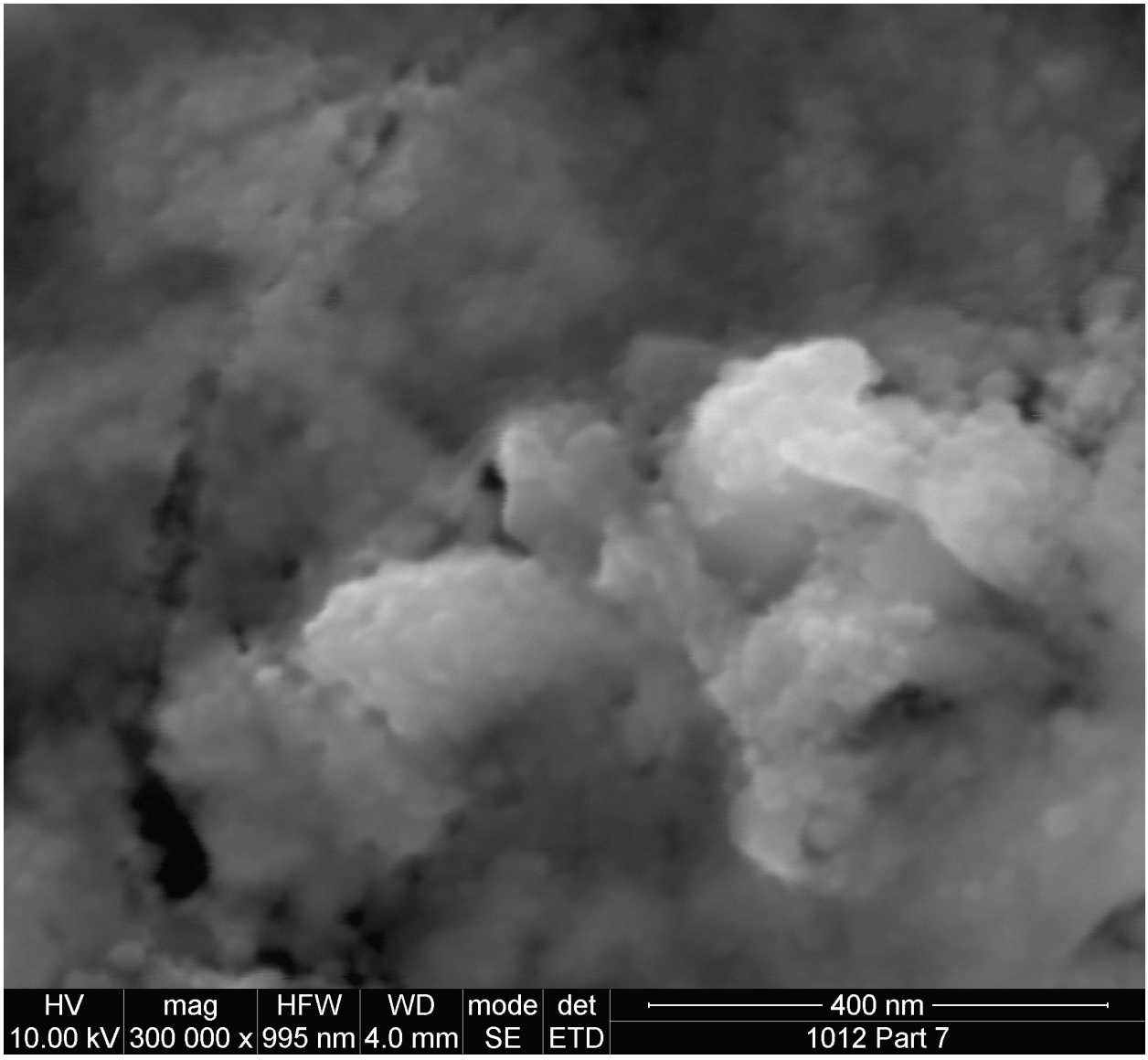

Figure 3.7: This SEM image has a resolution of 400 nm. While the image focus is poor at this resolution, the particles can be distinguished from each other and measured. The individual particle diameter varies between 50 and 70 nm, however, the results of a PCS analysis indicates that the particles agglomerate into 200 to 400 nm diameter masses.

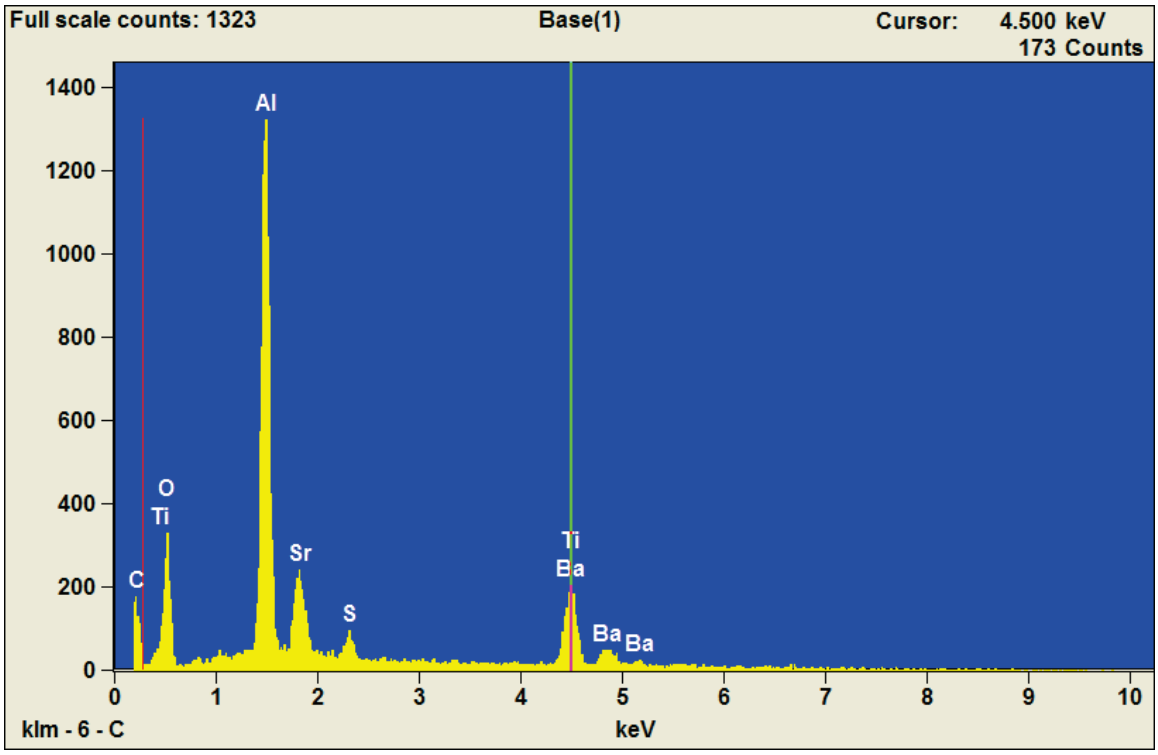

Figure 3.8: The results of the SEM-EDS indicate a strong barium, titanium, strontium and aluminum presence. The sample is contained in an aluminum weigh boat indicated by an aluminum line.

3.2 Physical Characteristics of Selected Dielectric Oils

The dielectric oils selected for high voltage switch self-break jitter characterization are also required to meet various other specifications. The use of an oil switch system in practical environments requires that the oil have both a long stable-state lifetime and viable viscosity over a large temperature range. Not only must the oil exhibit stable characteristics, it must also be non-reactive with any metals, insulators, seals and pump systems it may contact during operation. Several oils were selected for the initial testing, however only three oils were selected for extensive testing: a PAO (poly-alpha-olefin), alkylbenzene, and 1-Hexadecene.

Nycodiel PAO is a new generation coolant for electronic systems, mainly military radar, embarked on aircraft, ships or ground equipment. Nycodiel is not sensitive to water, does exhibit a stable flash point during use, and does not produce gels which clog cooling systems and filters.

The exact chemical formula for Nycodiel is proprietary to the Nyco Corporation so it cannot be shown; however it is similar to the formula of figure 3.9. Nycodiel is a PAO conforming to specification MIL-PRF-87252C which indicates that it is stable over a large temperature range. Because of these features, PAO is a good candidate for future testing.

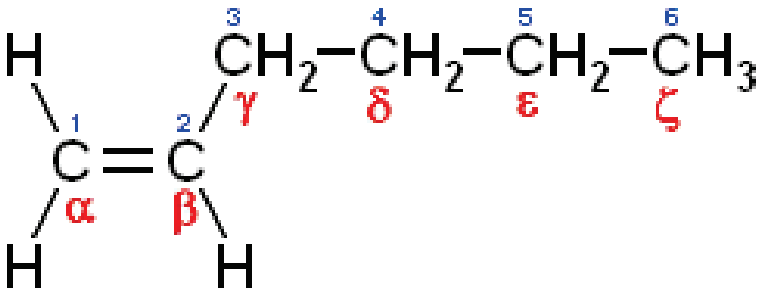

Figure 3.9. The exact Nycodiel chemical formula is proprietary, however as a PAO (poly-alpha-olefin) its formula is likely similar to the 1-Hexene above [15].

Nycodiel is a synthetic hydrocarbon-based fluid, with a viscosity of 5 cSt at 40°C [15]. Nycodiel exhibits remarkable jitter performance with the addition of the particle suspension. In some cases the switch jitter is reduced by a factor of two, which fixes Nycodiel as the best performing oil tested on HVADTS. We hope to have continued success with the Nycodiel as its stable temperature range is suited for a set of diverse applications. Nycodiel has a positive gassing tendency of +34.5 µL/min.

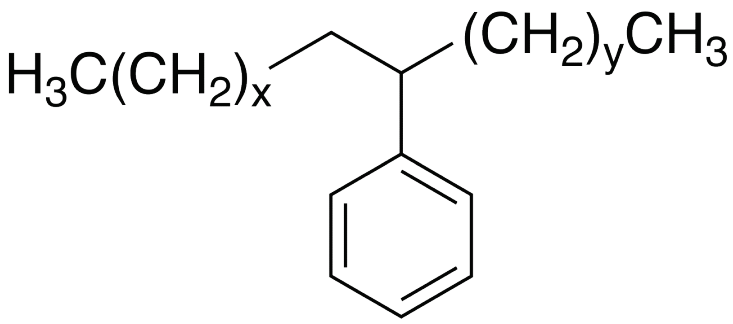

Figure 3.10: The chemical formula for linear alkylbenzene (LAB) is pictured in this figure. The benzene ring is located on the fourth series carbon.

Linear Alkyl Benzene (LAB) is a basic petrochemical intermediate derived by alkylation of benzene starting from n-paraffin feedstock and is used to produce LAS (Linear Alkylbenzene Sulphonate) [16]. LAB has a negative gassing tendency of -50 µL/min. It is thought that the negative gassing tendency might inhibit the formation of the gas bubbles that are the precursor to breakdown. LAB has a viscosity of 4.0-4.5 cSt at 40°C. The negative gassing tendency of LAB makes it an interesting testing candidate and could possibly serve as an additive to PAO.

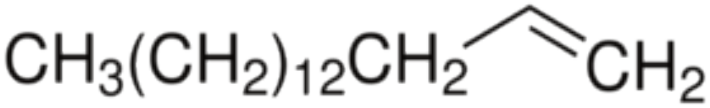

Figure 3.11: 1-Hexadecene is a large straight chain carbon with 15 carbon atoms.

The 1-Hexadecene is a straight chain hydrocarbon with 15 carbon atoms in series. Hexadecene is selected as a candidate oil due to its availability and purity. Hexadecene has a viscosity of 3.83 cSt at 25°C. The 1-Hexadecene is considered a control fluid and serves as a baseline oil for comparison [17]. The jitter performance of 1-Hexadecene is improved with a high-K particle additive.

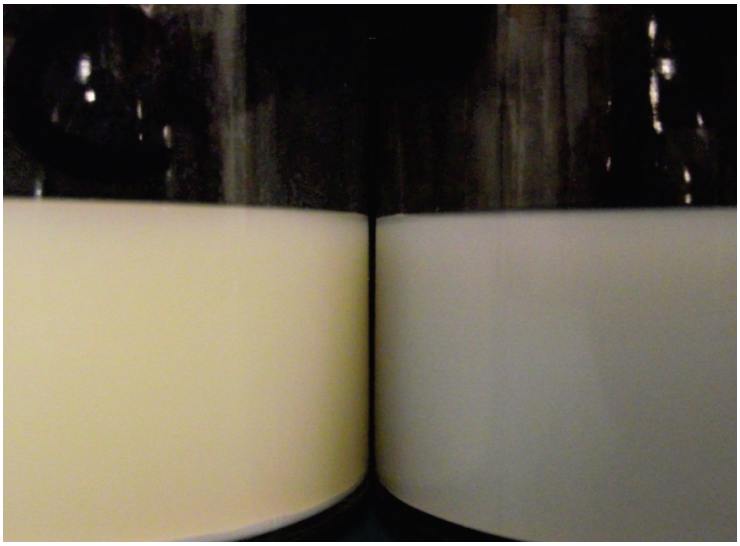

Figure 3.12: A photograph comparing the particle-infused Nycodiel PAO oil before testing (left) and after testing (right) demonstrates a strong carbon presence indicated by the darker color of the oil after testing.

3.3 Particle Suspension and Oil Test Procedure

The procedure developed and utilized by the Center for Physical and Power Electronics at the University of Missouri – Columbia for suspending high-K particles in dielectric oil is denoted in table 1. The procedure utilizes a chemical surfactant to coat the particles during sonication. Coating the particles prevents particle agglomeration and allows the particles to stay in suspension. After suspension, the particle-infused oil must be allowed to sit for at least 72 hours to allow the larger particles to fall to the bottom. Otherwise, the inline filter can become clogged with the larger particles rendering the filtration system ineffective at removing excess carbon.

Table 1. This table denotes the procedure for suspending particles in oil.

Step	**Instruction**
1	Procure 1-L of oil to be tested
2	Pre-filter oil through 0.45-um filter to remove any macroscopic impurities
3	Place oil in 1500-ml beaker, insert magnetic stirrer, place beaker on stir plate and commence stirring at stable speed
4	If test matrix calls for no additives skip to step 12, if surfactant only skip to step 7, otherwise continue to step 5
5	Place sonicator tip in oil solution and prepare it for operation
6	Start sonication, add 5% BST by weight and wait 30 minutes
7	Add surfactant 1% by weight and sonicate an additional 10 minutes, no sonication necessary if proceeding from step 4
8	If there are BST particles in solution take a sample for analysis, otherwise skip to step 12
9	Allow particles to settle for 2 days
10	Filter oil down to 3-um pore size
11	Take a sample for particle concentration analysis
12	Take a water concentration measurement
13	Sparge with dry nitrogen with magnetic stirrer engaged for at least 10 minutes (if desired)
14	Take a water concentration measurement no more than 5 minutes after sparging
15	Insert oil into test switch no more than 5 minutes after water tests
16	Take the necessary number of shots at the necessary pressures
17	Remove oil from switch
18	Take a water concentration measurement no more than 5 minutes after removal
19	Take a sample for particle concentration analysis
20	Run statistics and produce result
21	Repeat with any additional oils

Pre-filtration of the particle-infused oil is necessary so that the inline filter in the HVADTS system can perform its function of removing carbon by-products from the oil. Without the pre-filtering step, the filters immediately clog with larger particles, rendering the filter ineffective. Pre-filtration and inline filtration in all cases where particles are present is performed with a 3 μm cellulose filter. A new filter is installed and the switch is cleaned after the oil is tested. A 3 μm filter pore size has experimentally shown the best oil flow rates and jitter performance.

3.4 Particle Concentration Analysis

While the SEM images in section three are useful in determining an approximate particle size distribution, Photon Correlative Spectroscopy (PCS) is a more precise way of determining the particle size distribution. The particle size distribution is important when considering pre-filter and inline filter pore sizes, optimum particle concentrations, sedimentation times, and reproducible particle-infused oils to achieve the lowest jitter.

To determine the concentration of remaining particles by weight in the oils before and after testing, a proprietary drying method is employed. The method involves placing a small sample of the particle-infused oil on an aluminum weigh boat and drying it in a muffle furnace. The weight is recorded before and after the drying procedure and the concentration by weight is then simply known. The PCS and drying procedures are outlined in this section as well as a calculation to determine particle count.

3.4.1 Photon Correlation Spectroscopy

Photon Correlation Spectroscopy (PCS) is based on current dynamic light scattering techniques. The time decay of the near-order of the particles as a result of Brownian motion is used to evaluate the size of particles using the Stokes-Einstein relation. At constant temperature the method only requires the knowledge of the viscosity of the suspending fluid for an estimation of the average particle size and its distribution function.

The PCS analysis is performed by Particle Technology Labs in Chicago, IL [18]. Four samples were sent to the lab and analyzed: three PAO samples and an alkylbenzene sample. Figure 13 is a graph depicting the particle size distribution of a particle-infused PAO. The graph suggests that the mean particle diameter is approximately 238 nm. The full report on the four samples is contained in the appendix.

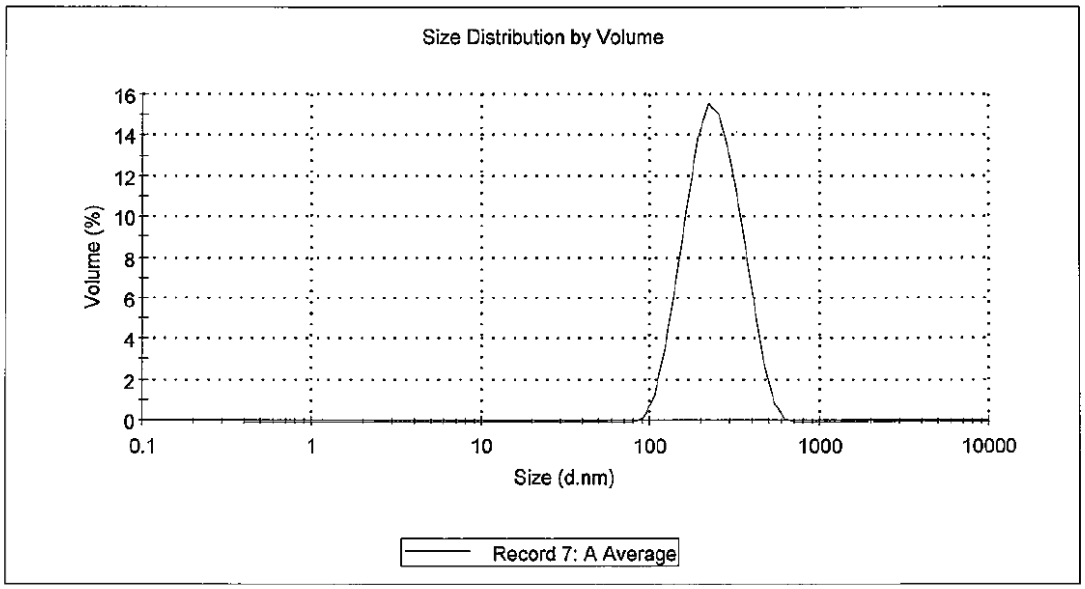

Figure 3.13: Results of the PCS analysis indicate that the mean particle size of the particles in this Nycodiel oil is 238.8 nm.

3.4.2 Oil Drying Method

The drying method of determining particle concentration by weight was developed by our chemist, Dan Crosby. Small 0.5 mL samples of the particle-infused oils are placed in aluminum weigh boats and evaporated in a muffle furnace at 555°C. Once the oil is vaporized and removed, only the particles remain. The sample is weighed before and after the drying process and the weight differential is indicative of the particle concentration by weight. Figure 14 is a photograph of particles in an aluminum weigh boat. The particle concentration is a necessary quantity to know, along with the particle size and density, in determining the particle count. The initial concentration before settling, pre-filtration, in-line filtering, and breakdown testing is 5% by weight.

Figure 3.14: After the drying method all the oil is evaporated and only the BST particles remain.

3.4.3 Particle Size, Concentration, and Count

Depending on the sample, it is apparent from the PCS analysis that the mean particle size varies between 200 and 400 nm. The drying method suggests that the particle concentration by weight is between 1 and 2%. Running a calculation with a particle size of 350 nm, a particle concentration of 1.5%, and a particle density of 5.2 g/cm^3 produces a particle count of approximately $9x10^{10}$ particles/mL [19].

Electrostatic simulations suggest that a particle size between 200 and 400 nm, a count greater than 10^{10} particles/mL and concentration greater than 1% by weight is sufficient to produce significant field enhancement in the bulk of the oil dielectric and on the electrode surface. The concentration is weight dependent and not volume dependent, since quantities are mixed by weight. The next section describes these PIC dielectric electrostatic simulations.

References

[9] TRS Technologies Incorporated, 2011.

[10] J. Hwang, M. Zahn, F. O'Sullivan, L. Pettersson, O Hjortstam and R. Liu, "Electron scavenging by conductive nanoparticles in oil insulated power transformers," *2009 Electrostatics Joint Conference*, Paper 1.1, 2009.

[11] F. O'Sullivan, J. G. Hwang, M. Zahn, O. Hjortstam, L. Pettersson, R. Liu, and P. Biller, "A model for the initiation and propagation of positive streamers in transformer oil," in *IEEE International Symposium on Electrical Insulation* ISEI08, Vancouver, British Columbia, Canada, June, pp. 210-214, 2008.

[12] F. M. O'Sullivan, "A model for the initiation and propagation of electrical streamers in transformer oil and transformer oil based nanofluids," Ph.D. dissertation, Massachusetts Institute of Technology, Cambridge, MA, USA, 2007.

[13] FEI Quanta 600F with EDS, FEI, www.fei.com, 2011.

[14] Y. Huang, J. Lee, J. Lee, Y. Jeong, S. Cheong, Y. Ahn and S. Kim, "Production and dispersion stability of nanoparticles in nanofluid," Powder Technology, Volume 186, Issue 2, August, 2008.

[15] Nyco Corporation, "Nycodiel" Technical Data Sheet. MSDS. 2011

[16] Alkylate 225, Huntsman Oil Co., "Linear AlkylBenzene" Technical Data Sheet. MSDS. 2011.

[17] "N-Hexane" Technical data sheet. MSDS. 2011

[18] Particle Technology Labs, Chicago IL, 2011.

[19] T. Remmel, M. Schulberg, S. Fujimura, H. Honma, H. Kobayashi, H. Kohno, S. Owen, R. Deslattes and J. Pedulla, "Barium Strontium Titanate thin film analysis," *ICPDS*, Vol. 43, 2000.

CHAPTER 4

PARTICLE-IN-CELL DIELECTRIC ELECTROSTATIC SIMULATIONS

The dielectric system was modeled and extensively simulated to develop a first-order understanding of the breakdown mechanisms affected when a dielectric is subjected to an electric field. The dielectric is modeled as a three-dimensional homogeneous background of material with a fixed dielectric constant into which a random distribution of particles is introduced; the particles having a dielectric constant much larger than the background dielectric. Conditions such as particle size, particle concentration, distance of a single particle from the electrodes, and effect of electrode field enhancements are investigated numerically. The simulations suggest that particle density is a critical parameter, with increased concentrations corresponding to increased average electric fields within the simulated dielectric sample. It is important to note, however, that the increase in average electric field is due to the effect of many localized field enhancements generated by the random distribution of polarized high-K particles near the electrode surface.

The results of the simulations indicate that the BST particles have a significant impact on the electric field distribution within the oil switch [20]. All simulations are performed in three dimensions with CST EM Studio [21]. Figure 4.1 is a three dimensional (3D) model of the electrode system that is used to simulate the effects of particles on the electric field, including a random dispersion of particles. Figures 4.2 and 4.3 illustrate a two-dimensional (2D) cutaway of a 3D simulation, and highlight the effect of the particles in the gap under steady state conditions. Figure 4.4 illustrates molecular reorientation of a uniformly fixed distribution of polarized particles.

The results of the field model indicate that the particles introduce a field enhancement effect on the electrode surface and within the bulk of the oil. The high dielectric constant associated

with a particle of BST ($\varepsilon_r \approx 2000$) excludes electric fields and concentrates them within the oil ($\varepsilon_r \approx 2$), thus producing an electric field enhancement at the BST-oil interface of 1000. It follows that a BST particle near the electrode surface will increase the local electric field in the oil and increase the probability of electron emission. The particle-generated electric field enhancement in the bulk of the oil may also help guide the breakdown streamer across the gap.

4.1 Average and Maximum Fields on a Smooth Electrode Surface

In the 3D gap model of figure 4.1, the particles are modeled as perfect spheres with adjustable radius and volume concentration percentage. Each simulation is performed with a random distribution of particles of fixed radius. The dimensions of the test gap for simulation purposes are held constant for all simulations. The gap length is fixed at 8 μm and the electrode diameter is set at 16 μm. The electrode potentials are set to 0 and 1000 volt which translates to an electric field of approximately 1.2 MV/cm across the gap. This electric field magnitude mimics experimental breakdown fields.

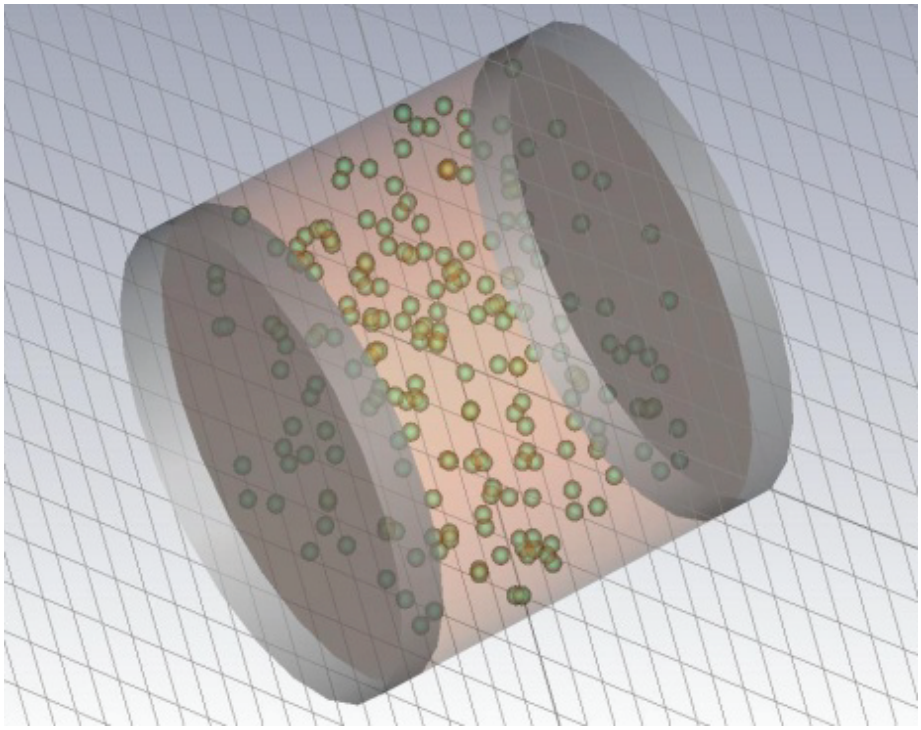

Figure 4.1: The PIC simulation test cell demonstrating a random particle insertion pictured is modeled in CST EM Studio Software Suite.

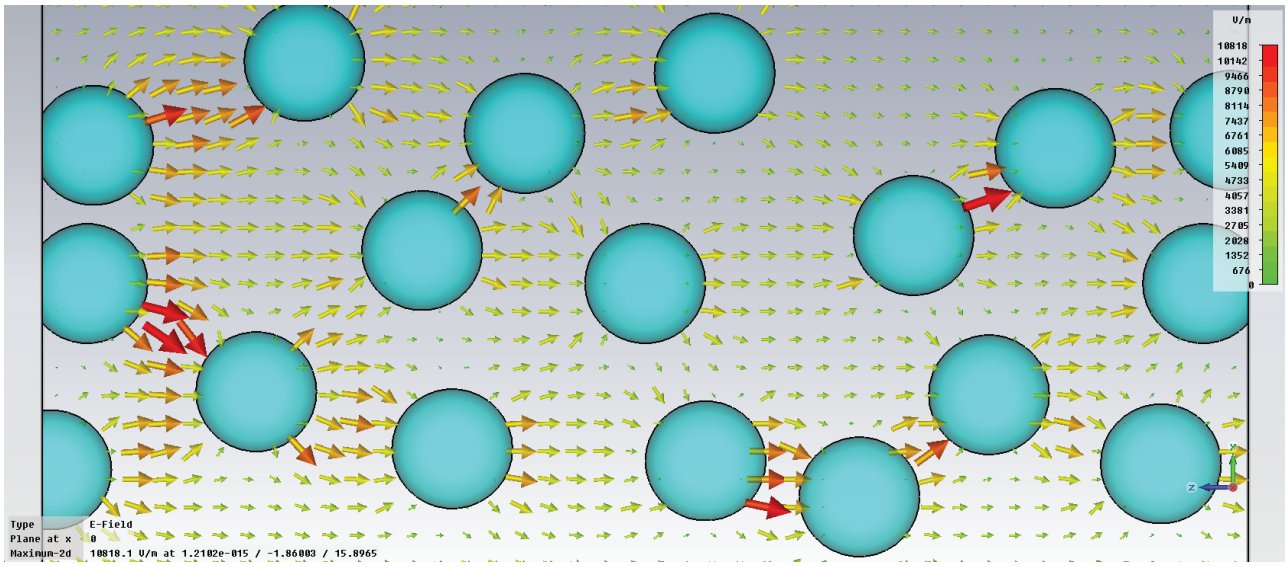

Figure 4.2: A 2D cutaway of a 3D simulation is pictured. The arrows represent the electric field intensity. The redder, larger arrows correspond to electric fields of greater magnitude.

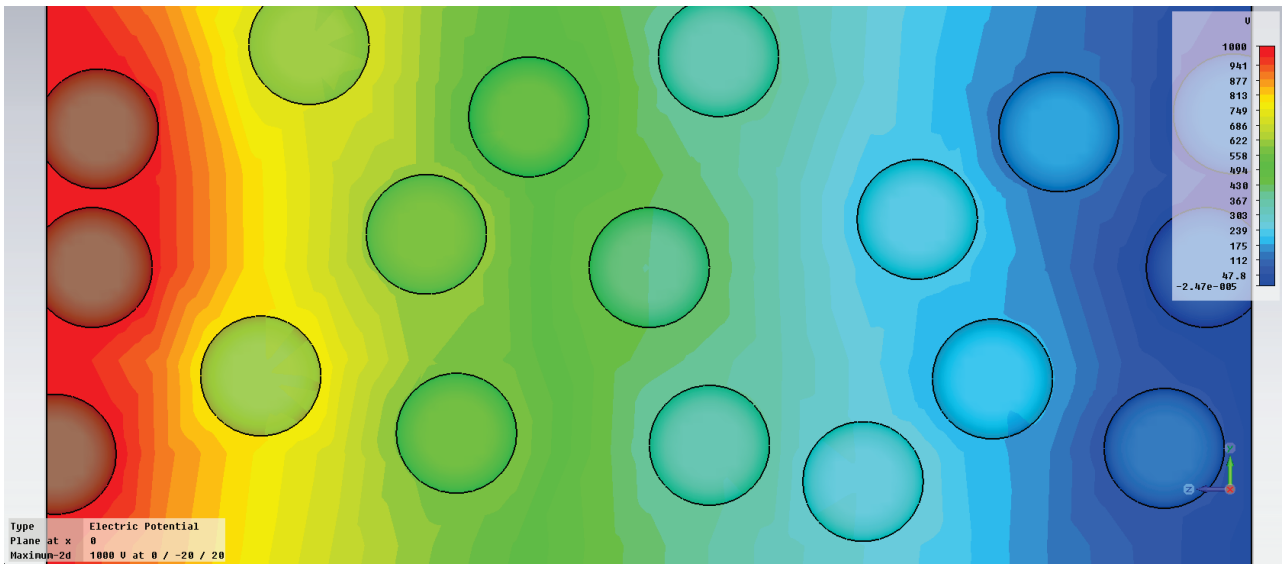

Figure 4.3: A 2D cutaway of a 3D simulation is pictured. The colors represent equipotential lines across the gap. This simulation is identical to the simulation of figure 4.2; however, the data is displayed differently.

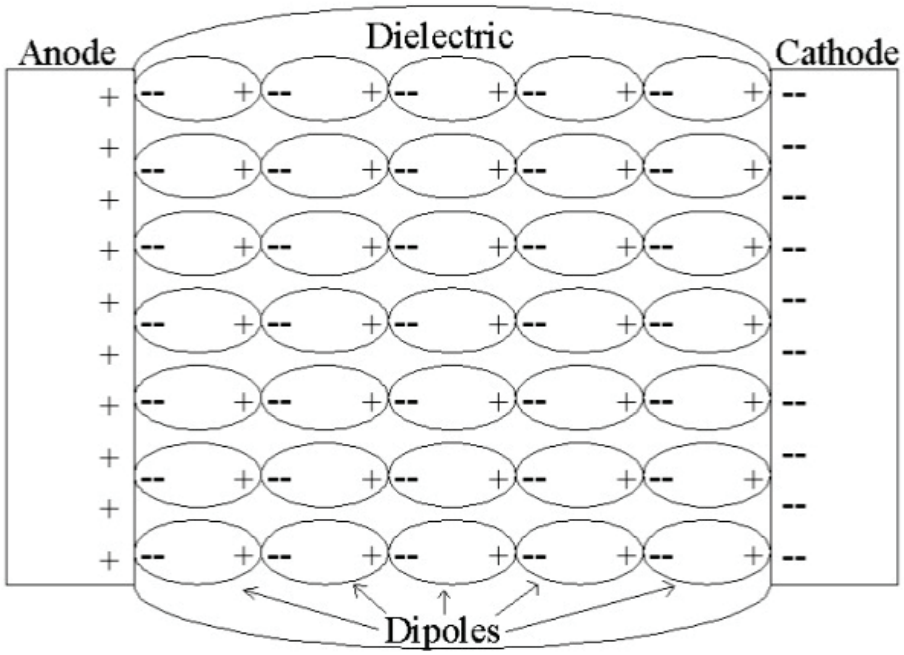

Figure 4.4: In the presence of an external electric field a polar molecule will reorient to compensate for the internal charge redistribution [23].

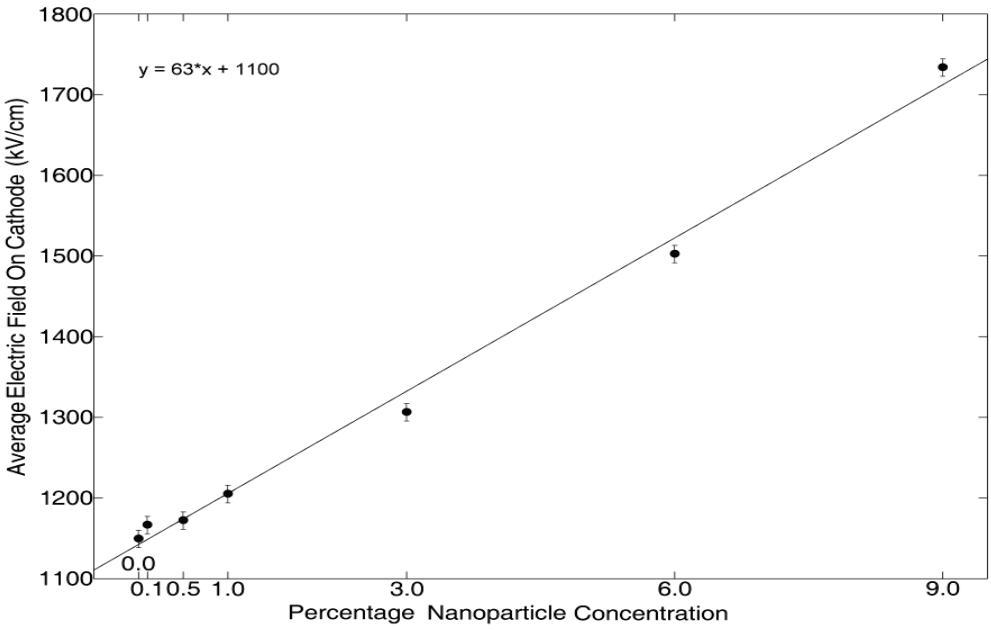

Figure 4.5: Cumulative results from simulations illustrate that an increasing particle concentration enhances the average electric field at the electrode surface. Particle radius is held constant at 350 nm. The standard deviation from the three simulations at each concentration is negligible.

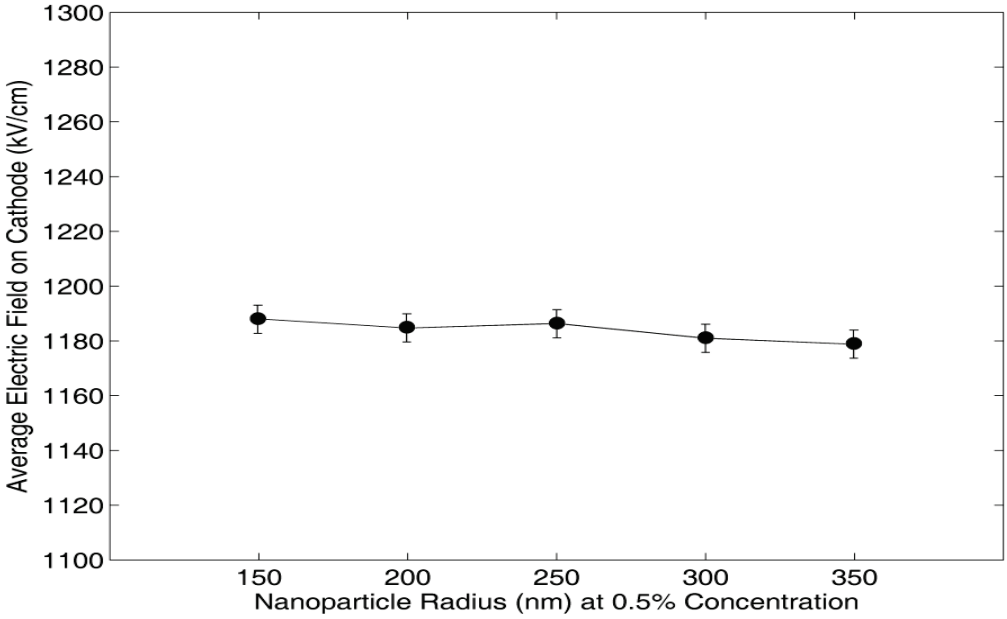

Figure 4.6: Cumulative results from a series of simulations demonstrate that there is no significant increase in the average electric field at the electrode with increasing particle size. The particle concentration is held constant at 0.5%. The standard deviation from the three simulations at each concentration is negligible.

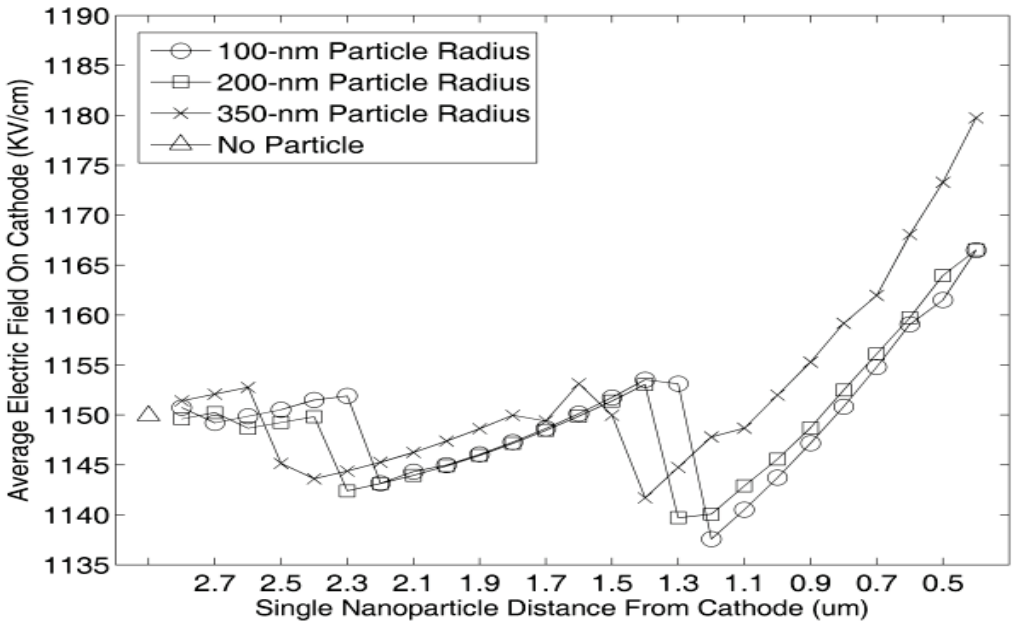

Figure 4.7: Cumulative results from a series of simulations illustrate how the distance of a single particle from the electrode influences the average electric field at the electrode for particle radii of 100, 200, and 350 nm. Each point is the result of a single simulation.

Figures 4.5 and 4.6 illustrate the effect of particle concentration and radius on the average electric field at the electrode surface. While particle concentration has a significant effect on the average electrode electric field, the particle radius is shown to not have a significant effect. Increasing the radius of the particles and maintaining a constant concentration reduces the number of particles in the PIC. While a larger particle generates enhancement over a larger electrode area, there are fewer particles resulting in minimal average field variation. The effect of size on experimental jitter is not known at this time; however, smaller particles are more practical as they stay in suspension longer.

Figure 4.7 shows the effect of a single particle on the average electrode field with varying particle distance and radius. The results indicate that an increasing particle concentration has a significant effect on the average electrode field. The results show an almost linear field increase of approximately 65 $\frac{kV/cm}{\%}$, indicating generous field enhancement at the surface of the electrode with an increasing concentration of perfectly spherical particles.

The distance of the particle's outer surface from the surface of the electrode has a significant effect on the average electric field at the electrode. At a distance greater than 0.8-μm from the electrode the electric field at the electrode surface is less than the field with no particles present. As the particle nears the electrode, the electric field on the electrode increases by approximately 40 $\frac{kV/cm}{\mu m}$. The particle distance simulations are repeated with particle radii of 200 nm and 350 nm. In each case the minimum average electrode field occurs when the particle is approximately 1.3 μm from the electrode surface. The minimum field distance shifts farther from the electrode for the larger particles. The trend of the simulation presented in Figure 4.7 may be the result of competing effects at the electrode surface. At certain distances the particles must decrease the electric field at various points on the electrode leading to a decrease in the average electrode field. The effect is more pronounced at smaller particle diameters. This could also be the result of artifacts present in the simulation.

Figure 4.8 shows that the local maximum electric field on the electrode decreases with an increasing particle distance. This result is not surprising as it is well known that the force between two charged objects exponentially decreases with increasing distance. This plot shows that a single 100-nm radius particle can increase the local electric field on the electrode nearly

40% from 1150 to 1575 kV. This suggests that an electron on the electrode surface near a suspended particle will have a much higher probability of emission from the electrode, increasing the chance that the area will be a site for microbubble formation and breakdown initiation.

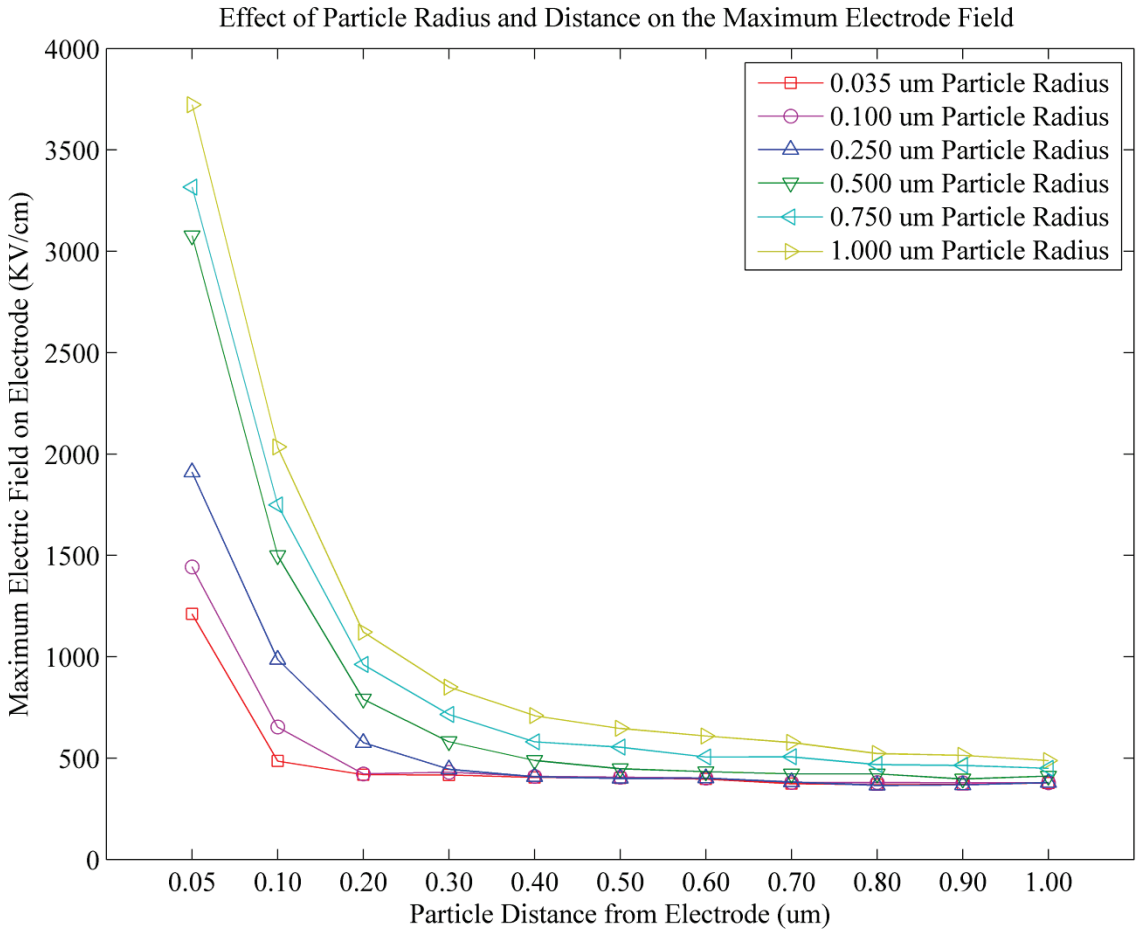

Figure 4.8: The maximum electric field strength at the electrode due to the presence of a single particle decreases with increasing particle distance. The larger particles generate a higher maximum electric field. Each point is the result of a single simulation.

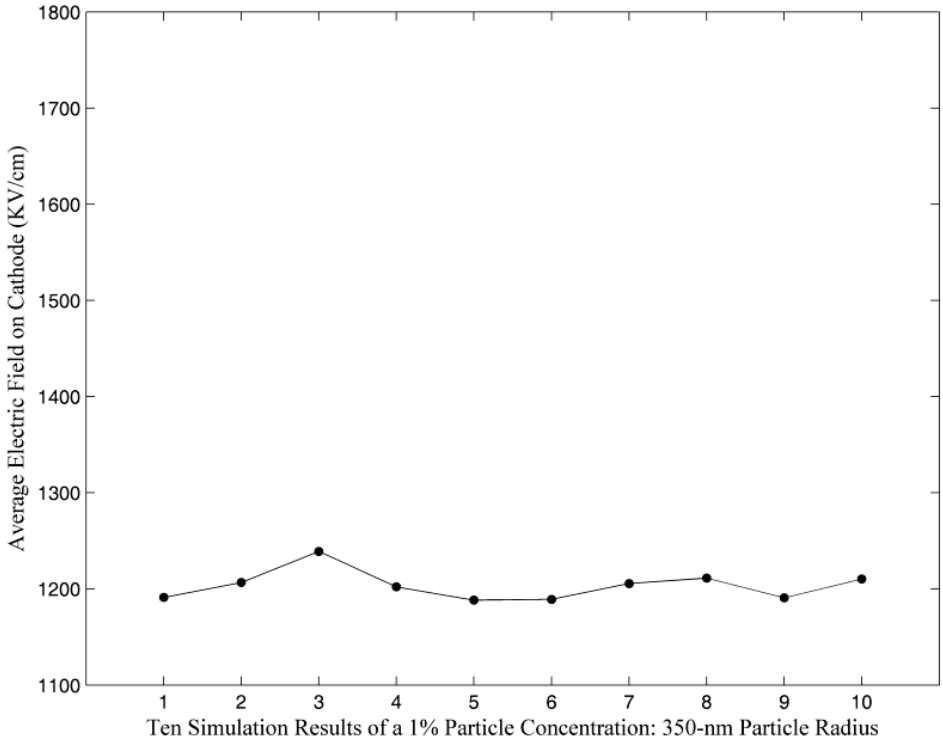

Figure 4.9: Results from a series of ten single 3D simulations show that the electric field at the electrode does not alter significantly due to a changing, random distribution of particles of fixed radii and concentration. Each point is the result of a single simulation.

Repeating electrostatic simulations with varying random particle distributions at a constant concentration and radius produces consistent average electrode electric field values. It appears that the particles initial distribution does not change the average electric field on the electrode significantly. Figure 4.9 shows the average electric field on the electrode with a 1% concentration of 350 nm radius particles with 10 separate initial random distributions.

Consideration must also be given to the effect of the dielectric constant of the particle. All the above simulations utilize a particle dielectric constant of 2000, which is the approximate dielectric constant of a BST particle. Figure 4.10 shows the effect on the average electric field with several particle concentrations and three dielectric constants. Figure 4.11 shows the effect of the dielectric constant of a single particle on the electrodes maximum electric field.

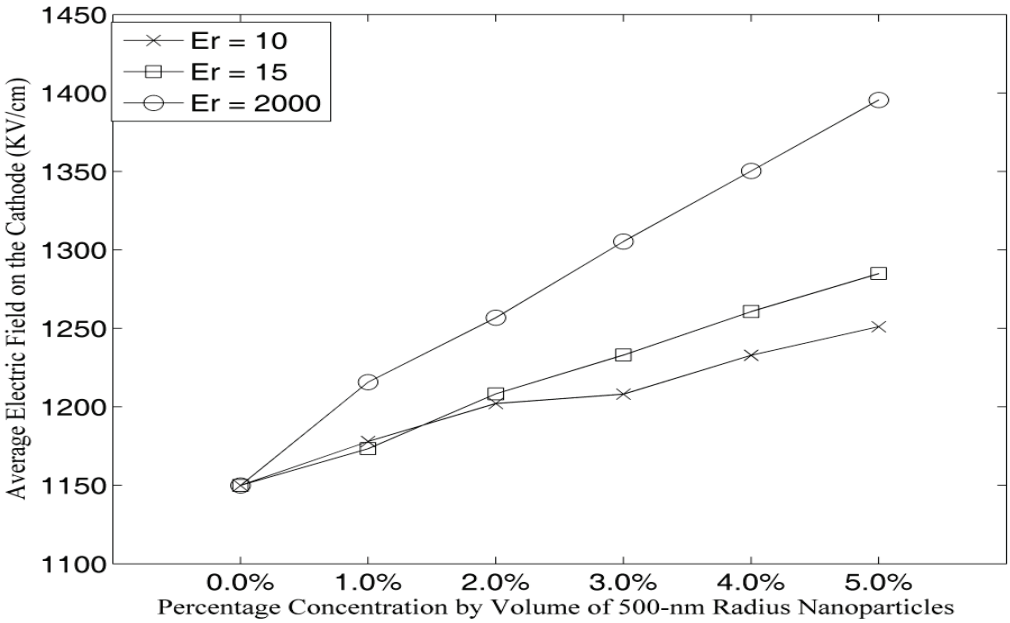

Figure 4.10: Cumulative results from the simulations show that the average electrode electric field increases with different particle dielectric constants and volumetric densities. A constant particle radius of 500 nm is utilized. Each point is the result of a single simulation.

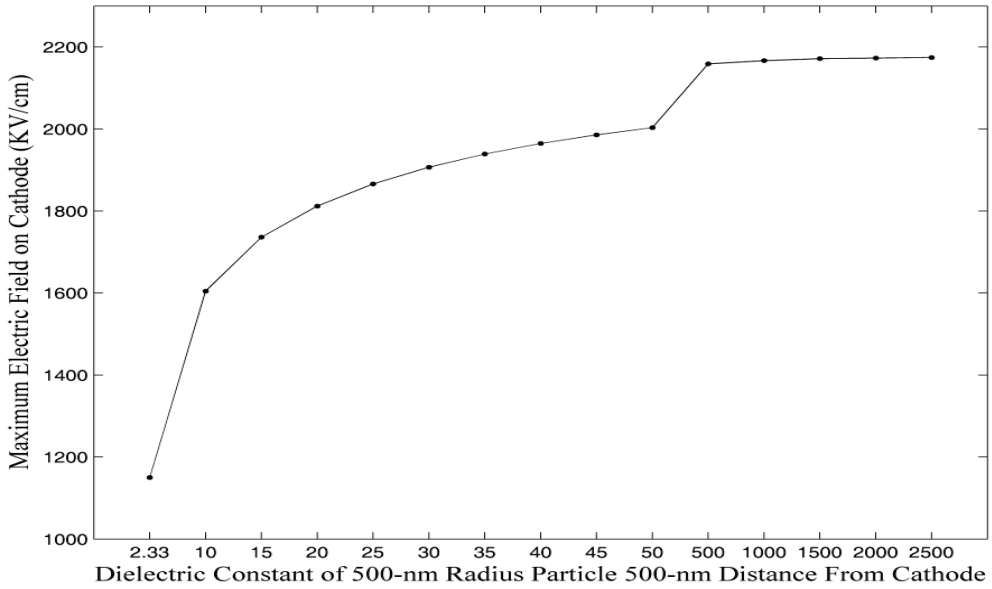

Figure 4.11: Results from several simulations examine the peak electric field at the electrode as a function of the dielectric constant of a single particle. The peak electric field asymptotically approaches a maximum value of approximately 2.1 MV/cm as the relative dielectric constant increases beyond 2500. Each point is the result of a single simulation.

The simulations indicate that the electric field at the electrode is influenced by the particle concentration, dielectric constant and distance from the electrode. The distribution of the particles prior to application of high voltage is evidently less significant. In practice the particle radius may also significantly impact breakdown. The smaller and more numerous the particles are, the more chances that a particle may be localized near the electrode to generate a field sufficient to initiate a breakdown event. Also, more electric field gradients may be present to aid in streamer propagation across the gap. It is important to remember the increase in the average electric field on the electrode is not due to a uniform effect. It is the effect of many localized field enhancements that contribute to this overall average field increase.

4.2 Average and Maximum Fields on a Rough Electrode Surface

To ensure that the inherent computational error involved in the simulation process does not affect the results, each value presented is the average value from a series of three separate simulations, unless otherwise noted. In the case of all random field enhancement insertions, each of the three recorded field values in the series is simulated using different random insertions. This is done to show that the results are valid with any field enhancement spatial distribution, as would be the case on an actual deformed electrode surface. Figure 4.9 indicates that there is a small difference between simulations with different particle spatial distribution with the other variables held constant. Error bars were included in simulations with non-negligible standard deviations between runs.

The average electric field interactions on the electrode surface are measured directly from the electrode surface. The average field is found by integrating the field vectors, in V/m, over the surface of the face, m^2, which gives a result in units of V-m. Dividing this value by the total surface area gives the average field in terms of V/m. Simulations incorporate tetrahedral meshing and tangential boundary conditions with an accuracy of 10^{-6}.

The cathode and the anode are assigned voltage potentials of 0 V and 100 V, respectively. The potentials generate an average field of 126 KV/cm with an 8 μm gap between smooth electrode surfaces. All values presented are in electric field units of KV/cm. The simulation results of the previous section (figures 4.1 through 4.11) are produced with cathode and anode

voltages of 0 V and 1000 V, resulting in an average electric field an order of magnitude greater than the following simulations.

The limiting factor of the simulations is the simulation computation time. For a majority of the simulations the particle count is less than 500 and the simulations take 5 to 10 minutes to process. However, once the particle count reaches or exceeds 1000, the simulations can take several hours or days to process. This time constraint limits both the particle concentration and size. A high particle concentration matched with a low particle size results in a large particle count. The simulations are structured to limit the particle count to less than 1000.

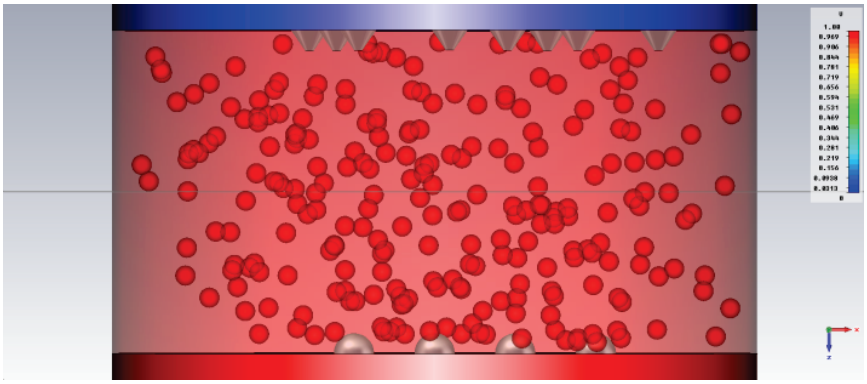

Figure 4.12: This picture shows the x-z plane of a simulation cell with five fixed spheres on the anode and eight random cones on the cathode. The simulation cell is a 3D cell; particles and electrode enhancements along the y plane are not actually in contact with one another. Approximately 245 particles are produced with a particle concentration of 1% and a particle diameter and dielectric constant of 0.5 µm and 2000, respectively.

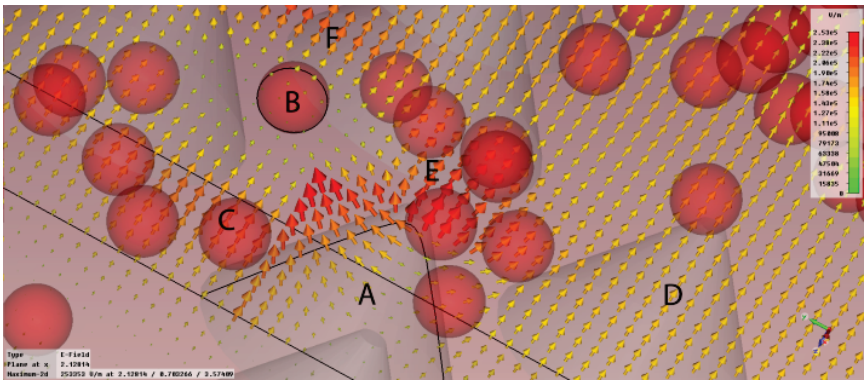

Figure 4.13: This 3D picture of section of a simulation cell shows a 2D slice of the fields generated by a particle and conical electrode field enhancement. The black lines indicate the 2D field-slice of the 3D simulation. Objects without a back outline do not contribute to the fields in the slice as they exist elsewhere on the x axis.

The letter A in figure 4.13 indicates a conical structure and B indicates a particle. The letter C indicates field enhancement on the smooth surface due to the particle B. The letter D indicates the electric field with no enhancement. The letter E indicates enhancement due to the conical field enhancement and F indicates the enhancement due to the particle in the bulk of the oil. The fields between A and B are the result of the interaction between the particle B and conical field enhancement A and have the greatest magnitude in the image-space.

All of the results in this section are obtained from 3D simulations. Figure 4.13 is included as a visual aid. It is apparent from that figure that the strongest field lines are located between the A and B enhancements and the weakest fields are at D where there are no field enhancements. These enhanced fields are thought to be responsible for the apparent breakdown strength reduction of the dielectric oil in our experimental oil switch.

The simulation variables that are changed to produce the curves of the following results are the number of field enhancements, size of field enhancements, type of field enhancements (hemisphere or cone), size of particles, and particle concentration. Figure 4.14 is an image of the simulation cell depicting the electrode surface from which the average field values are derived.

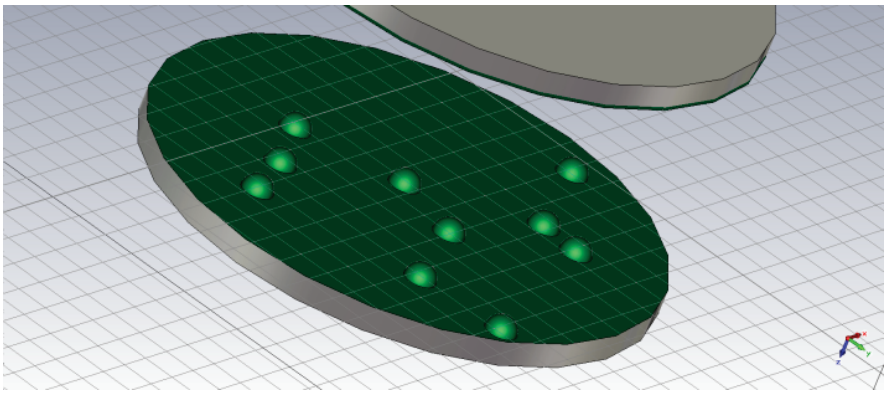

Figure 4.14: This image highlights the green surface of the electrode from which the average field values are derived. Ten hemispheres with 0.5 μm radii are randomly inserted in this simulation instance.

The results of figure 4.15 are obtained from varying the number of randomly placed conical field enhancements with and without particles. The conical field enhancements have the

following dimensions: top radius: 0.1 µm, bottom radius: 0.5 µm, and length: 0.5 µm. The particles are inserted at a size and concentration of 0.25 µm radius and 1% for a total of 245 particles in the simulation cell.

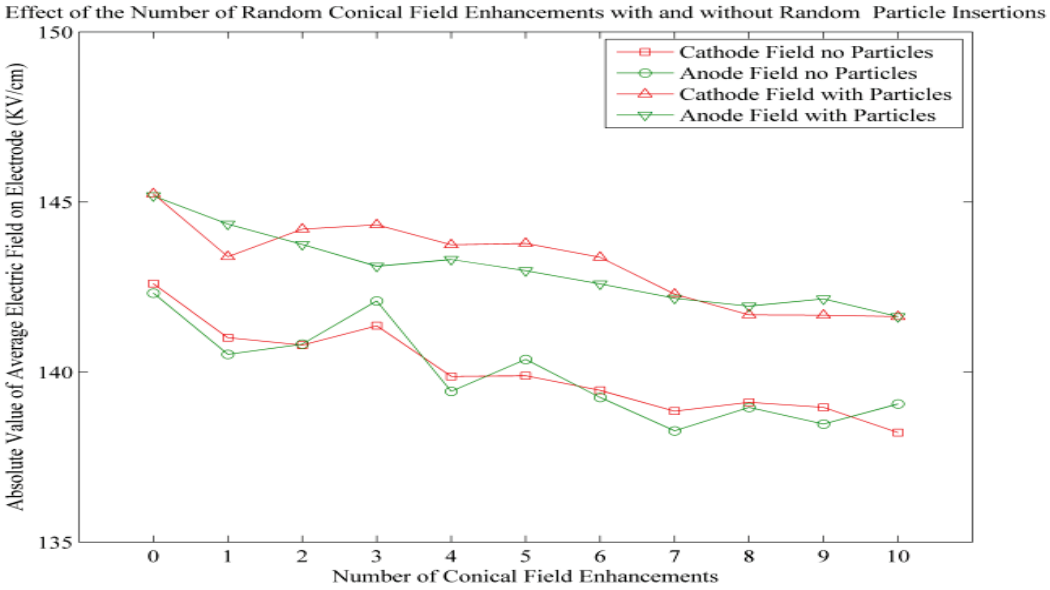

Figure 4.15: The results show that the average field on the electrodes decreases with increasing number of randomly placed conical field enhancements with and without particle insertions.

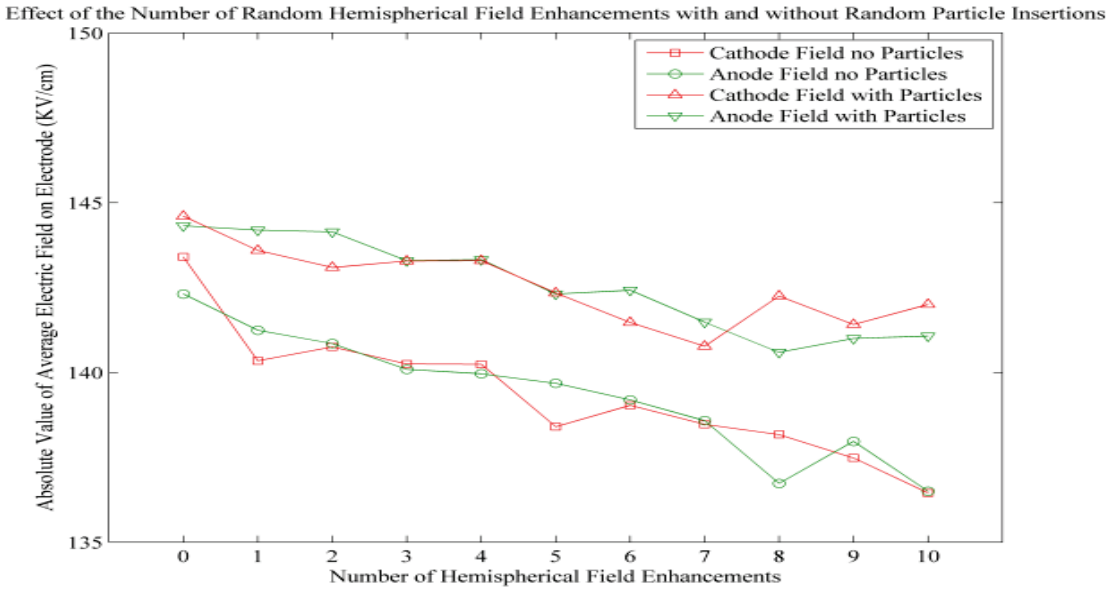

Figure 4.16: The results show that the average field on the electrodes decreases with increasing number of randomly placed hemispherical field enhancements with and without particle insertions.

The results of figure 4.16 are obtained from varying the number of hemispherical field enhancements with and without particles as is done in figure 4.15. The hemispherical field enhancements are created using spheres with a radius of 0.5 μm. The hemispheres are inserted in random locations.

The results of figures 4.15 and 4.16 indicate that increasing the number of field enhancements on the surface of an electrode slightly decreases the average field. While the fields at the tip of the electrode enhancements are enhanced, the fields near the base of the enhancement are reduced as seen in figure 4.17. The presence of the particles increases the average field in every instance, but does not prevent the gradual decrease in average field values with increasing number of field enhancements.

The simulations suggest that the effect of the field reductions near the base of the enhancement has a significantly greater cumulative effect that the field increases on the top of the enhancements with increasing number of enhancements resulting in a linear decay of the average field. It is important to note that the average electric field on the electrode surface is affected by many localized field effects and not a general effect. The local effects are generated by the inserted particle and electrode field enhancements.

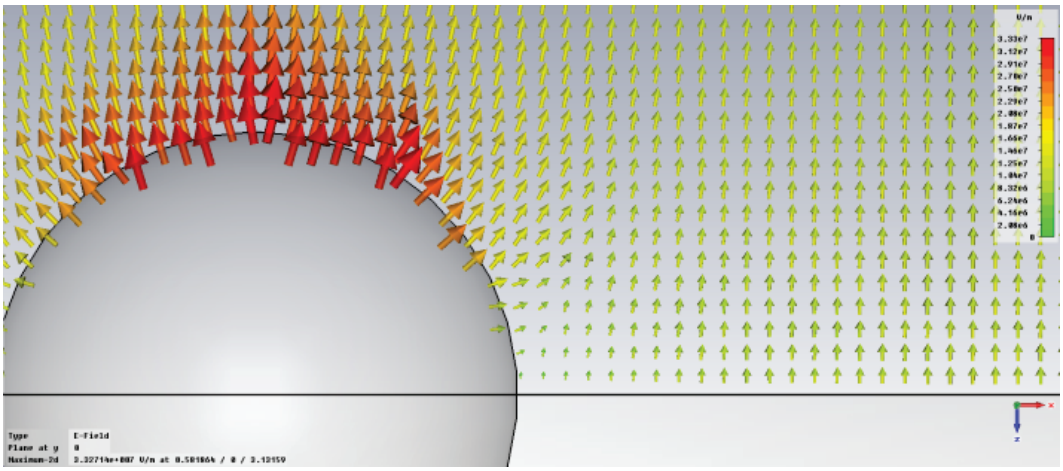

Figure 4.17: The image shows that while the maximum field on the top of the hemispherical enhancement is 330 KV/cm, the fields at the base are reduced to 20.8 KV/cm. The results of the simulation indicate that these reduced fields are responsible for the decrease in the average field with increasing number of field enhancements.

Ten conical and hemispherical field enhancements are simulated at five and four different sizes with and without particles present. The four lengths of the cones are 0.5, 0.75, 1.0, 1.25, and 1.5 µm. The top and bottom of the cones are held constant at radii of 0.1 and 0.5 µm, respectively. The four radii of spheres are 0.5, 0.75, 1.0, and 1.25 µm. There is not enough space on the electrode surface to simulate ten hemispheres at a 1.5 µm radius. All of the electrode field enhancements are randomly inserted.

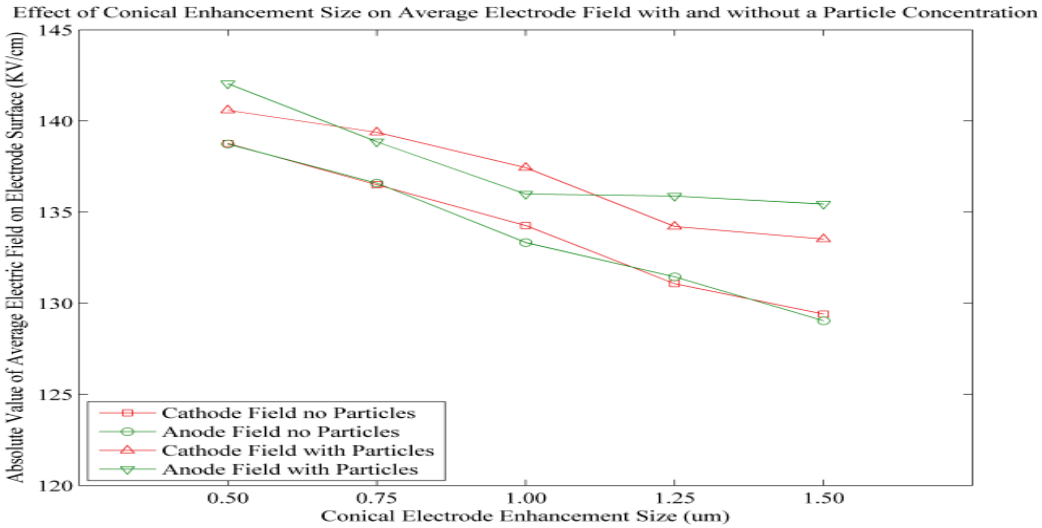

Figure 4.18: The results show increasing the size of the conical field enhancements decreases the average electrode surface field.

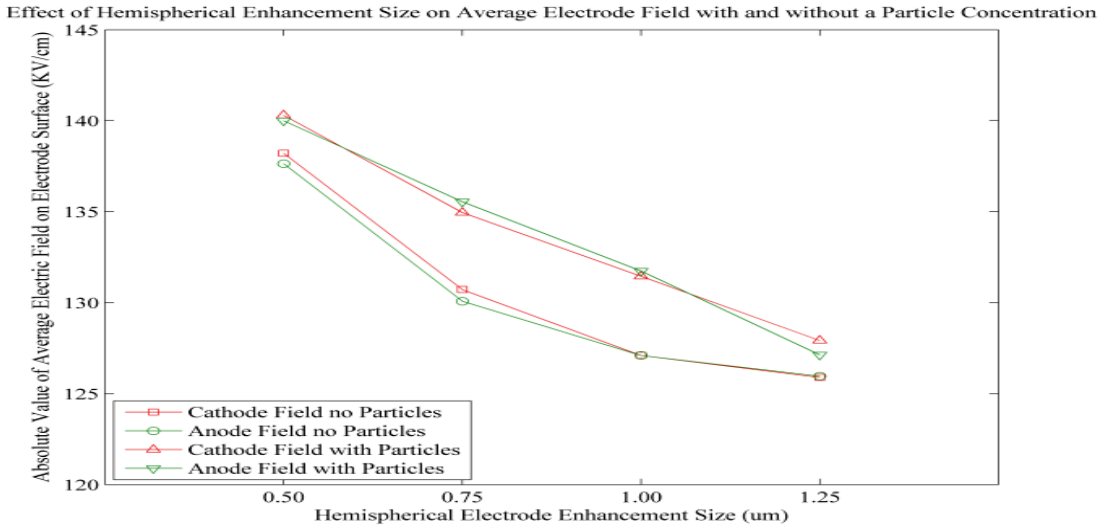

Figure 4.19: The results show increasing the size of the hemispherical field enhancements decreases the average electrode surface field.

The simulations of figures 4.18 and 4.19 demonstrate that the particles increase the average fields on the electrode surface possibly contributing to the reduction in breakdown strength of the oil dielectric. The results also show that as the size of the conical and hemispherical enhancements increase there is a decrease in the average electric field on the electrode. As the conical and hemispherical electrode field enhancements increase in size, there is a greater ratio of base area to top area. The fields at the base of a field enhancement are considerable reduced and act to decrease the average electrode fields, as is illustrated in figure 4.17.

The results of figure 4.20 are obtained from varying the particle concentration in the simulation cell. The randomly distributed particle concentrations are 0.0, 0.5, 1.0, 2.0, 3.0, and 4.0% by volume. These concentrations translate to particle counts of 0, 123, 245, 491, 736, and 982, respectively. The cones have a length of 0.5 μm and a bottom and top radius of 1 and 0.1 μm while the hemispheres have a 0.5 μm radius.

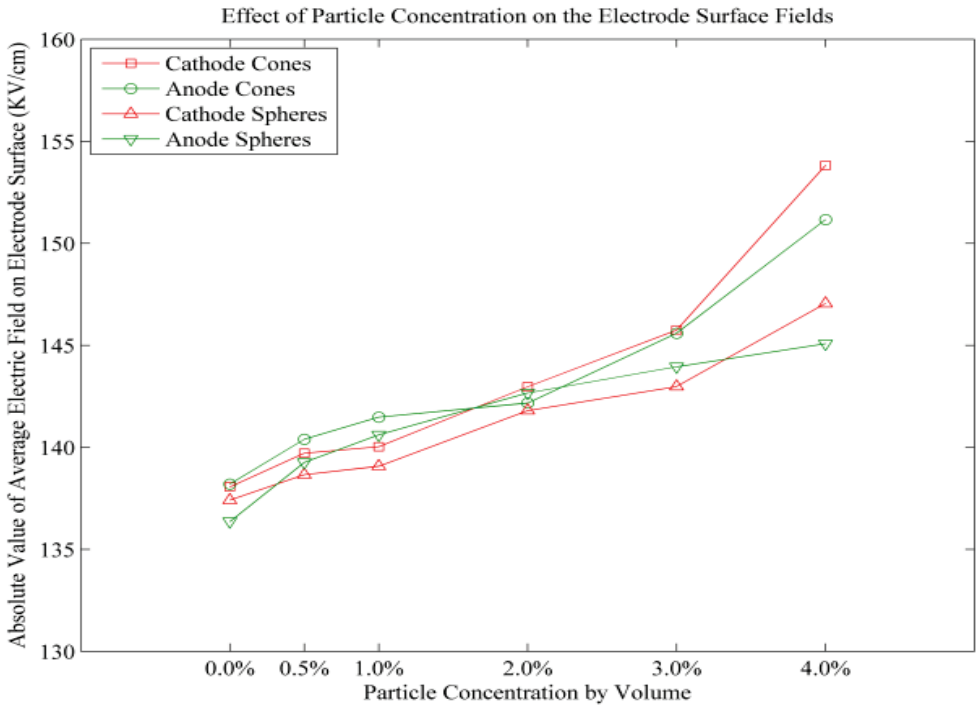

Figure 4.20: The results show that increasing the particle concentration increases the average electric field on the electrode surfaces.

The simulations of figure 4.20 demonstrate that the particles concentration increases the average fields on the electrode surface. It is thought that the particle concentration during experimental testing is approximately 1.75%. According to figure 4.20, a concentration of 1.0% is sufficient to generate increases of $10\frac{KV}{cm}$ in the average electrode field.

The results of figure 4.21 are obtained from varying the particle radius in the simulation cell. The randomly distributed particles are inserted at a 1% concentration by volume with radii of 0.15, 0.25, 0.35, 0.45, 0.55, and 0.65 µm. These radii translate to particle counts of 1136, 245, 89, 42, 31, and 14, respectively. Ten hemispheres are randomly inserted with at a 0.5 µm radius.

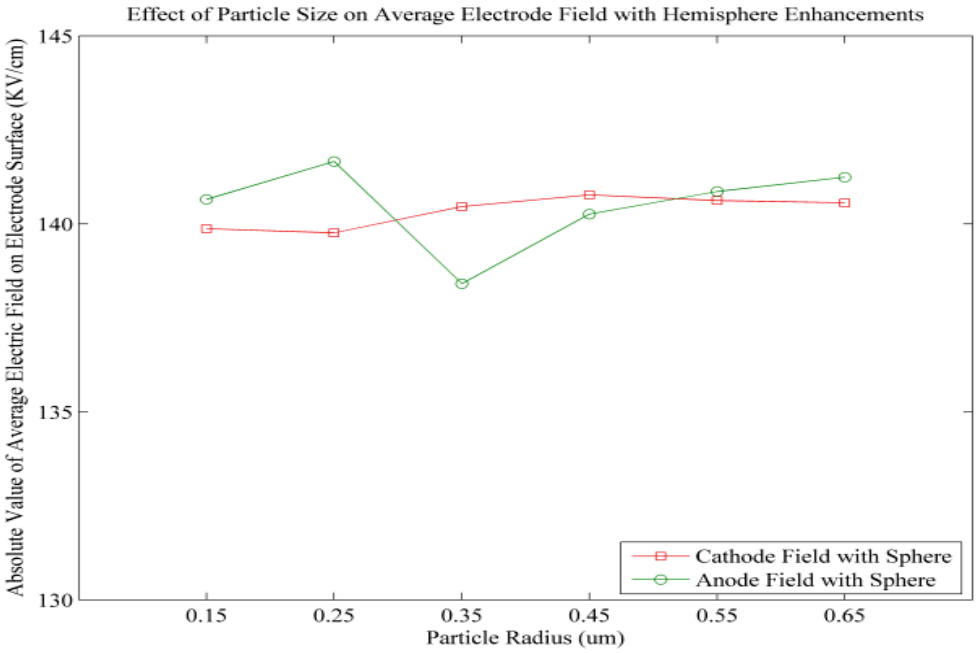

Figure 4.21: The results show that increasing the radius of the particle enhancements has no significant effect on the average electrode field. Each point is the result of a single simulation.

The results of figure 4.21 indicate that increasing the radius of the inserted particles in the simulation cell has little impact on the average electric field at the electrode surface. A small decrease in average electric field is found with increasing radius in previous simulations with smooth electrode surfaces is seen in figure 4.6. It is clear that the concentration of particles plays a much larger role than their radius on the average electrode field. It is important to note that as

the particle radius increases with a constant volume concentration, the number of particles in suspension is reduced.

In practice, however, the particle radius may significantly impact breakdown. The smaller and more numerous the particles are, the more chances that a particle may be localized near the electrode to generate a field sufficient enough to initiate a breakdown. Also, the smaller and more numerous the particles are, the more electric field paths may be present to aid in streamer propagation across the gap. It is important to remember the increase in the average electric field on the electrode is not due to a uniform effect. It is the effect of many localized field enhancements that contribute to the overall average field increase.

Figure 4.22: A previously smooth one inch diameter electrode is subjected to 230 breakdowns on the single-shot test stand. The deformations increase the probability that a subsequent breakdown will initiate on or near the site.

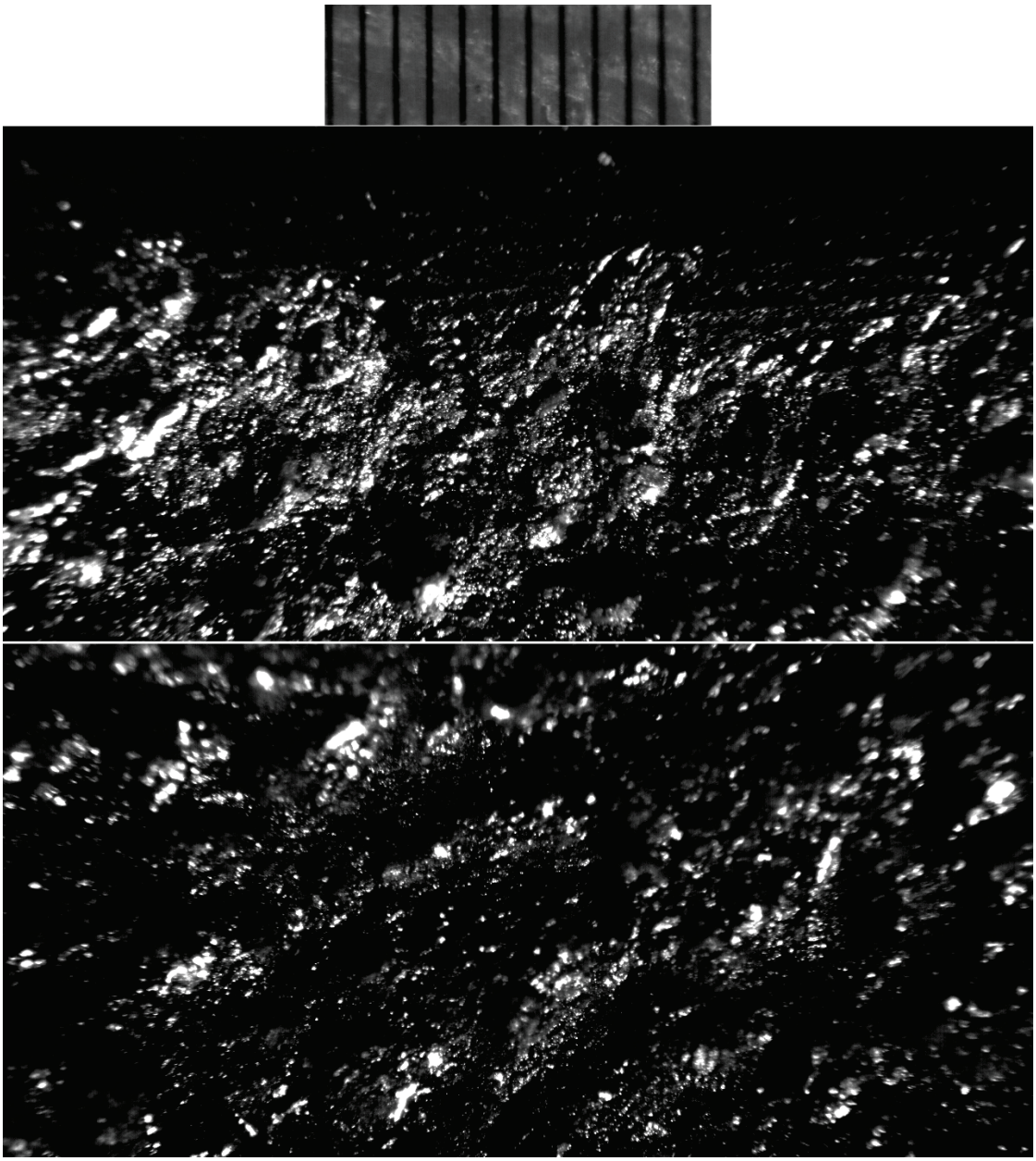

Figure 4.23: This image is a photograph of electrode deformation on the UMC rep-rate oil switch. The grating lines at the top of the image are 100 μm thick for reference. Shown above the line are erosion patterns near the top of the erosion band and below the line shows erosion patterns near the center of the erosion band. The entire band is 1 cm thick and extends the complete circumference of the hemispherical electrode [22]. The pattern is a product of approximately 10^6 breakdowns. Surface profilometry suggests that the average depth is approximately 25 μm.

4.3 Average Fields on a Field-Transparent Surface

The existing particle code is modified so that electric field interactions between the particles and the electrode field enhancements can be analyzed. Figure 4.24 illustrates a sample simulation cell matrix with five fixed spheres on the anode and eight random cones on the cathode. Particles with a 0.25 μm radius are inserted at a 1% concentration. The perfect electrical conductor (PEC) electrodes are 16 μm wide, 0.8 μm thick and set 8 μm apart. This distance is sufficient to prevent the field enhancements on one electrode from interacting with the fields on the opposite electrode. The dielectric constant of the oil background matrix is set at 2 for all simulations.

The magnitude of the average electric field on the electrode is determined by creating a field-transparent surface parallel to the electrode 0.1 μm from the top of the electrode field enhancement. The cathode and the anode are assigned voltage potentials of 0 V and 100 V, respectively. The potentials generate an average field of 125 KV/cm with an 8 μm gap between electrode surfaces.

The field enhancement on the electrode surface can either be a hemisphere or a cone. These hemispheres and cones represent deformation on surface of an electrode due to repeated discharges. The hemisphere is formed by imbedding a sphere in the PEC plate. The sphere can be set at any radius.

The cone has three adjustment parameters: top radius, bottom radius, and length. The top radius of the cone can be set to zero if a pin structure is desired. Twelve field enhancements of either type can be placed on each electrode. While the shape of the enhancements can be modified, all the enhancements on either electrode must be the same size and shape. Figure 4.25 is an image depicting the equipotential field lines of the simulation cell with a hemisphere and cone enhancement. It is clear from the image that the field enhancements only affect local electric fields near the electrode surface. Each point is the result of one simulation.

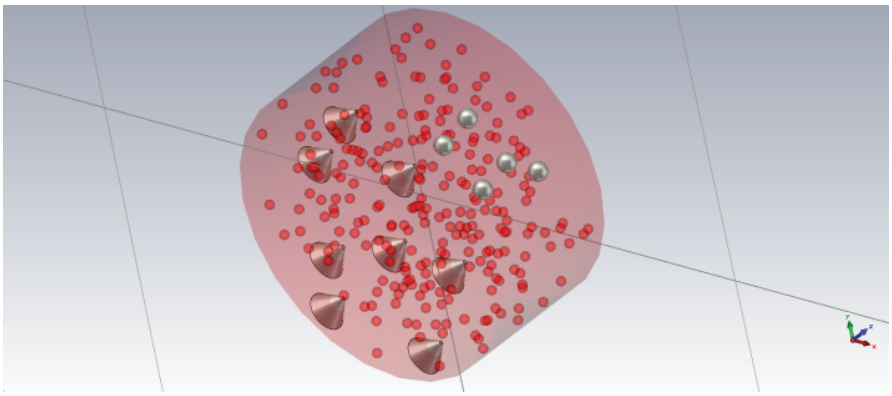

Figure 4.24: This picture shows the simulation cell as a perspective image with the plates hidden so the field enhancements and particles can be clearly seen. The axis is included on the bottom-right corner for analysis.

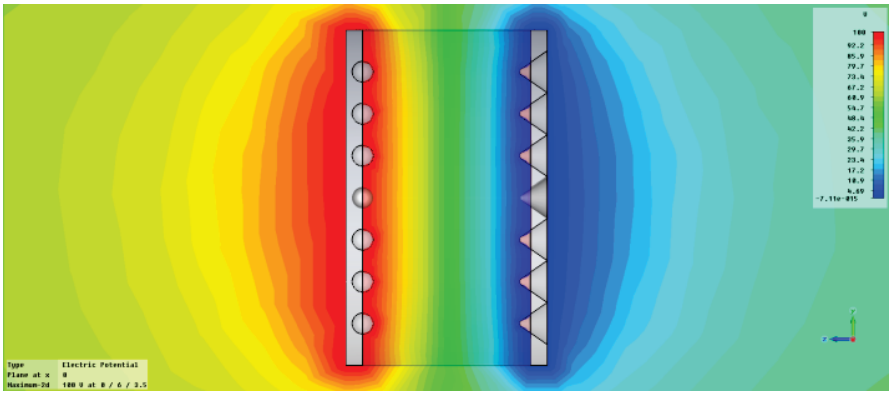

Figure 4.25: This image depicts contour equipotential field lines of the simulation cell with hemispherical and conical field enhancements. This graph shows that the effect of the electrode field enhancement is localized on the electrode surface

The magnitude of the average electric field interaction on the electrodes is determined by creating a field-transparent surface parallel to the electrode 0.1 μm from the top of the field enhancements. These surfaces are pictured in figure 4.26. The average value of the field lines acting on the surface is a good indication of the interaction fields between the electrode and particle enhancements. The simulation variables that are changed to produce the curves of figures 4.27 through 4.36 are the number of field enhancements, size of field enhancements, shape of field enhancements, type of field enhancements (hemisphere or cone), size of particles, and particle concentration.

It must be noted that all the fields recorded in this section are acting on the field-transparent surface, or FT-surface, located 0.1 μm above the electrode surface, and not the actual electrode surface. This section seeks to analyze field interactions between the particles and the electrode field enhancements, not the entire electrode surface. It has been shown previously that the average field on a face contouring the electrode surface is reduced by electrode enhancements and increased by particle enhancements in the previous sections.

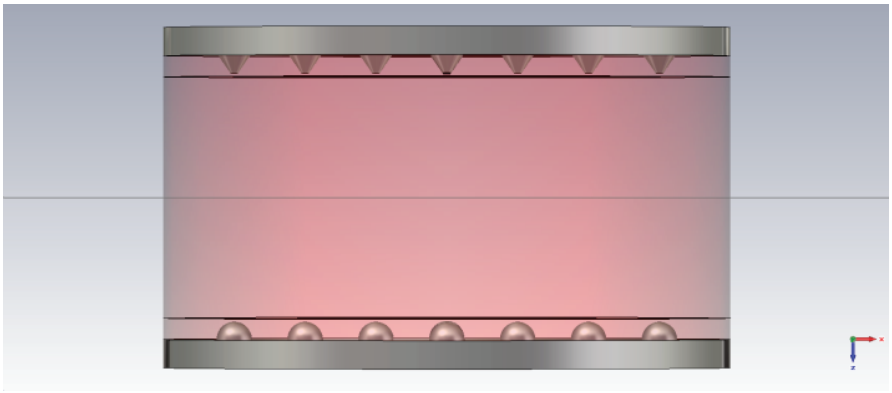

Figure 4.26: This picture shows the field-transparent surfaces above the field enhancements that are used to measure the average electric field interactions between the electrode and particle enhancements. The surfaces have no effect on the local electric fields and merely act to measure the interaction between simulated fields.

The average electric field interactions on the electrode surface are measured utilizing the field-transparent surfaces of figure 4.26. The average field is found by integrating the field lines, in V/m, over the surface of the face, m^2, which gives a result in units of V-m. Dividing this value by the total FT-surface area gives the average field in terms of V/m. Simulations incorporated tetrahedral meshing and tangential boundary conditions with an accuracy of $1E^{-6}$.

The cathode and the anode are assigned voltage potentials of 0 V and 100 V, respectively. The potentials generate an average field of 126 KV/cm with an 8 μm gap between smooth electrode surfaces. All values presented are in electric field units of KV/cm.

It is important to note that the average electric field on the FT-surface is affected by many localized field effects and not a general effect. The local effects are generated by the inserted particle and electrode field enhancements shown in figure 4.24.

The results of figure 4.27 are obtained from varying the number of conical field enhancements with and without particles. The conical field enhancements have the following dimensions: top radius: 0.1 µm, bottom radius: 0.5 µm, and length: 0.5 µm. The particles are inserted at a size and concentration of 0.25 µm radius and 1% for a total of 245 particles in the simulation cell.

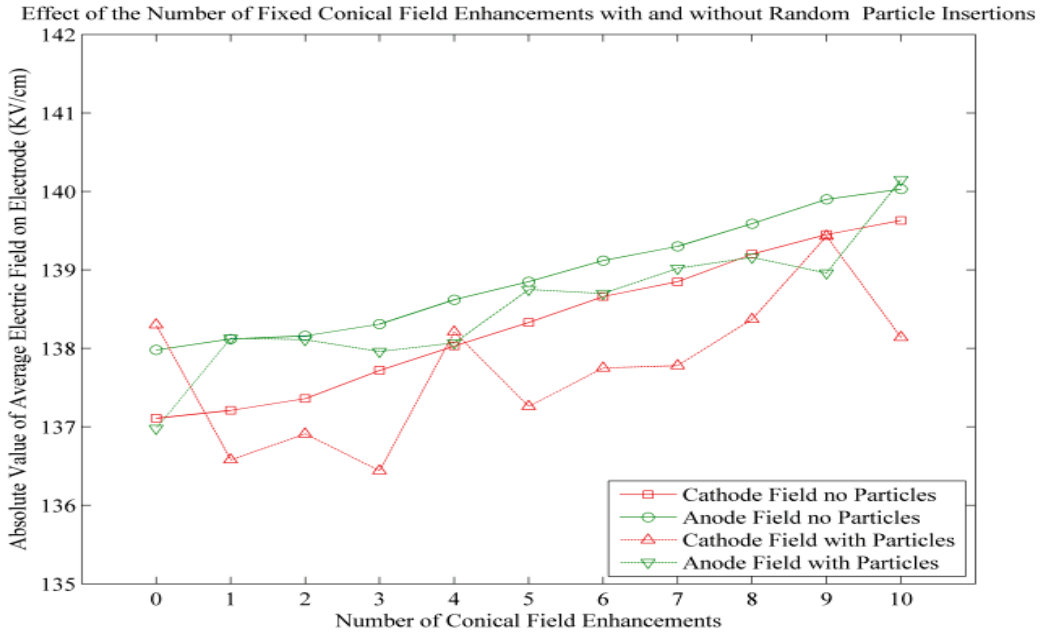

Figure 4.27: This graph shows the effect of the number of conical field enhancements on the average anode and cathode FT-surfaces with and without a random particle insertion. Each point is the result of one simulation.

Figure 4.27 demonstrates that increasing the number of fixed field enhancements increases the total field on the FT-surfaces with and without particles present. The introduction of the particles causes field perturbations on both the anode and cathode surfaces. This is an indication that the particles have a disruptive effect on the fields generated by the electrode enhancements.

The results of figure 4.28 are obtained from varying the number of hemispherical field enhancements with and without particles as is done in figure 4.27. The hemispherical field enhancements are created using spheres with a radius of 0.5 µm. The hemispheres are inserted in fixed locations.

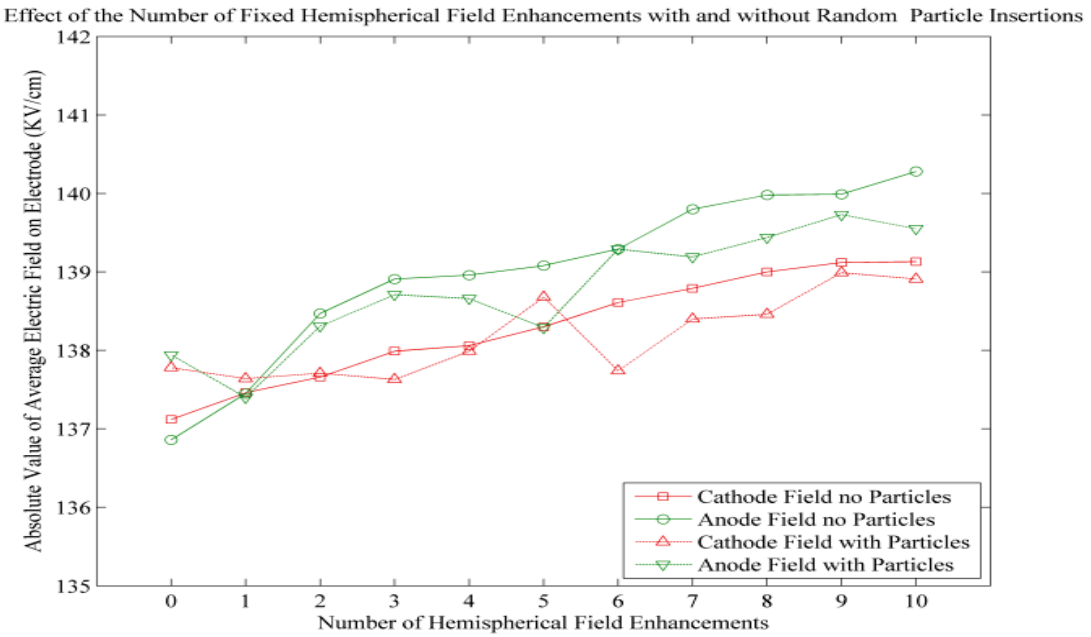

Figure 4.28: This graph shows the effect of the number of hemispherical field enhancements on the average anode and cathode FT-surface with and without a random particle insertion. Each point is the result of one simulation.

Figure 4.28 once again demonstrates that increasing the number of fixed field electrode enhancements increases the total field on the FT-surface with and without random particles present. The particles, as in figure 4.27, act to disrupt the fields on the enhancement surface.

The electrode surface conditions in an oil spark gap switch change with every breakdown event. In some cases, the switch operates at frequencies of 100 Hz or more. Simulations consisting of fixed electrode and particle field enhancements do not sufficiently match these conditions. By simulating each instance with a random distribution of field enhancements, actual surface conditions can be modeled.

The results of figures 4.29 and 4.30 are obtained by inserting 10 random conical and 10 random hemispherical field enhancements, respectively, with random particle insertions. Each data point from the figures is the result of one simulation, not an average of 3. The purpose of these simulations is to determine if a random field enhancement insertion paired with a random particle insertion produces significantly different results.

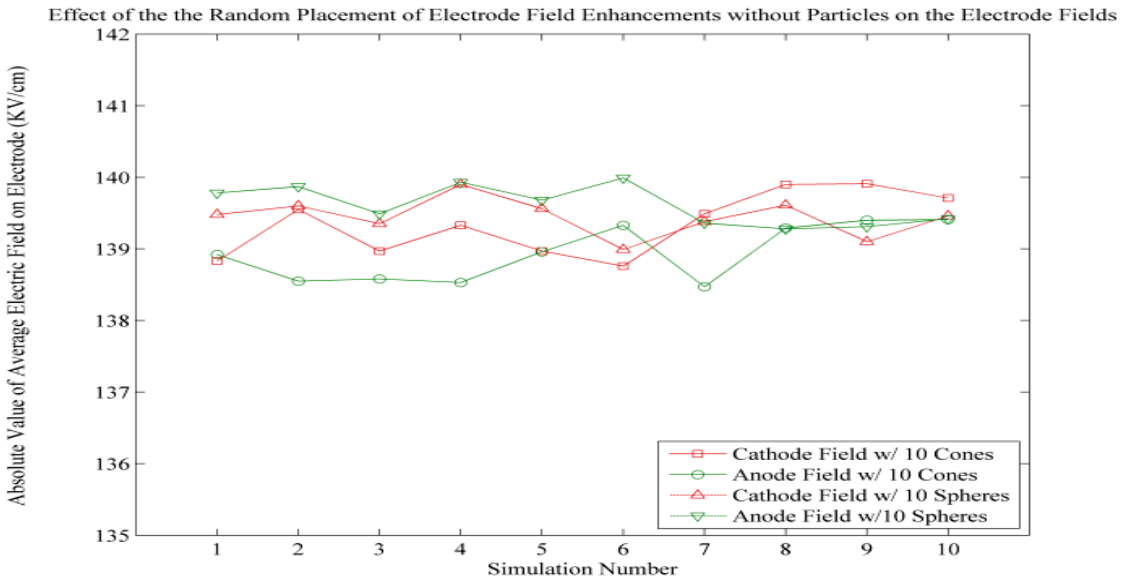

Figure 4.29: This graph shows the effect of the number of conical and hemispherical electrode field enhancements on the average anode and cathode FT-surfaces without a random particle insertion. Each of the points is the result of a single simulation.

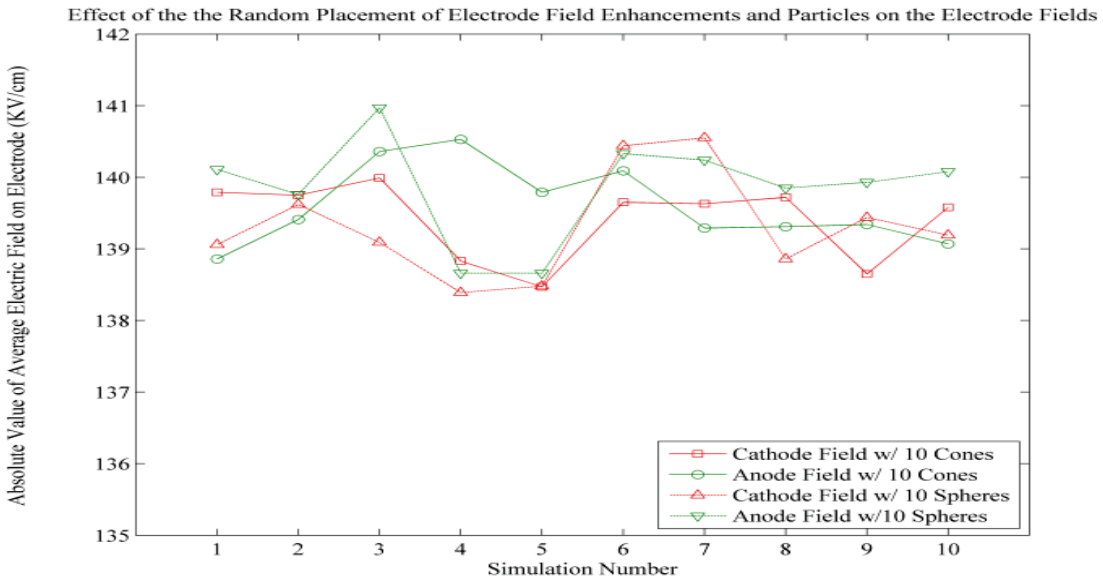

Figure 4.30: This graph shows the effect of the random insertion of conical and hemispherical electrode field enhancements on the average anode and cathode FT-surfaces with a random particle insertion. The particles produce field fluctuations between simulations on the FT-surface that are not seen in figure 4.29 when no particles are inserted. Each of the points is the result of a single simulation.

The results of figure 4.29 indicate that random distributions of electrode field enhancements do not produce large variations in the average electrode field on the FT-surface. The random insertion of particles paired with the random insertion of electrode field enhancements of figure 4.30, however, results in variations of the average electrode field between simulations.

Ten conical and hemispherical field enhancements are simulated at four different sizes with and without particles present. The four lengths of the cones are 0.5, 0.75, 1.0, and 1.25 µm. The top and bottom of the cones are held constant at radii of 0.1 and 0.5 µm, respectively. The four radii of spheres are 0.5, 0.75, 1.0, and 1.25 µm. All of the electrode field enhancements are randomly inserted.

Figure 4.31 shows a simulation with particles and 1.25 µm cones. The particles are inserted randomly with a 0.25 µm radius and 1% concentration. The FT-surfaces are adjusted so that they remain 0.1 µm from the top of the electrode field enhancements. The purpose of these simulations is to determine if field enhancement size has any effect on interactions between electrode field enhancement and the particles.

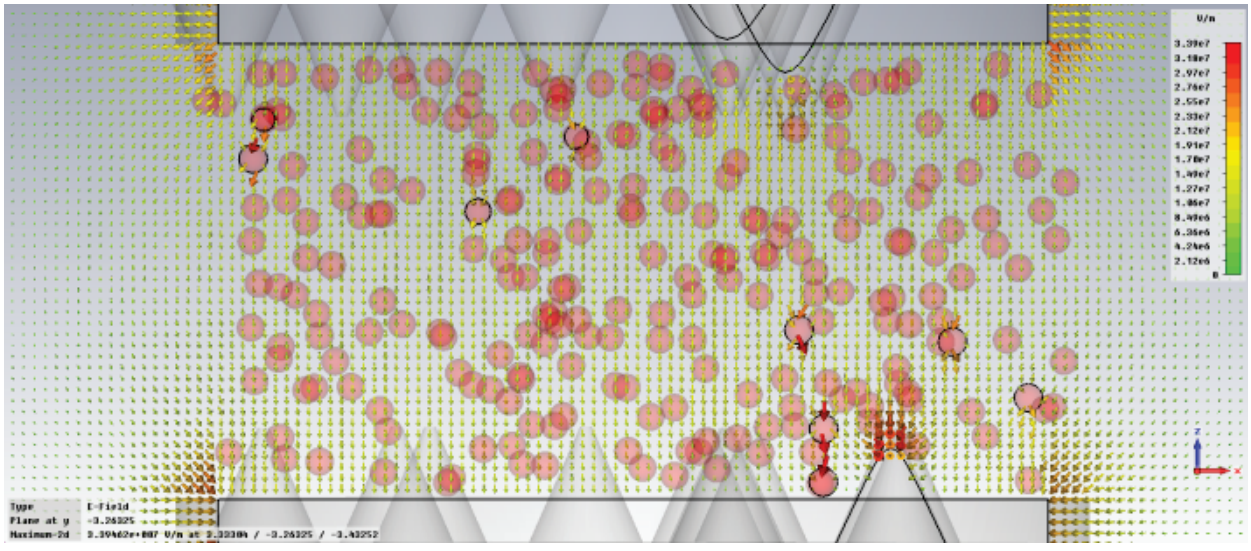

Figure 4.31: This is an image of the simulation results with a 1.25 µm cone sizes and 1% particle distribution with 0.25 µm particle radii.

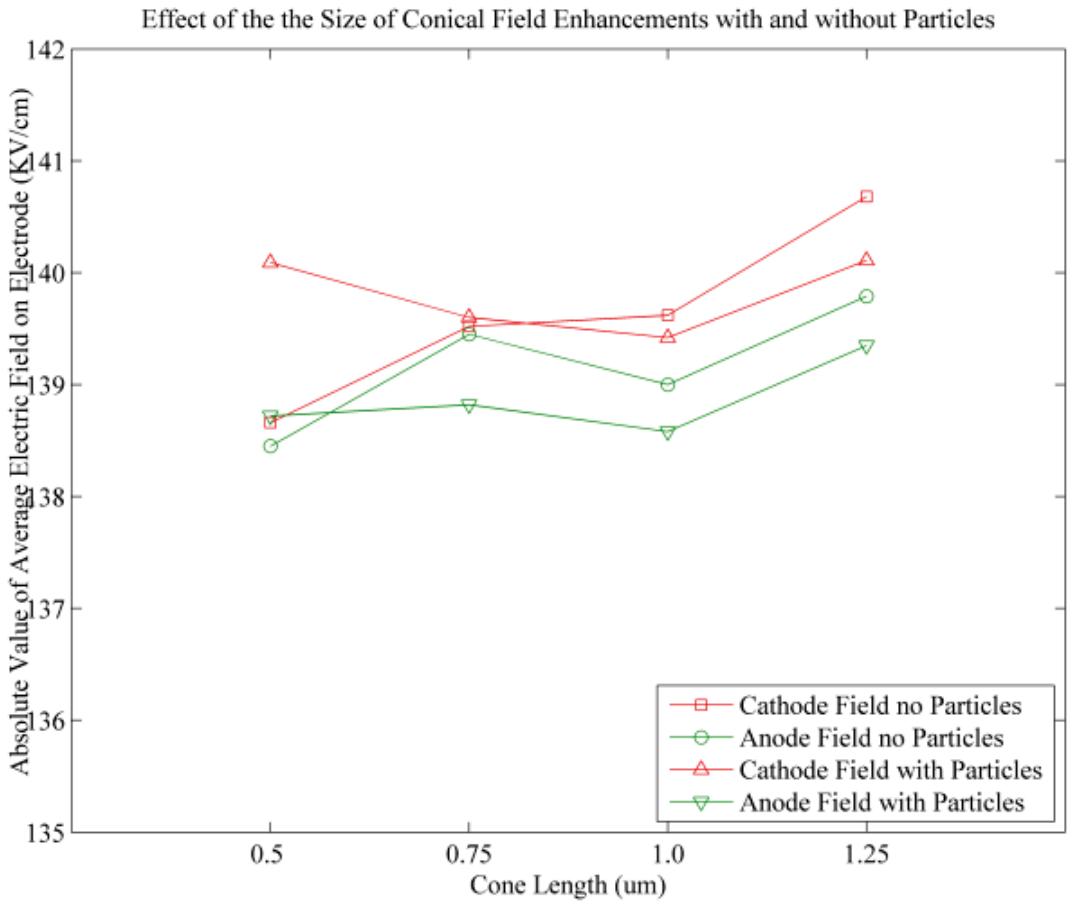

Figure 4.32: This graph shows that changing the length of the 10 cones has negligible effect on the average electrode field on the FT-surface with and without particles.

Figure 4.32 demonstrates that increasing the length of the cones does not significantly increase the average electrode field. The surface area of the cone tip is small and the locally generated enhancement has negligible impact on the average enhancement. Figure 4.33 shows that increasing the radii of the hemispheres enhances the average electric field. The larger the hemisphere, the more surface area of the FT-surface is affected by a spherical enhancement, increasing the average electric field. The effect of the local fields of the particles on FT-surface is negligible in both cases. Each simulation is the average of 3 simulations. The effect of changing radius of the spheres is much greater than the effect of the particles, so the standard deviation of the runs is negligible on the range of the axis. Averaging the simulations together diminishes the field-scattering effect the particles have on the FT-surface.

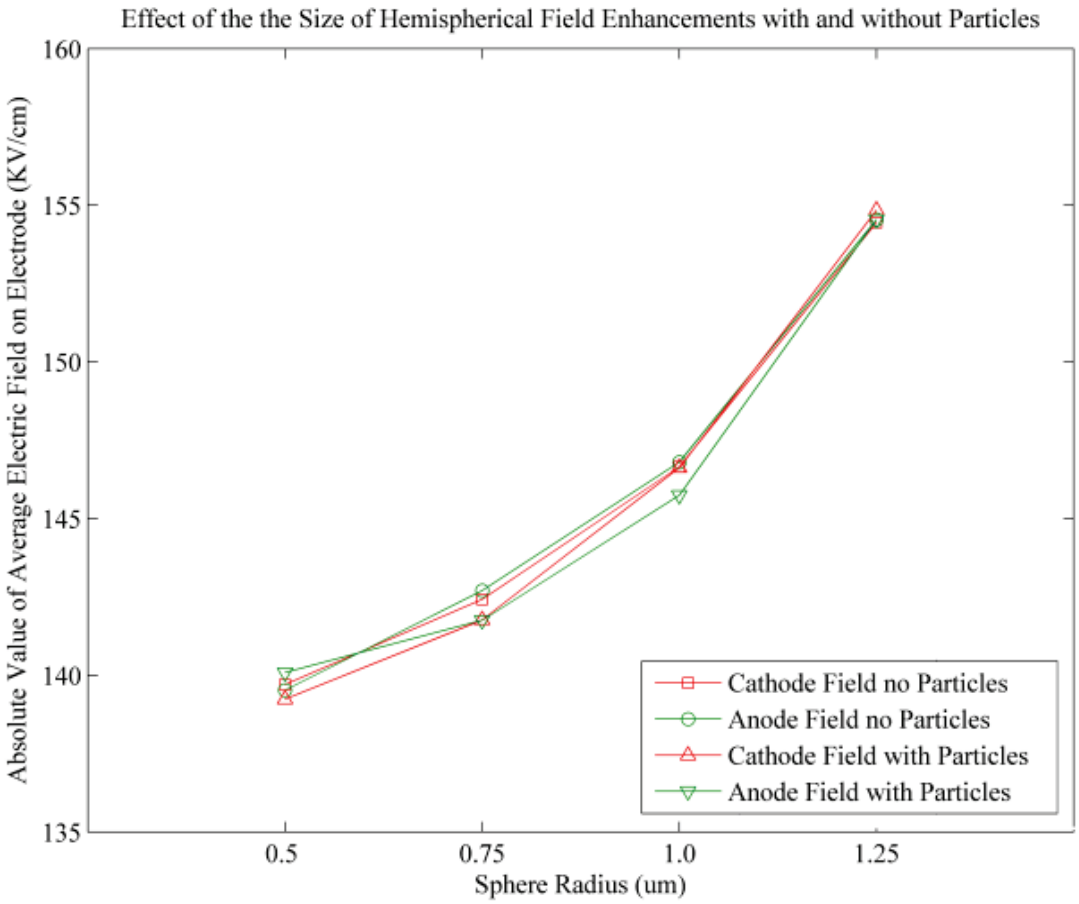

Figure 4.33: This image shows that changing the radius of the 10 hemispheres significantly increases the average electric field on the FT-surface with and without a particle concentration.

Another factor to consider is the top radius of the conical field enhancements. As the radius of the cone's tip decreases, the surface area of the cone tip decreases and the local field is enhanced. The results are shown in figure 4.34. The bottom radius and length are held at 1.0 and 0.5 µm while the top radius is simulated at 0.0, 0.2, 0.4, 0.6, 0.8, and 1.0 µm. The effect is simulated with 10 cones, with and without a 1% particle concentration. The effect of changing radius of the cones is much greater than the effect of the particles, so the standard deviation of the runs is negligible compared to the field range.

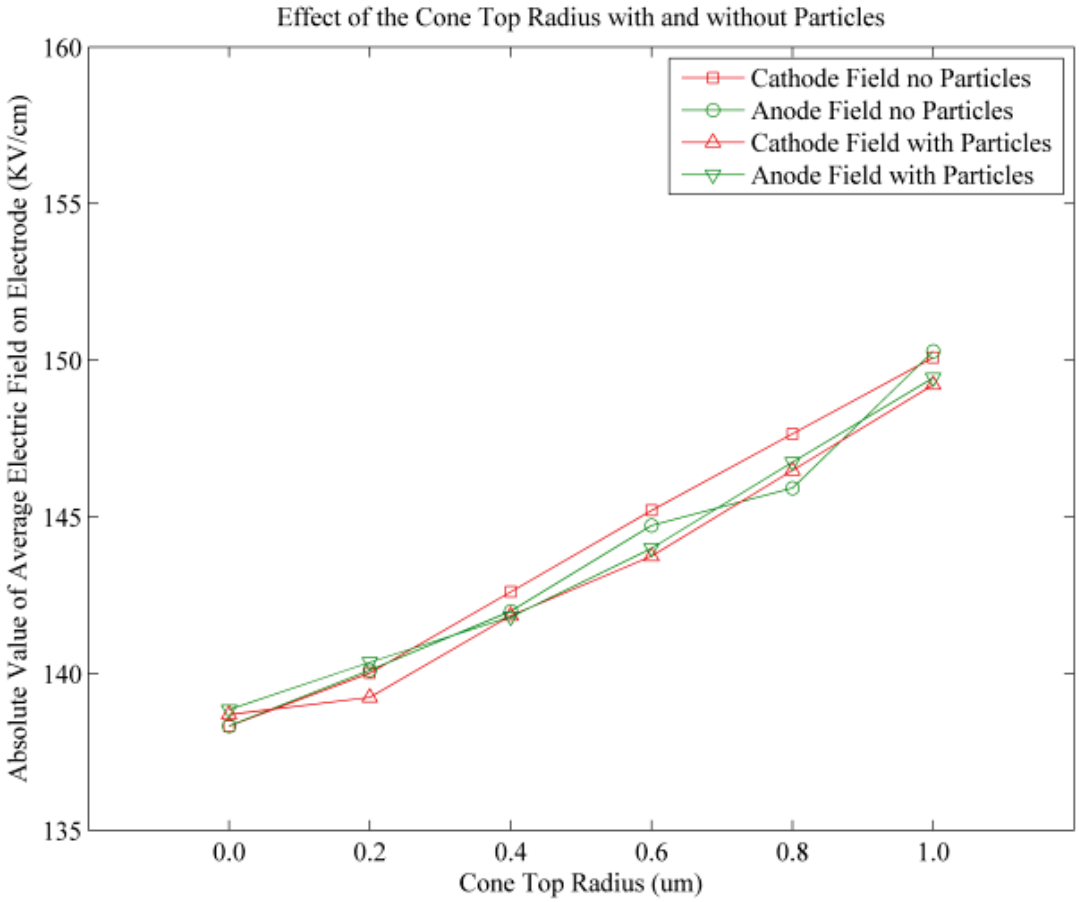

Figure 4.34: This image shows that changing the top radius of the 10 cone insertions significantly increases the average electric field on the FT-surface with and without particles. Similar to the results of figure 4.33, the larger the cones top radii, the more field enhancement surface area can contribute to the average field effect. At a top radius of 1 µm, the cone is a cylinder.

The previous sections demonstrate that increasing the concentration of high-k particles increases the fields on the electrode surface. Figure 4.35 indicates that the particle concentration has a negligible effect on the field-transparent surface. Ten randomly inserted cones and hemispheres are simulated with particle concentrations of 0.0, 0.5, 1, 2, 3, and 4% by volume. These concentrations translate to particle counts of 0, 123, 245, 491, 736, and 982, respectively. The cones have a length of 0.5 µm and a bottom and top radius of 1 and 0.1 µm while the hemispheres have a 0.5 µm radius.

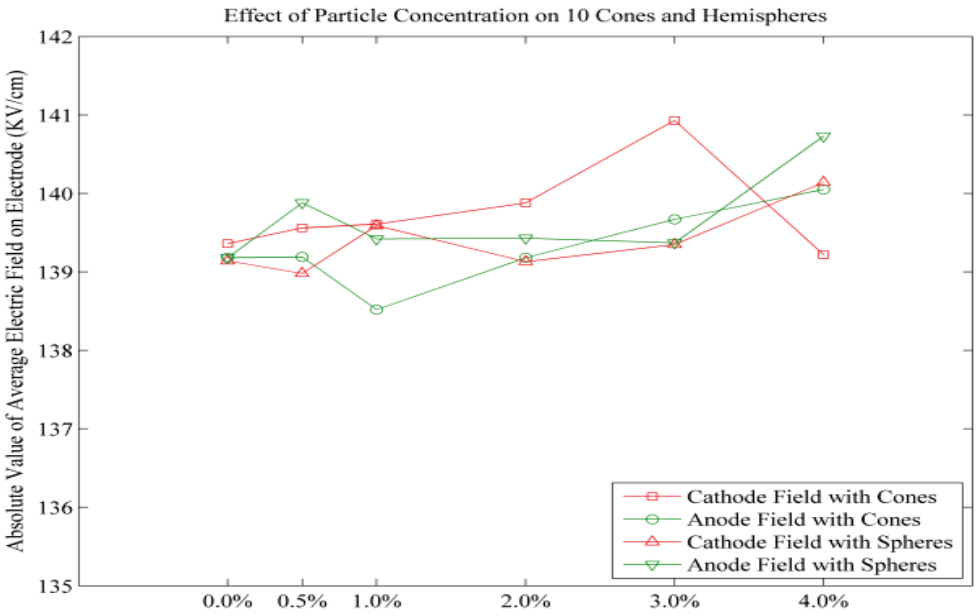

Figure 4.35: This image shows that changing the concentration of the particles has a slight impact on the average field acting on the FT-surface at particle concentrations above 0.0% with major fluctuations at and above 1%.

The disrupting effect of the particle concentration on the average FT-surface fields is a strong indicator of the field "smoothing" effect being investigated. Unlike our previous studies that demonstrated an increased average electric field on the electrode surface, the particles can exist on the FT-surface. It is well known that the electric fields within a high-K particle are negligible compared to the fields existing outside of the particle [23].

As the number of particles increases, there is a greater probability that a cross section of the particle will exist on the FT-surface. When the fields are averaged across the FT-surface, any particle that crosses the FT-surface will contribute negligible field values to the averaging calculation.

The previous sections indicate that a particle concentration increases the average field on the actual surface of the electrode in the presence of electrode field enhancements. In the simulations of figure 4.35, however, the increased enhancement is counteracted by particles existing on the FT-surface. This balance is a further example of how the particles and electrode field enhancements interact to "smooth" the fields on the electrode enhancements.

Previous sections indicate that increasing the size of high-K particles does not significantly affect the average electric field on the electrode surface [20, 24]. As the size of the particles increases with a constant volume concentration, there is a reduced number of inserted particles. For particle radii of 0.25, 0.3, 0.35, 0.4, 0.45, and 0.5 μm, the number of particles inserted are 245, 142, 89, 60, 45, and 31. The cones have a length of 0.5 μm and a bottom and top radius of 1 and 0.1 μm while the hemispheres have a 0.5 μm radius.

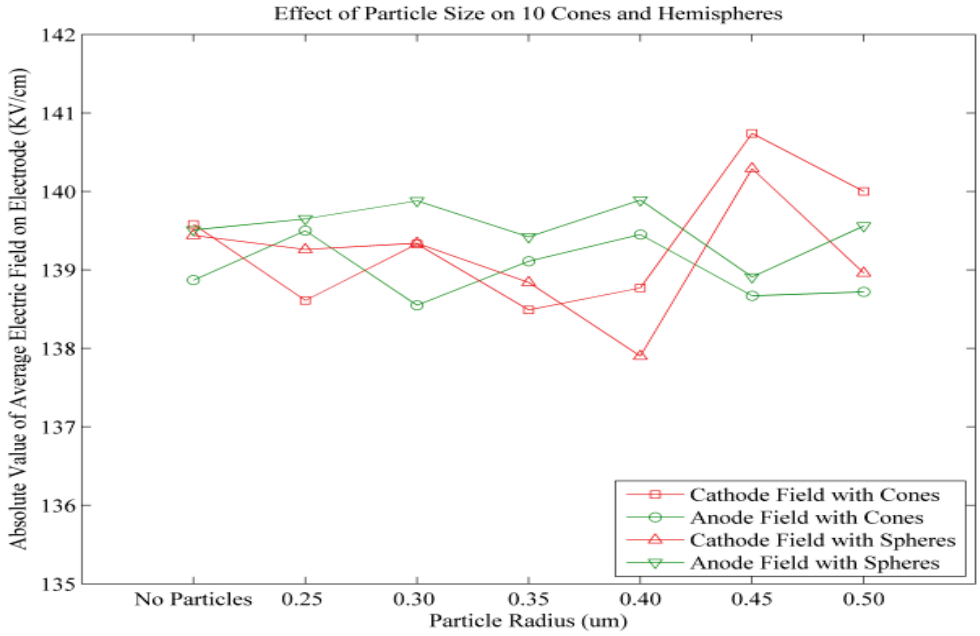

Figure 4.36: This image shows that changing the size of the particles has an impact on the average field acting on the FT-surface at larger particle radii. The field fluctuations are most apparent at particle radii at and above 0.30 μm.

The results of figure 4.36 once again indicate that the average field on the FT-surfaces is influenced by the presence of the particles. Both figures 4.35 and 4.36 show significant field disruptions due to the particles. The disruptions in the average FT-surface fields are caused by changes in local field maxima due to the presence of the high–K particles which, even when averaged over three simulations and random distributions, cause disruption of the average FT-surface fields indicating that the "smoothing" effect may be a plausible theory to explain the apparent jitter reduction in our oil spark gaps.

4.4 Maximum Fields on Electrode Surface Maxima

The simulations studying the interaction between the particles and the conical and hemispherical electrode enhancements on the average field on a FT-surface indicates that the particles "smooth" the electric field profile across the electrode surface, which would otherwise be localized solely on the tips of the electrode enhancements. The following section analyzes the maximum fields generated by different particle and electrode enhancement geometrical configurations.

Figures 4.37 through 4.41 show several of the simulation models used to demonstrate a particle's effect on the maximum electrode enhancement field. It is obvious from the results that the particle and electrode enhancements boost the maximum electric field on the electrode surface. The results of figure 4.40 indicate that this increase may be as high as 566.56% of the non-enhanced value.

The higher field significantly increases the chance that an electron will emit from that location and initiate a breakdown even. This effect is maximized when the particle is positioned directly above the electrode field enhancement. However, this is not always the case, as will be shown later in this section. The field enhancement effect can be scaled to any gap voltage and length by multiplying the field enhancements described below by a scale factor determined by the equation: $X_{scalar} = \frac{Volt\ (V)}{Distance(cm)} \cdot (\frac{1}{126000})$. The gap voltage and distance for the simulations is 100V and 8μm, respectively. One of the experimental setups utilized a voltage and gap spacing of 250 KV and 1.6 mm, respectively, generating a scalar of 12.4.

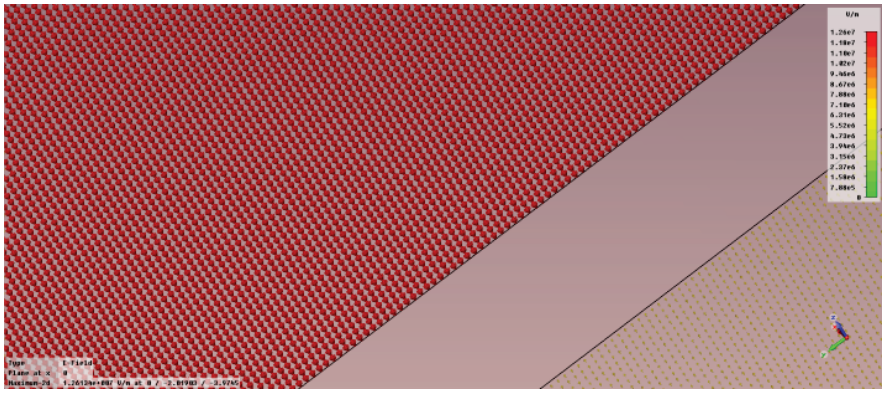

Figure 4.37: This image shows that without any particle or electrode field enhancements the maximum field on the smooth electrode surface is 126 KV/cm.

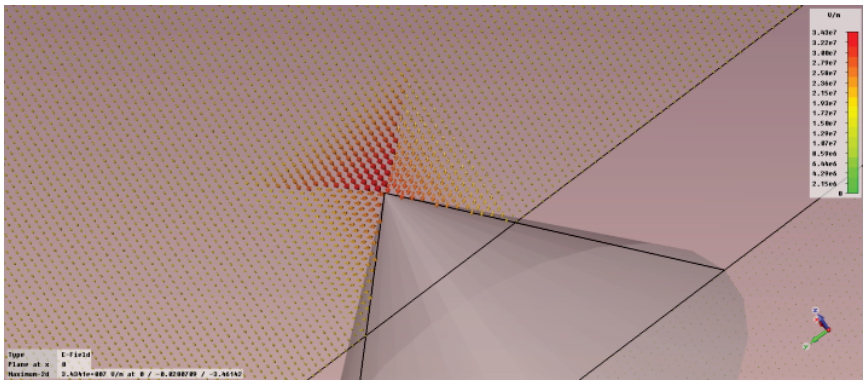

Figure 4.38: This image shows that the conical field enhancement on the electrode surface generates a maximum field of 361.11 KV/cm. This is an increase of 289% from the non-enhanced 125 KV/cm of figure 4.37**.**

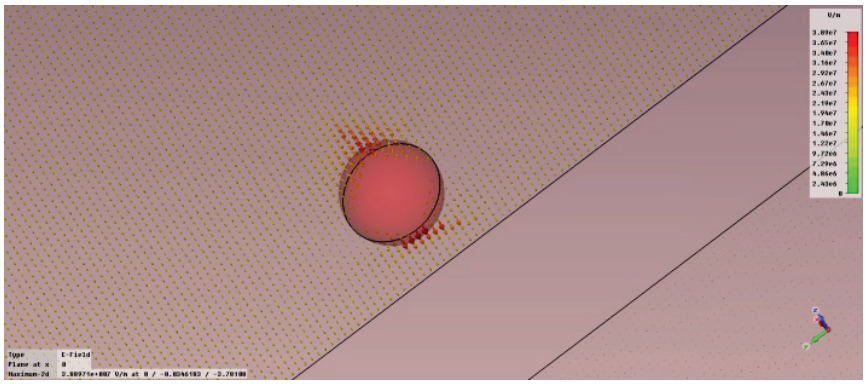

Figure 4.39: This image shows that a high-K particle near the electrode surface generates a maximum field on the surface of 451 KV/cm. This is a 25% increase from the 361.11 KV/cm results of figure 4.38.

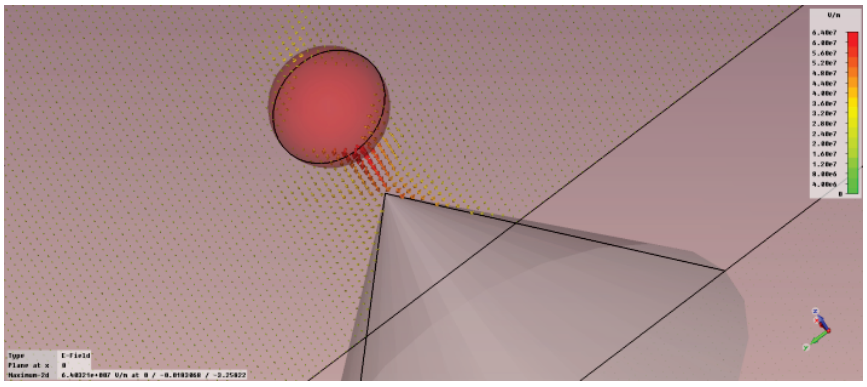

Figure 4.40: This image shows that the presence of a particle near the tip of an electrode field enhancement generates a maximum field of 708.2 KV/cm. This is an increase of 57% from the results of figure 4.39.

It is apparent from the results of figures 4.38 through 4.41 that a polarized particle with a radius of 0.25 μm generates a greater field maximum on the electrode surface than the cone with a bottom and top radius of 1 and 0 μm. However, the interaction between both of the enhancements generates the greatest field enhancement of 566.56% compared to no enhancement at all. Figure 4.41 depicts a simulation where the particle is located in the space between two hemispherical electrode enhancements.

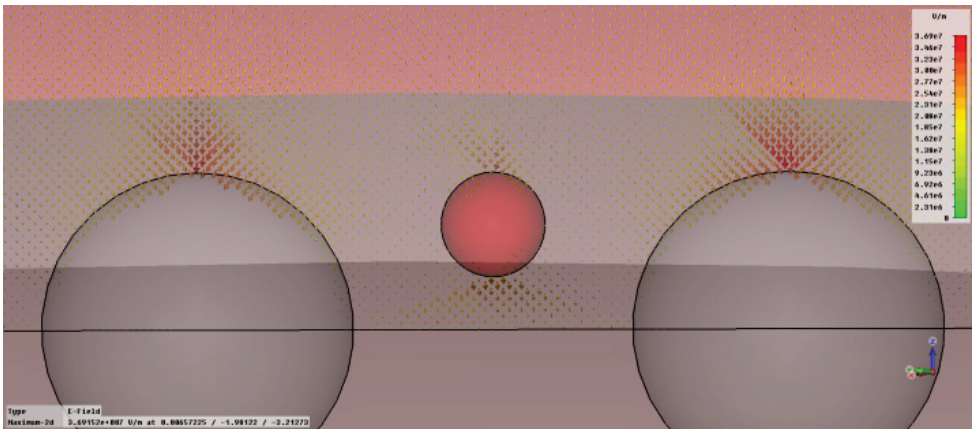

Figure 4.41: This image shows that the presence of a particle in the trough between two electrode enhancements is capable of generating fields on the surface of the electrode comparable to the fields generated by the electrode enhancements.

Figure 4.41 is a key example of the "smoothing" effect the particles have on a rough electrode surface. The field at the tip of the hemispherical enhancements is 347 KV/cm, which is 275% of the 126 KV/cm field found in the trough between the enhancements with no particles present. The particle generates a field of 284.13 KV/cm on the electrode surface, which is 81.88% of the field at the tip of the electrode. The probability that a breakdown event is initiated on the tip of the electrode enhancement is reduced by the presence of the particle.

The remainder of this section covers variations regarding the electrode and particle geometrical arrangements seen in figures 4.42 and 4.43. The type and size of the field enhancements are changed and the maximum field values on the electrode surface are reported.

In these simulations the maximum fields are reported while varying the size of conical and hemispherical field enhancements. The simulations are performed with and without the presence of a particle with a 0.25 μm radius. The edge of the particle is located 0.10 μm from the

enhancement. Figure 4.42 shows the conical and hemispherical simulation results. The enhancement positions are fixed and there are no random insertions, each value is the average of three separate simulations. All simulations are performed on the anode electrode. The maximum field with no field enhancements is 126 KV/cm.

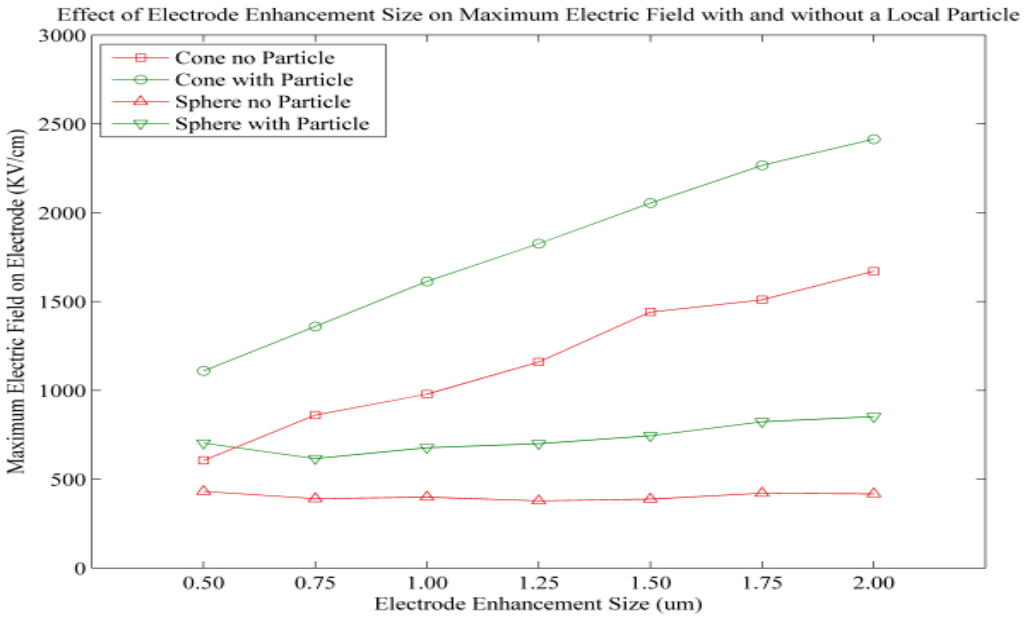

Figure 4.42: This graph demonstrates that increasing the length of the conical enhancement increases the maximum electric field while increasing the hemisphere size does not significantly change the maximum field. The presence of the particle increases the maximum field in both cases. The standard deviation is negligible due to the range of the field axis.

It is well known that the radius of curvature of an electrode enhancement influences the electron emission characteristics [25]. The radius of curvature of an electron emitter is proportional to the fields on the surface of the emitter. An electrode enhancement, such as a cone, has a small radius of curvature, while a sphere has a larger radius of curvature. The results from figure 4.42 indicate, as expected, that increasing the length of the conical enhancement decreases the radius of curvature thus increasing the maximum field at the tip. The hemispherical enhancement, as it increases in size, has a marked decrease in its radius of curvature.

The radius of curvature of a cone is proportional with the angle between its base and side if the ratio between the top and bottom cone radii remains constant. However, as the length of the cone increases, the angle between the bottom and side of the cone increases at a decaying rate.

As such, the rate of increase of the maximum field of conical enhancement results of figure 4.42 should decay with increasing length. However, there is no apparent reduction in the rate of increase of the maximum field. This is because as the cone length increases, the distance between the anode cone tip and the flat cathode electrode is reduced. The decrease of the gap spacing serves to increase the field between the electrodes and counteract the standard rate decay generated by the decreasing rate of radius of curvature with increasing cone length.

The same gap-narrowing effect can be seen with the hemispherical data of figure 4.42. As the radius of the hemisphere increases, there is decay in the radius of curvature. This effect should produce lower field values with increasing hemisphere size, but the gap narrowing prevents this effect from being observed in the simulations.

Figure 4.43 shows the results of the same simulation conditions with the simulated gap widened from 8 μm to 80 μm, the potential on the anode is changed from 100 to 1000V to maintain the same field values. The figure shows that there is a decrease of the rate of increase of the maximum field at larger cone lengths and a decrease in the electric field with increasing sphere radius as the effect of the gap-narrowing is less pronounced at the widened gap. This indicates that the gap is increased, the effect of the field enhancements is less apparent.

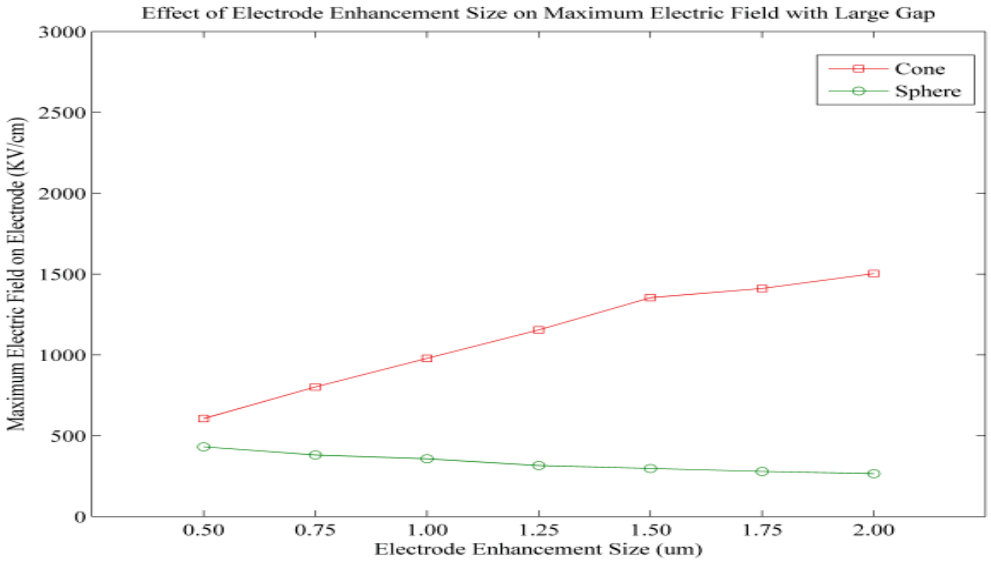

Figure 4.43: The graph shows the maximum fields on the cones and hemispheres with a larger gap. The effect of the gap-narrowing is significantly less pronounced compared to figure 4.42. No particles are inserted.

4.5 Maximum Fields on Electrode Surface Minima

Simulations have been conducted to investigate the theory that the particles have a "smoothing" effect on the electrode surface. It is thought that particles generate field enhancements on electrode surfaces in the depressions between electrode maxima as in figure 4.41. The results from figure 4.44 indicate that the average electric field on the electrode surface minima, or any surface not covered by a field enhancement, increases with increasing particle concentration. The FT-surface is located directly on the surface of the electrode. The FT-surface does not cover the electrode enhancements as this simulation serves to measure the average field increase on the electrode minima.

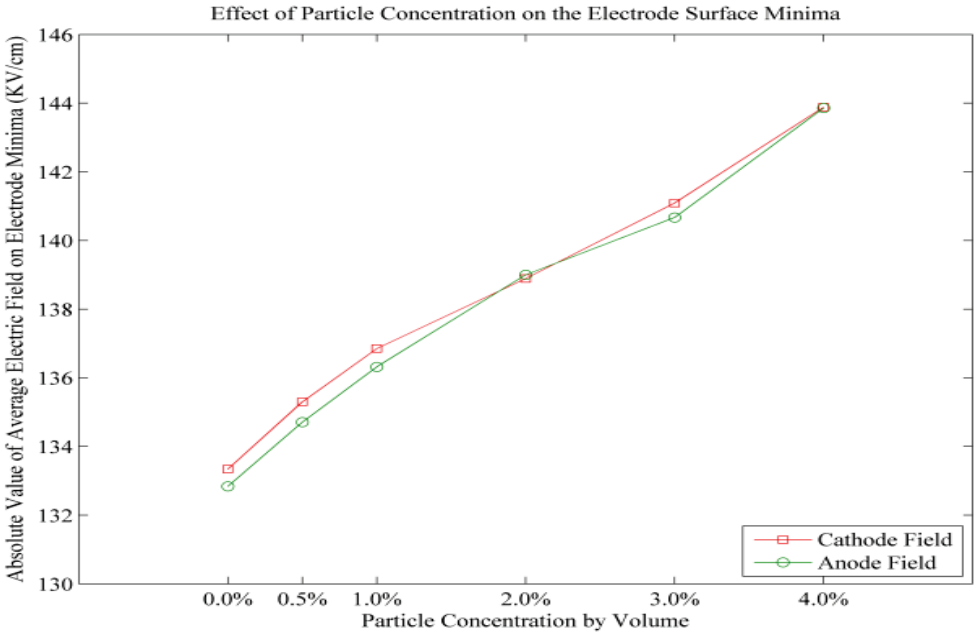

Figure 4.44: This graph shows an increase of the average electric on the electrode surface minima with increasing particle concentration. The electrode surface minima are any part of the surface that is not covered by a field enhancement.

Figure 4.44 is a simulation depicting the effect of the particles enhancement on the electrode surface minima. The result supports the theory that the particles can increase the fields on the surface minima increasing the probability that a breakdown will originate from the site; increasing the number of sites of probable breakdowns across the electrode surface.

References

[20] C. Yeckel and R. Curry, "Electrostatic field simulation study of nanoparticles suspended in synthetic insulating oil*," IEEE Transactions on Plasma Science*, June, 2010.

[21] CST Computer Simulation Technology. 2009. *CST EM STUDIO*. Framingham, MA: CST Computer Simulation Technology AG.

[22] P. Norgard, R. Curry and R. Sears, "PAO synthetic oil: a new paradigm in repetitive high-pressure oil switches," *IEEE Transactions on Plasma Science*, Vol. 34, No. 5, October, 2006.

[23] C. Balanis, *Advanced Engineering Electromagnetics*, John Wiley and Sons, NJ, 1989.

[24] C. Yeckel and R. Curry, "Field enhancement simulation study of a nanoparticle-infused dielectric oil with roughened electrodes," *18th International Pulsed Power Conference*, 2011.

[25] R. Del Vecchio, "Geometric effects in the electrical breakdown of transformer oil," *IEEE Transactions on Power Delivery*, April, 2004.

CHAPTER 5

OPTICAL PROFILOMETRY OF ELECTRODE SURFACE

As demonstrated by the simulations in the previous section, deformations on the surface of an electrode generate localized electric field enhancements that allow electrons to emit at lower applied voltages. The emission of electrons at lower voltages is suspected to be a contributor to poor jitter performance. The size of the deformations is proportional to the amount of energy discharged during the breakdown event. The deformations are generated during normal operation of the switch system. This section reports images generated by an optical profilometer utilized to scan the surface of both smooth and deformed electrode surfaces. The electrode material is 17-4PH stainless steel that has been precipitation hardened to C38 Rockwell hardness.

Figure 5.1: The two electrode surfaces utilized in the experimental analysis are the rough and smooth surfaces pictured. The rough surface (left) is generated with the use of sand-blasting and the smooth surface (right) is generated with 1200-grit sandpaper.

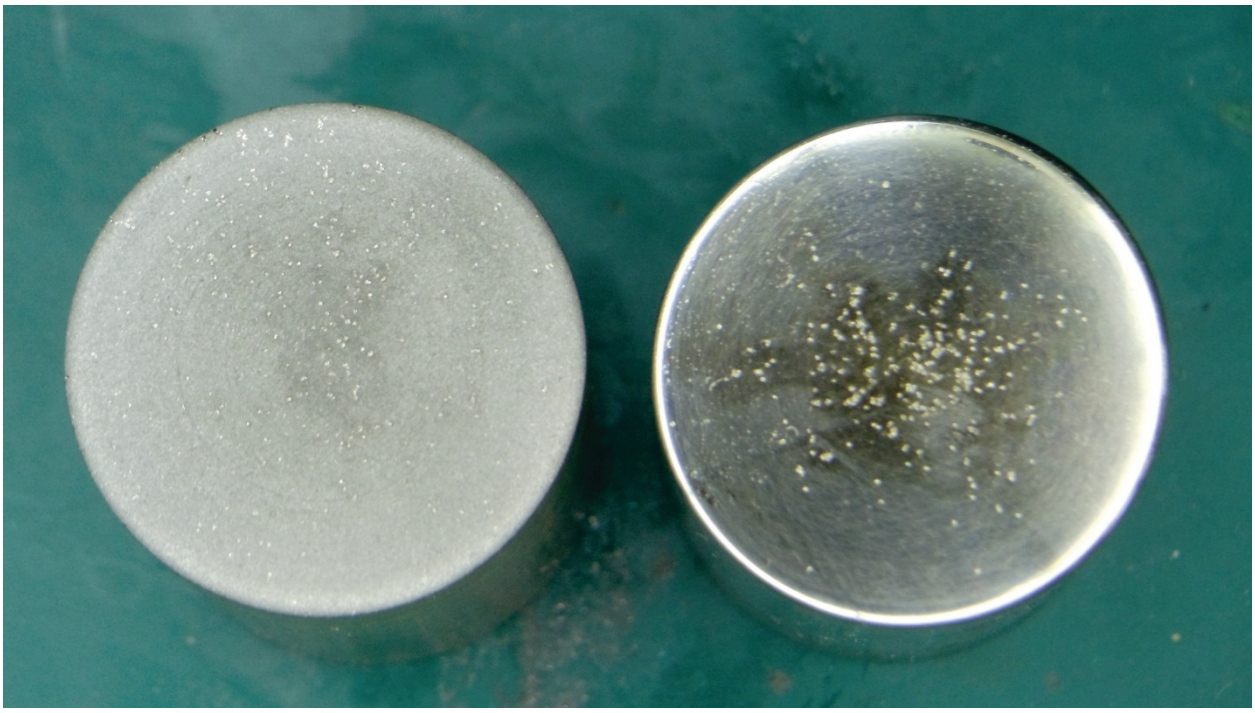

Figure 5.2: After 230 breakdowns, the rough and smooth electrode surfaces are pitted by breakdown arcs. The carbon on the surface is also a byproduct of the breakdown discharge.

Figure 5.2 is a photograph of the rough and smooth electrode surface after being subjected to 230 breakdowns in the HVADTS system. Figure 5.3 is the rough electrode after an acetone cleaning procedure removes all traces of carbon and other ion impurity layers. These cleaned surfaces are scanned with the optical profilometer to produce the images and graphs of figures 5.4 through 5.13. The optical profilometer hardware and software was developed by the Veeco Corporation [26]. The optical profilometer is useful in determining the width and depth of the breakdown deformations and the roughness factor, Ra, of the smooth and rough electrode surfaces.

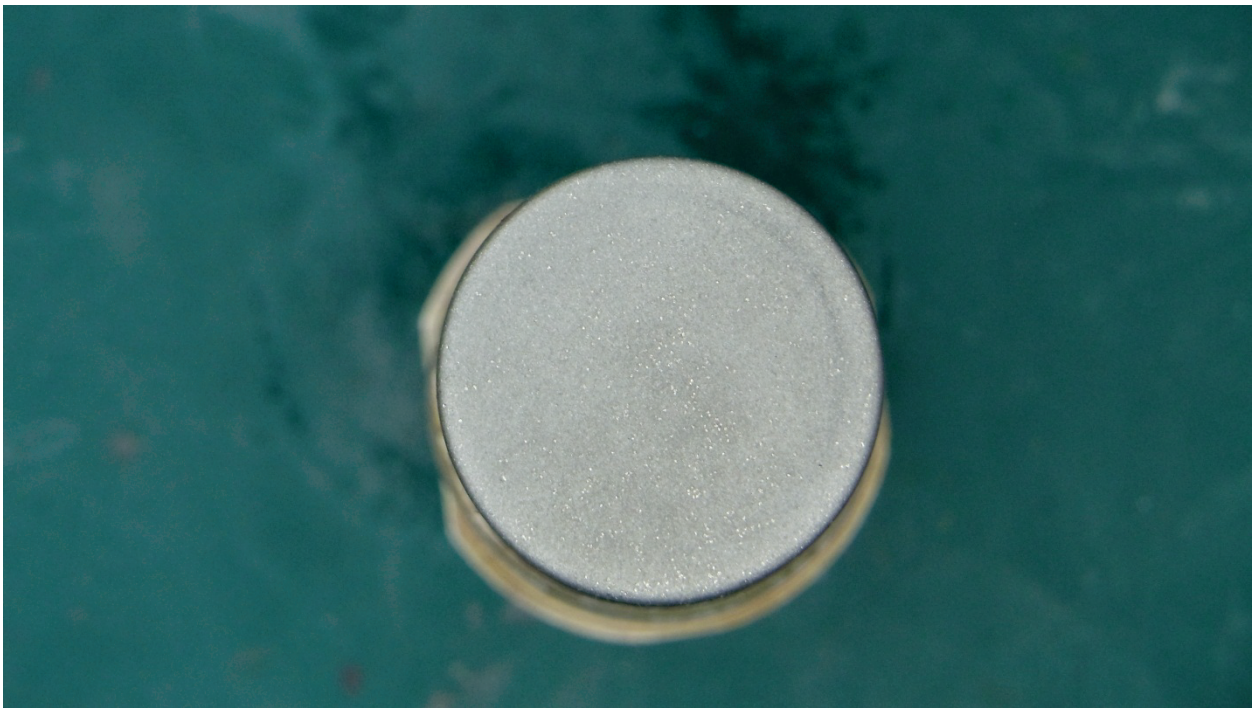

Figure 5.3: The rough electrode shows no trace of carbon after the acetone cleaning procedure. The electrode is ready to be reinstalled in the HVADTS system.

5.1 Smooth Electrode Surface Profilometry

The optical profilometer utilized in obtaining the results of figures 5.4 through 5.13 is a white-light interferometer developed by Veeco Inc. This device splits an optical beam and reflects it off of the surface of the electrode back into a lens. A computer then processes the scanned data and displays a digitized representation of the surface. The splitting of the beam is an efficient way for the optical profilometer to minimalize obstruction and errors in the data. During this process, fringes are created as a result of the overlapping of the two beams which is also an indicator that the optic lens is in focus with the sample surface. Once in focus, the image is ready to be scanned and then analyzed. To read the variations in the surface, the interferometer adjusts the focus automatically. As the focus changes throughout the sample it reads the heights of the peaks and the depths of the pits in the area of the sample and generates a surface profile.

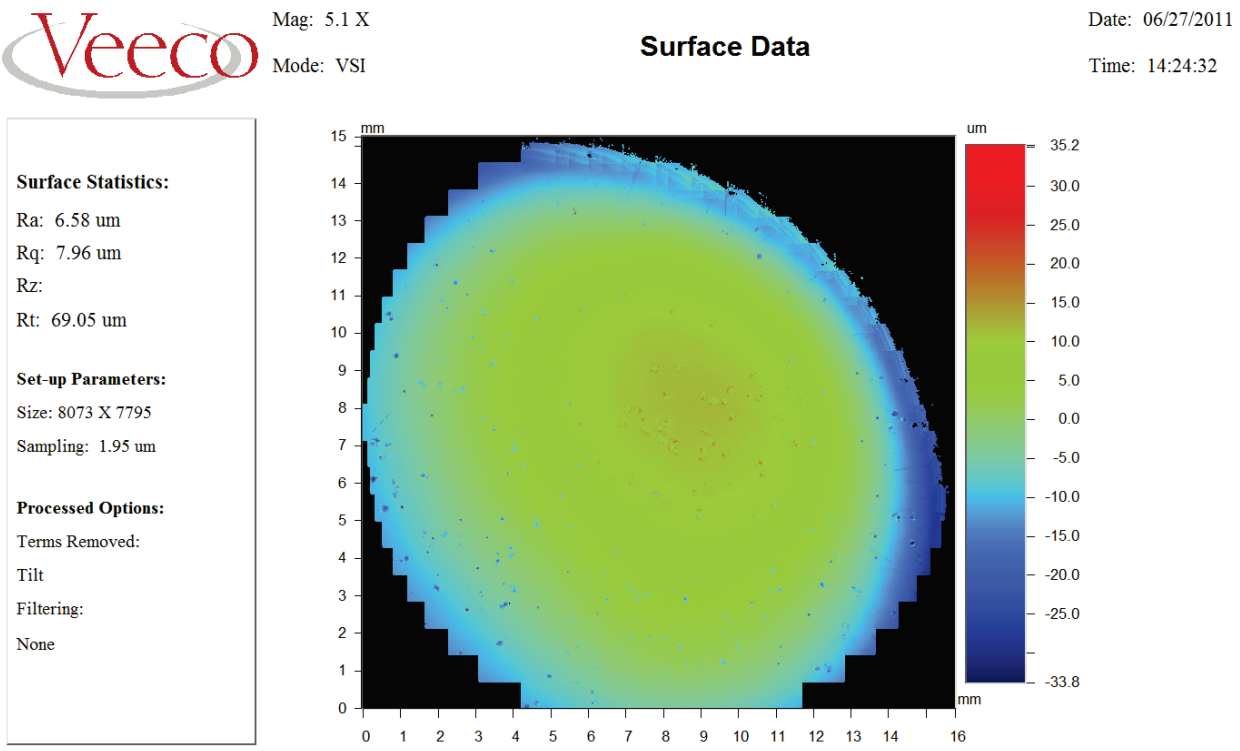

Figure 5.4: The result of an optical profilometer from the smooth surface of figure 5.1 indicates the pits generated by the breakdown arcs and also a rounding effect generated by the polishing procedure.

Figure 5.4 indicates that the figure-8 method of polishing the electrode surface generates a Rogowski profile on the electrode surface. It appears that the near-planar profile does not affect the breakdown locations significantly, as the breakdown deformation scatter is random across the electrode surface. The height differential between the edge and the center of the electrode is nearly 60 µm. As the electrode matches a Rogowski profile, the fields between the two electrodes can still be considered uniform. The results indicate an average deformation depth of 19 µm on the smooth electrode surface.

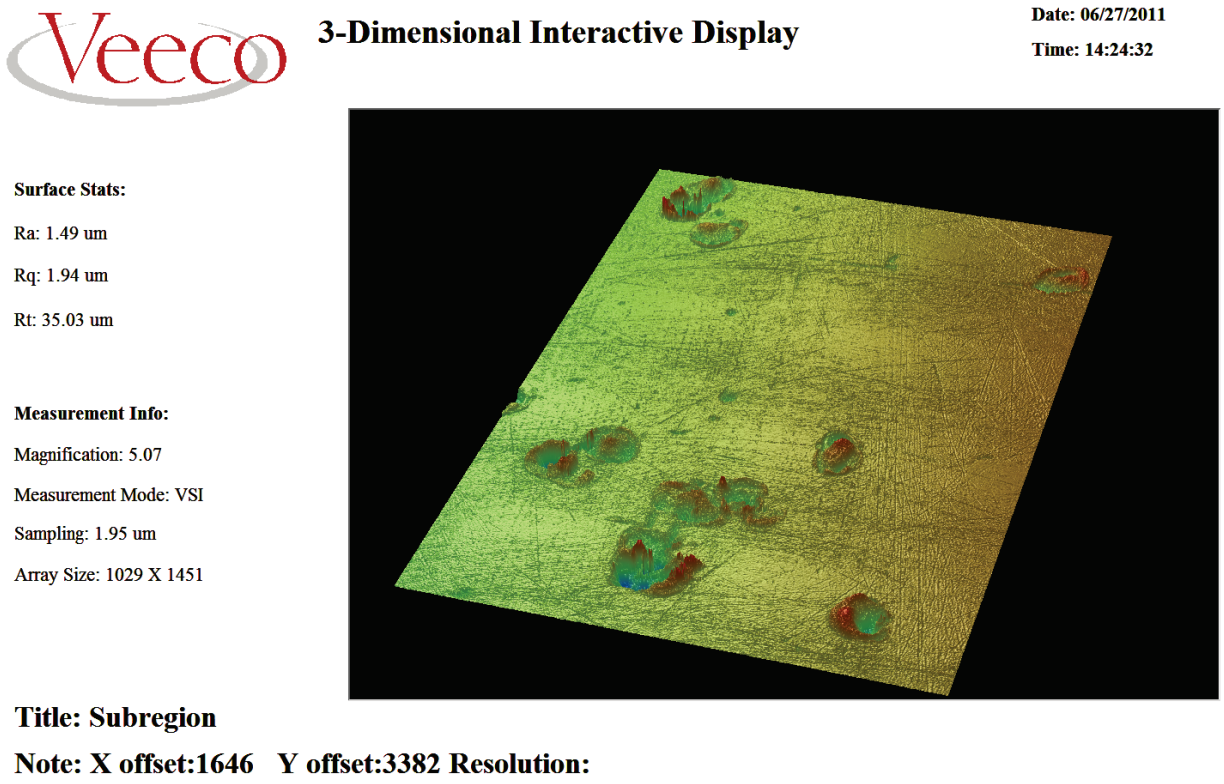

Figure 5.5: A subregion of the results from figure 5.4 indicates a surface roughness factor, Ra, of 1.49 µm. The arc pits are easily discernable.

Figure 5.5 clearly shows a 3D profile of several breakdown deformations at 5X magnification. The breakdowns appear to be clustered, indicating that there is a high probability that subsequent breakdowns occur near a previous breakdown site. The experimental data suggests that a smooth electrode surface produces higher rates of jitter than a rough electrode surface. On a smooth electrode surface, a breakdown event can occur on either a smooth or deformed section of the electrode. If the breakdown occurs on a smooth section, the electrons require a higher voltage to emit due to limited enhancement in that area. If the breakdown occurs on a rough section (previous breakdown cluster) of the smooth electrode, the electrons would not require as much voltage to emit due to field enhancement; and the breakdown can occur at a lower voltage. This combination of high and low breakdowns over a 100-shot test cycle on a smooth electrode surface, results in higher rates of jitter.

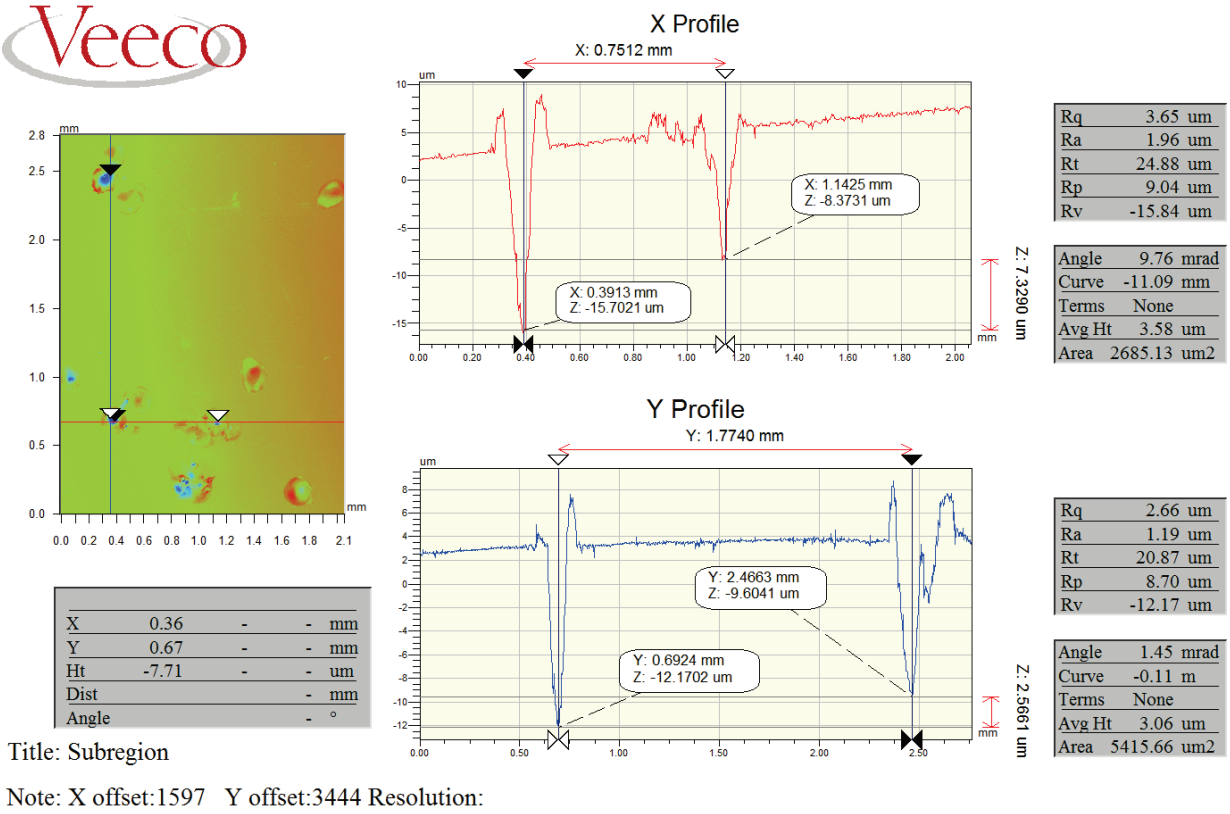

Figure 5.6: Analysis of two pits from the surface of figure 5.5 indicates an average pit width and depth of 100 and 18 µm, respectively. The field enhancements on the edges of the pit are apparent.

On a rough electrode surface no smooth surfaces exist, so there is negligible probability that a breakdown will initiate on a smooth surface. As such, the breakdown must initiate on an enhancement. This theory is supported by the experimental data which indicates a lower mean breakdown and jitter for rough electrodes compared to smooth electrodes. This is possibly the reason we are seeing lower jitter with the rough electrodes.

It is apparent from profilometer results that the deformations of the smooth electrode surface have a smaller diameter and more depth than the deformations on the rough electrode surface. Figures 5.6 and 5.8 indicate that the average depth of the deformations on the smooth electrode surface is approximately 19 µm. Figures 5.11 and 5.13 indicate that the average depth of the deformations on the rough electrode surface is approximately 14 µm. The magnitude of the protrusion depth is directly proportional to the height of the protrusions on the edges of the

deformation as demonstrated by figures 5.6, 5.8, 5.11 and 5.13. The enhanced radius of curvature of the protrusions on the smooth electrode surface is possibly contributing to higher jitter rates.

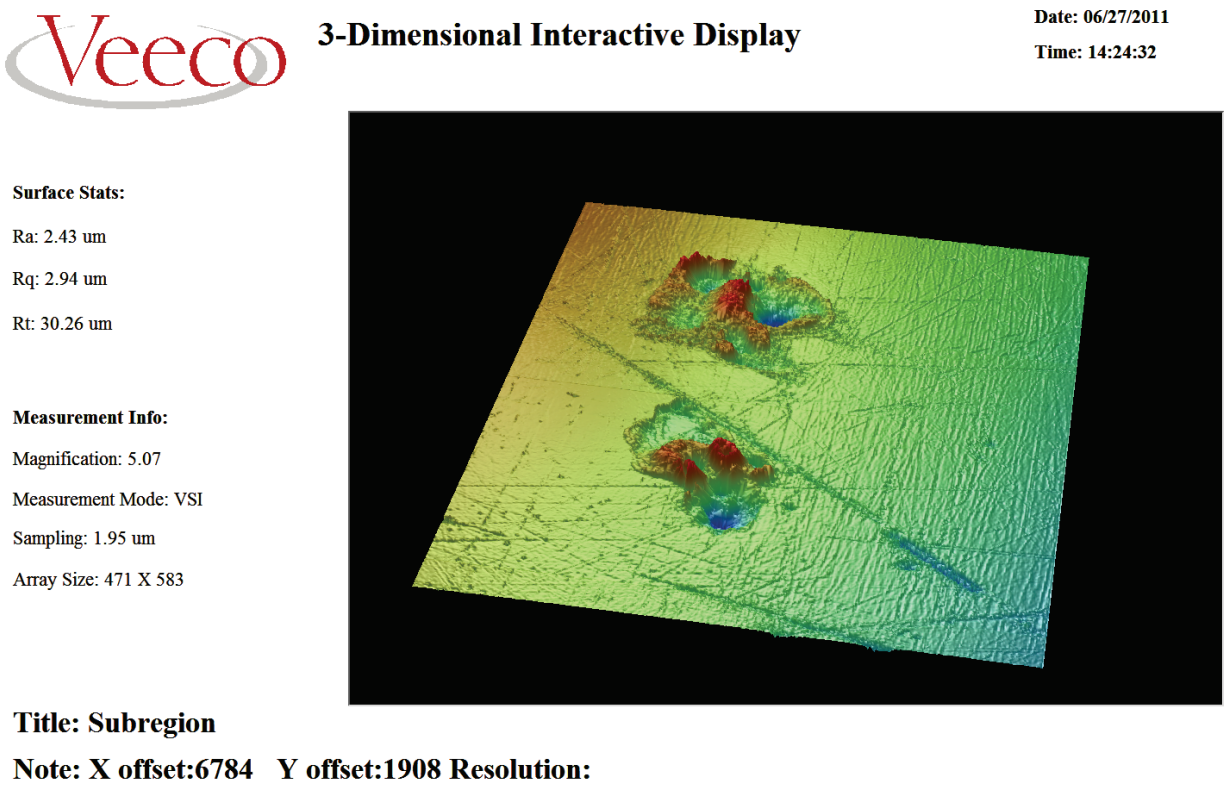

Figure 5.7: A second subregion of the results from figure 5.4 indicates a surface roughness factor, Ra, of 2.43 µm. The arc pits are easily discernable. The scratch through the center of the sample is a result of the polishing procedure.

Figures 5.6 and 5.8 indicate that the average diameter of the deformations on the smooth electrode surface is approximately 100 µm. Figures 5.8 and 5.11 indicate that the average diameter of the deformations on the rough electrode surface is approximately 150 µm. Like the depth of the deformations, the figures indicate that the larger the diameter the lower the radius of curvature of the field enhancement on the edge.

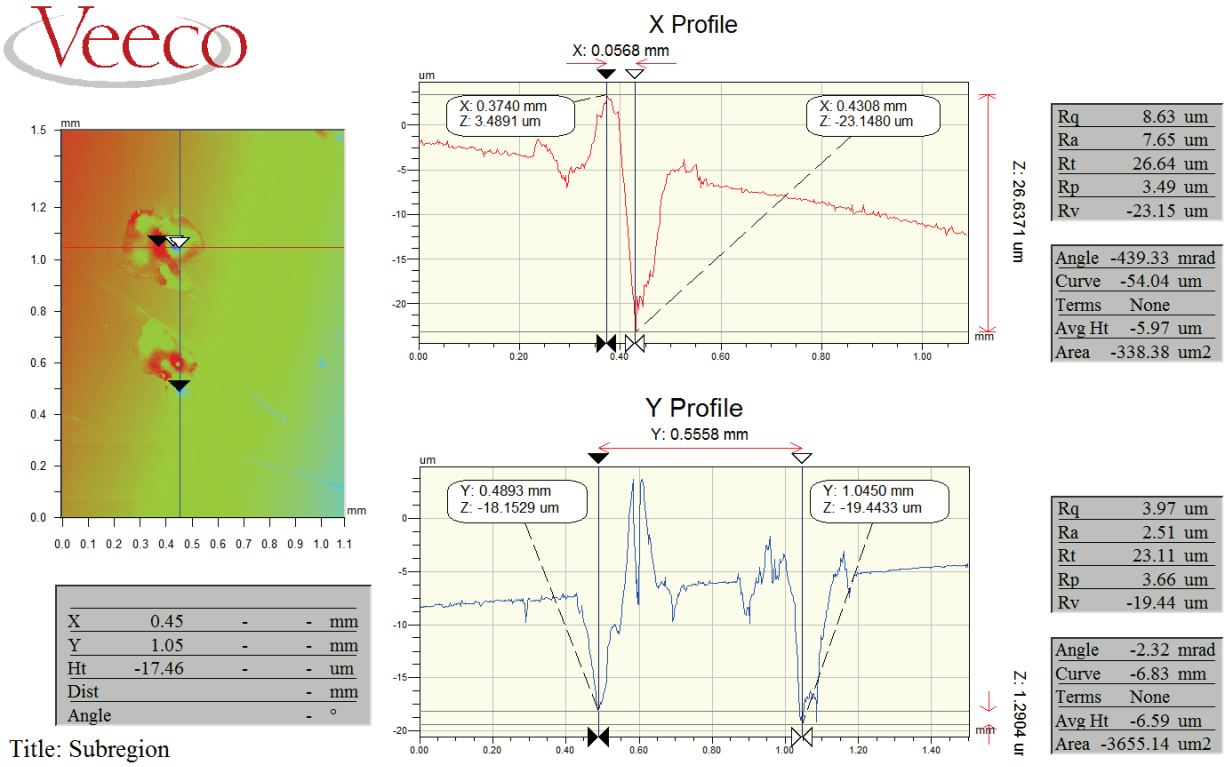

Figure 5.8: Analysis of two pits from the surface of figure 5.7 indicates an average pit width and depth of 100 and 20 µm, respectively.

5.2 Rough Electrode Surface Profilometry

Figures 5.5, 5.7, 5.10 and 5.12 are good indications of the surface roughness factor, Ra, for the smooth and rough electrode surfaces. Surface roughness, Ra, is the arithmetic average of absolute values of the height and depth of the surface: A higher relative value indicates a greater average distance from zero, and a rougher surface. Figures 5.5 and 5.7 indicate that the smooth electrode surface has an approximate surface roughness of 1.96. Figures 5.10 and 5.12 indicate that the rough electrode surface has twice the approximate surface roughness at 4.13. The results indicate an average deformation depth of 13 µm on the rough electrode surface.

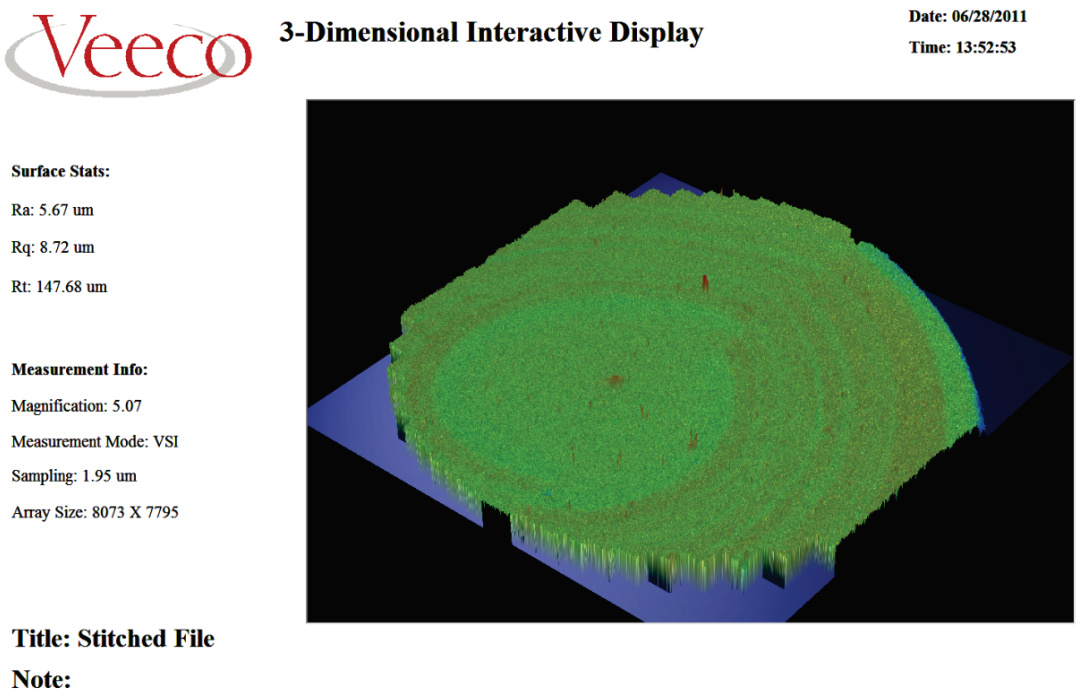

Figure 5.9: The result of an optical profilometer from the rough surface of figure 5.3 indicates that the sand-blasting procedure generates circular surface roughness stratification.

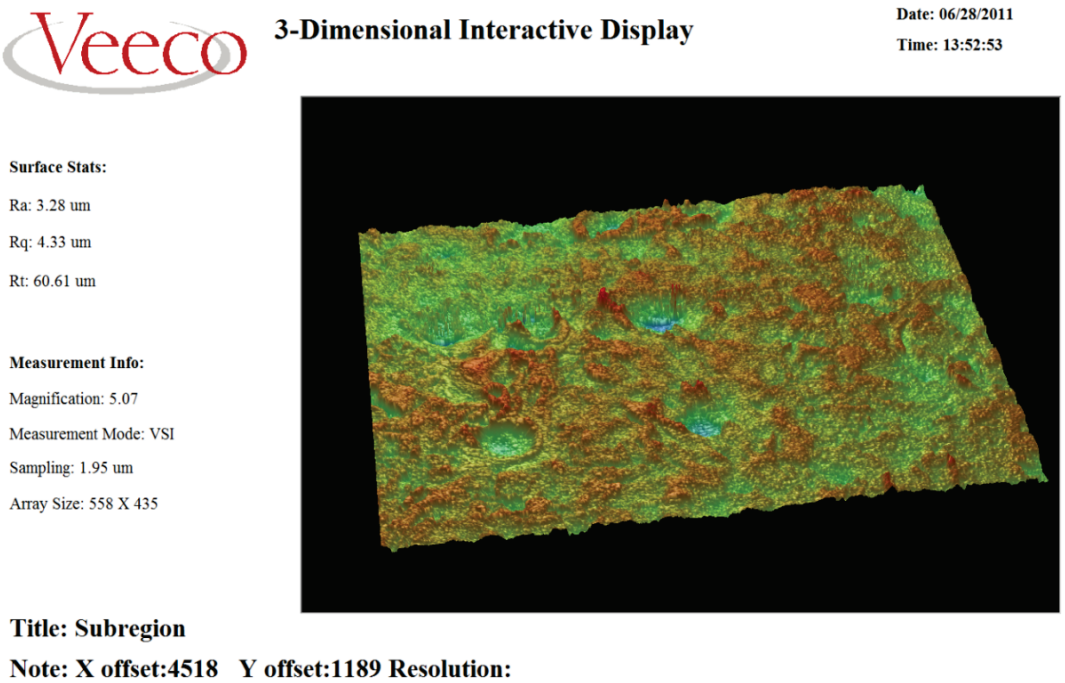

Figure 5.10: A subregion of the results from figure 5.9 indicates a surface roughness factor, Ra, of 3.28 μm. The arc pits are less easily discernable than those of the smooth electrode surface.

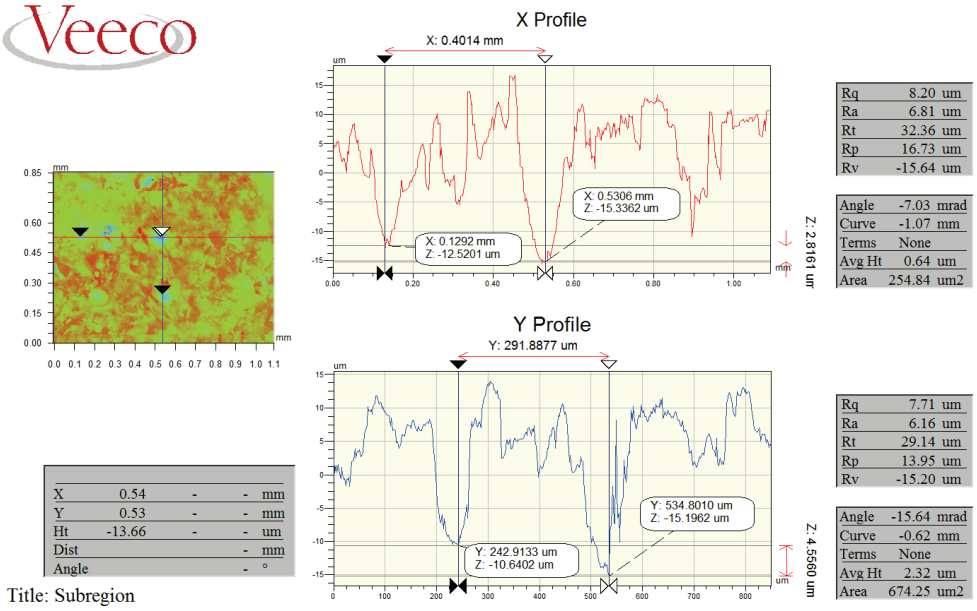

Figure 5.11: Analysis of two pits from the surface of figure 5.10 indicates an average pit width and depth of 150 and 13 µm, respectively. The field enhancements on the edges of the pit are difficult to discern from the roughness generated by the sand-blasting procedure.

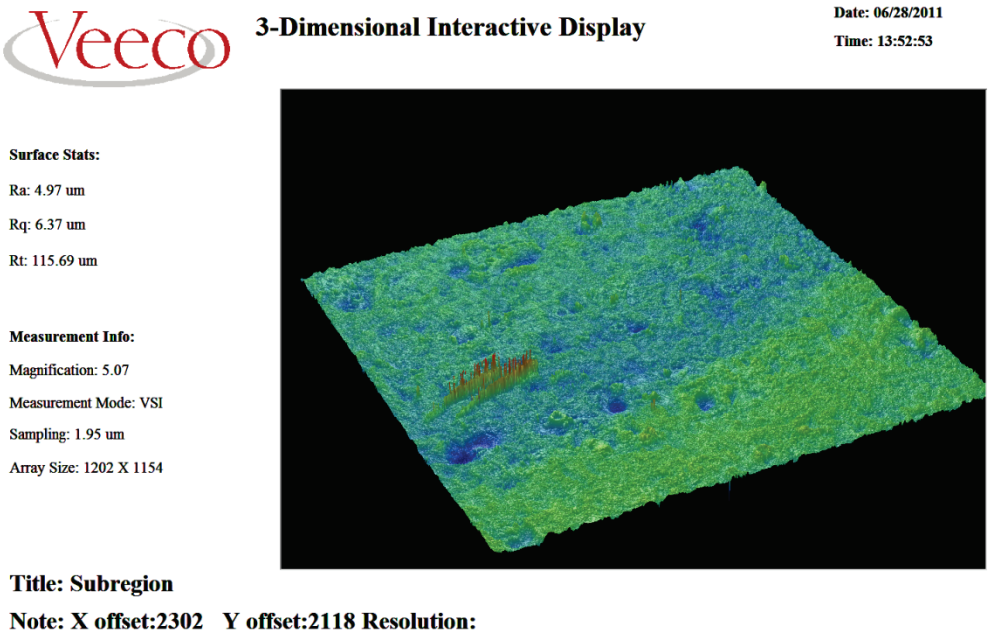

Figure 5.12: A second subregion of the results from figure 5.9 indicates a surface roughness factor, Ra, of 4.97 µm The arc pits are less easily discernable than those of the smooth electrode surface. The strange field enhancement located in the lower-left center is an artifact of the optical profilometer scanning method and does not exist.

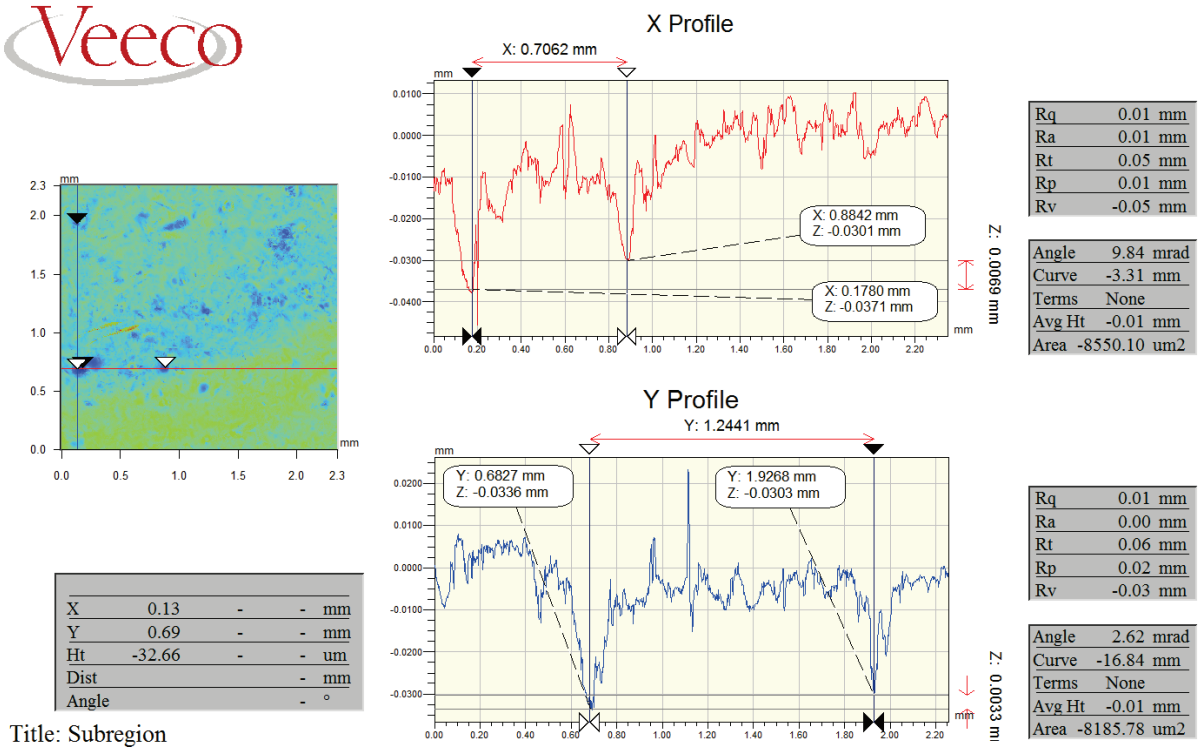

Figure 5.13: Analysis of two pits from the surface of figure 5.12 indicates an average pit width and depth of 150 and 15 µm, respectively. The field enhancements on the edges of the pit are difficult to discern from the roughness generated by the sand-blasting procedure.

The results of the optical profilometer scan demonstrate that the deformations on the electrode surface produced by breakdown events generate greater field enhancement on the smooth surface than the rough surface. The edges of the deformation on the smooth electrode surface have greater radius of curvature than similar deformations on the rough electrode surface. This suggests that the higher rates of jitter demonstrated by the smooth electrode surface are the result of these sharper features.

On the smooth electrode surface, breakdowns can initiate on the tip of a deformation protrusion or on a smooth section. On a rough electrode surface, breakdowns can initiate only on a deformation protrusion. This suggests that the lower jitter demonstrated by the rough electrode is possibly a result of a more uniform field distribution. A suspension of high-K particles further levels the electric field profile, limiting the extreme breakdown values that contribute to switch jitter.

References

[26] Veeco Corporation, Optical Profilometer Hardware and Software, 2011.

CHAPTER 6

HVADTS SYSTEM CHARACTERISTICS

All the experimental breakdown test data in this report is obtained from the MU High Voltage Advanced Dielectric Test Stand (HVADTS). The HVADTS is a single shot system capable of generating a 250-kV voltage pulse across a liquid with a rise-time of 1.6-µs. A photograph of the test stand is shown in Figure 6.1. Figure 6.2 provides a schematic diagram of the core elements of the pulse generator.

Figure 6.1: The HVADTS system is composed of a Marx Generator which drives a CLC circuit. The load consists of an oil switch in series with a 200 Ω water resistor.

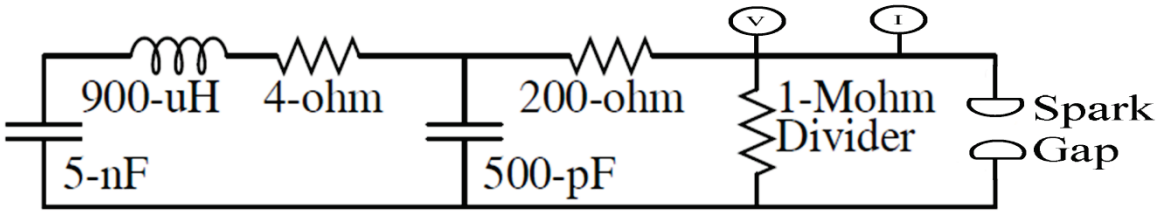

Figure 6.2: The schematic of the HVADTS circuit is pictured here. The 5 nF erected Marx capacitance discharges through a 900 μH inductor into a 500 pF capacitor stack. The high pressure oil switch shorts the capacitor stack to ground through a 200 Ω resistor.

The HVADTS consists of a Marx-generator that pulse charges a peaking capacitor through an inductor. The voltage developed on the peaking capacitor is simultaneously applied to the high pressure test switch, which contains the test fluid between two, planar, 2.54 cm diameter, 17-4PH stainless steel electrodes, that have been precipitation hardened to C38 Rockwell hardness. The inter-electrode gap is externally adjustable, and for the majority of experiments conducted is restricted to 0.16 cm. The voltage applied across the electrodes rises 20-80% at the rate of 300 kV/μs. The switch is designed for self-breakdown operation. The high pressure switch, shown in Figure 6.3, has a maximum voltage and pressure rating of 300 KV and 2000 psig (13.789 MPa), respectively.

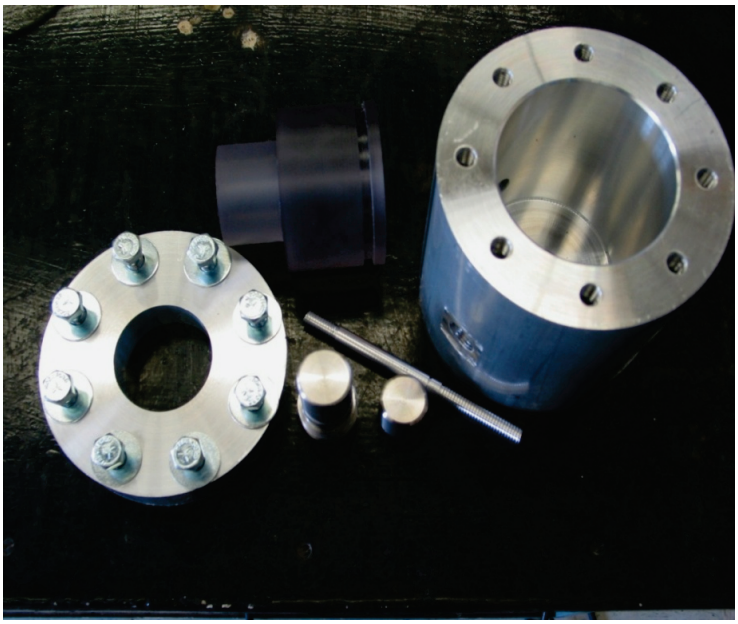

Figure 6.3: Photograph of the disassembled high pressure oil switch.

Figures 6.4 through 6.11 are photographs of the HVADTS hardware. Figure 6.4 shows the Marx generator, which has been reconditioned and modified with an additional stage to produce a greater output voltage. Figure 6.5 shows the 900 μH inductor. The air-core inductor is wound in two parts on G-10 forms. Figure 6.6 shows the high voltage capacitor stack, high pressure switch, load, and fluid reconditioning system. The switch is mounted to a steel plate which may be raised out of the oil bath to facilitate switch filling and maintenance. The high voltage portion of HVADTS is submerged in transformer oil during operation for safety and to prevent accidental breakdown due to the voltages achieved during a pulsed discharge.

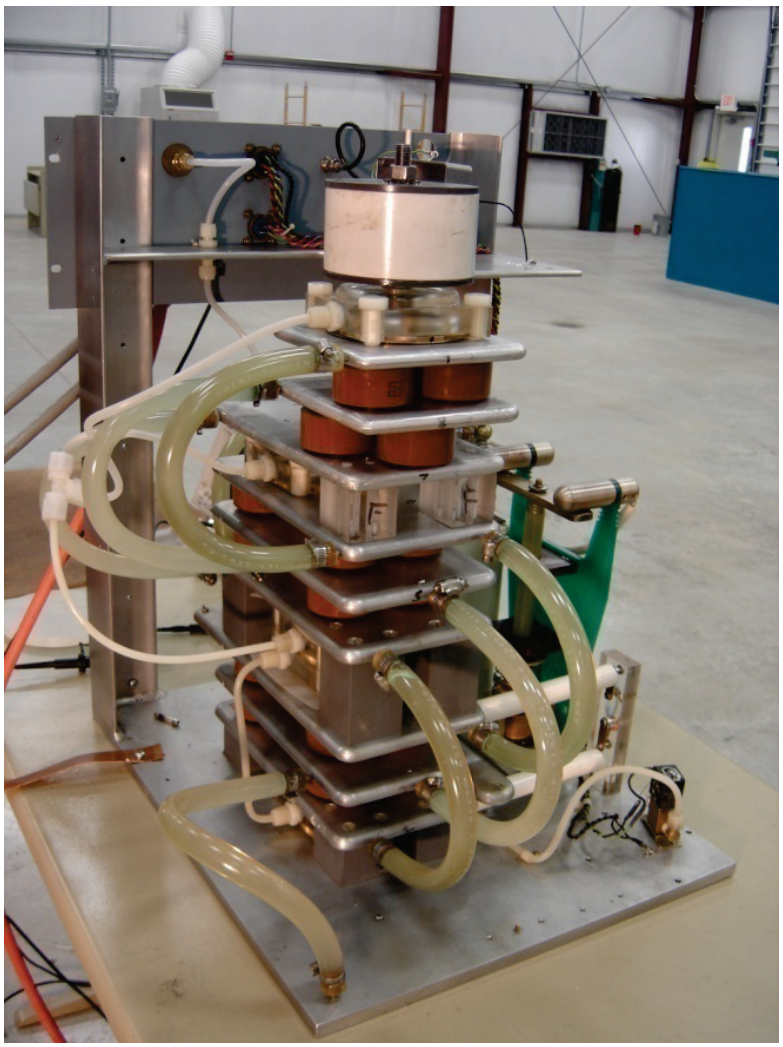

Figure 6.4: Photograph of the modified Marx generator. The Marx produces a 21-J pulse with a peak output voltage of 150 kV.

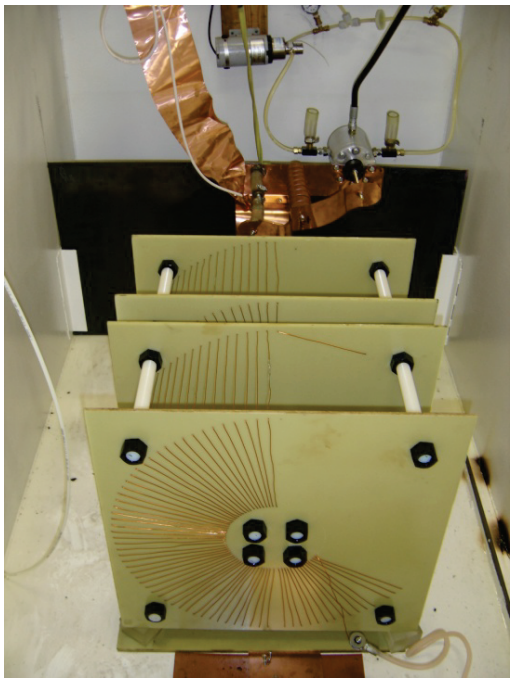

Figure 6.5: Photograph of the 900 μH inductor wound on two G-10 forms. The inductor isolates the Marx generator from the peaking capacitor and switch.

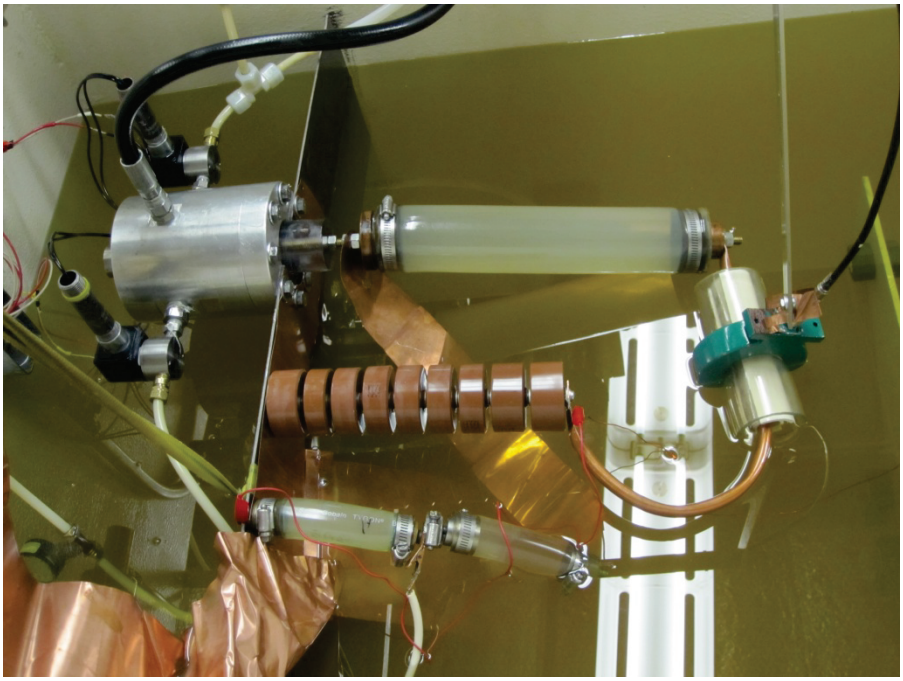

Figure 6.6: Photograph of the peaking capacitor, switch, voltage divider, current transformer, load resistor and oil reconditioning circuit.

The oil is reconditioned immediately prior to breakdown testing, and again following each breakdown. The reconditioning process involves flushing the oil from the switch and filtering macroparticle contaminants. Two solenoid isolation valves, shown in figure 6.7, allow the oil to be pumped through a 1 – 5 μm inline filter element. The oil is generally allowed to circulate for at least one minute following a breakdown. After reconditioning, the isolation valves are closed and a hand pump is used to pressurize the high pressure switch through a hydraulic translator. The total volume of fluid required to fill the system, including the switch, is approximately 800 mL.

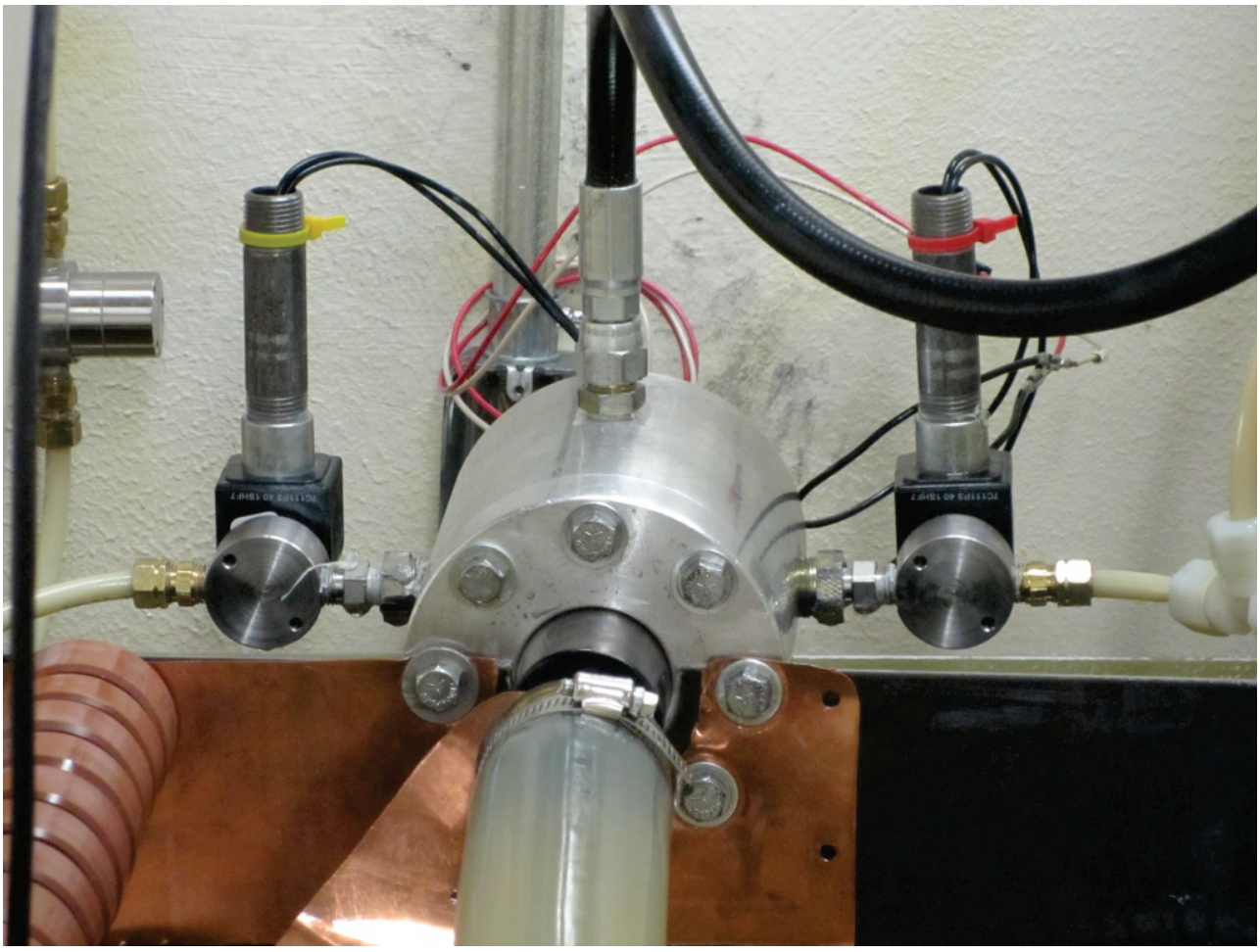

Figure 6.7: This photograph shows the switch installed in the circuit with the high pressure solenoid valves visible on each side.

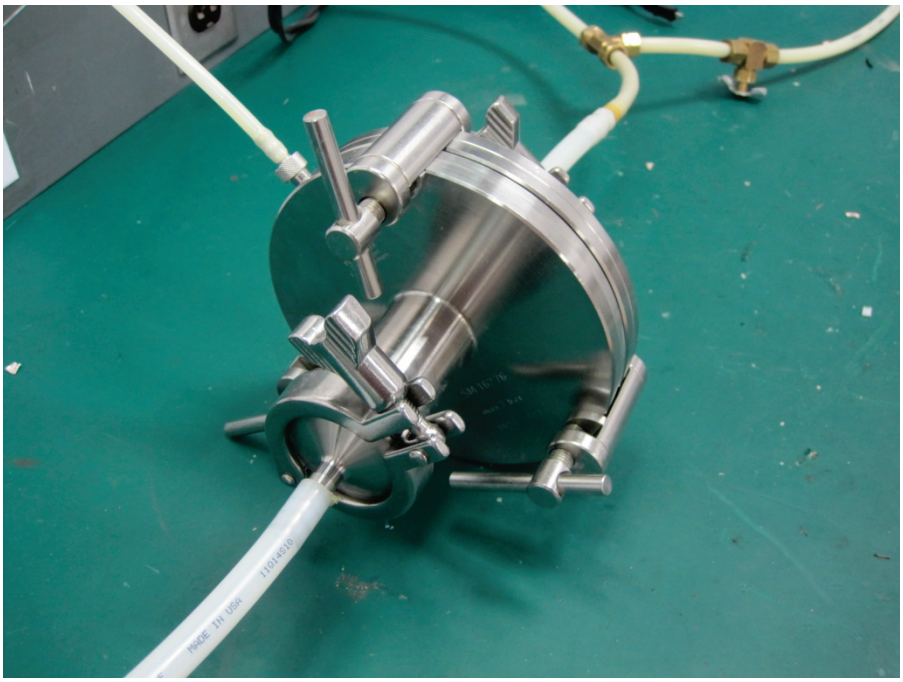

Figure 6.8: The Sartorius filter housing allows for large 142 mm filters to be installed in the oil reconditioning system minimizing the pressure drop of the filter.

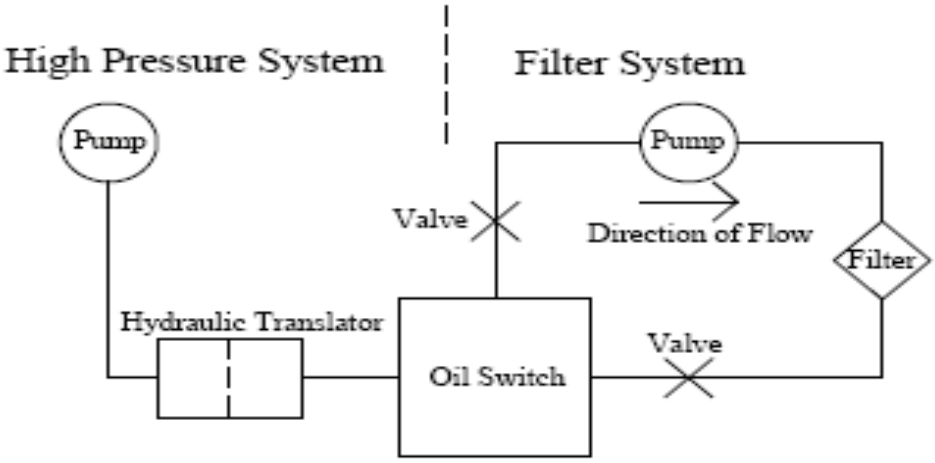

Figure 6.9: A Schematic diagram of the high-pressure and oil-reconditioning circuit is pictured.

The sample oils are evaluated for water content prior to high voltage testing utilizing a JM Science Aqua Counter model AQ-300 coulometric titrator, shown in Figure 6.10. The AQ-300 uses the Karl-Fischer titration method to determine total dissolved water [27]. It is an established fact that the presence of dissolved water in an oil dielectric has an impact on the self-breakdown jitter of non-aqueous liquid switches [28, 29].

Figure 6.10: The JM Science Aqua Counter AQ-300 coulometric titrator used to perform water concentration analysis.

The breakdown voltage is monitored utilizing a Northstar Research high voltage probe, model PVM-6 [30]. The PVM-6 has a peak voltage rating of 100 kV, an 80-MHz bandwidth, and provides a 1000:1 voltage division ratio at the output. The switch voltage is designed for up to 250 KV; therefore an additional voltage divider having a 4.26:1 voltage division ratio is used across the switch terminals to bring the measured voltage within the dynamic range of the PVM-6. Figure 6.11 shows the PVM-6 installed in HVADTS.

Figure 6.11: The Northstar Research PVM-6 100 kV, 80 MHz high voltage probe used to monitor the transient switch voltage.

The high pressure switch is operated utilizing a gap separation that would permit self-breakdown at approximately 80 % of peak voltage. Figure 83 illustrates a typical waveform in which breakdown occurs at 150.11 kV, or approximately 63.2 % of 250 kV. The noise evident on the leading edge of the waveform (t = 1.4 μs) has been attributed to noise generated by the Marx Bank trigger generator.

Figures 6.13 and 6.14 illustrate the open circuit voltage pulse. The voltage is seen to peak at 255 KV and ring at a frequency of 250 KHz. Figures 6.15 and 6.16 show the current through the oil switch after breakdown has occurred. The waveform can be seen to peak at 2 KA at a frequency of 50 MHz. The HVADTS has proven to be a reliable system performing over 10^4 shots since last maintenance.

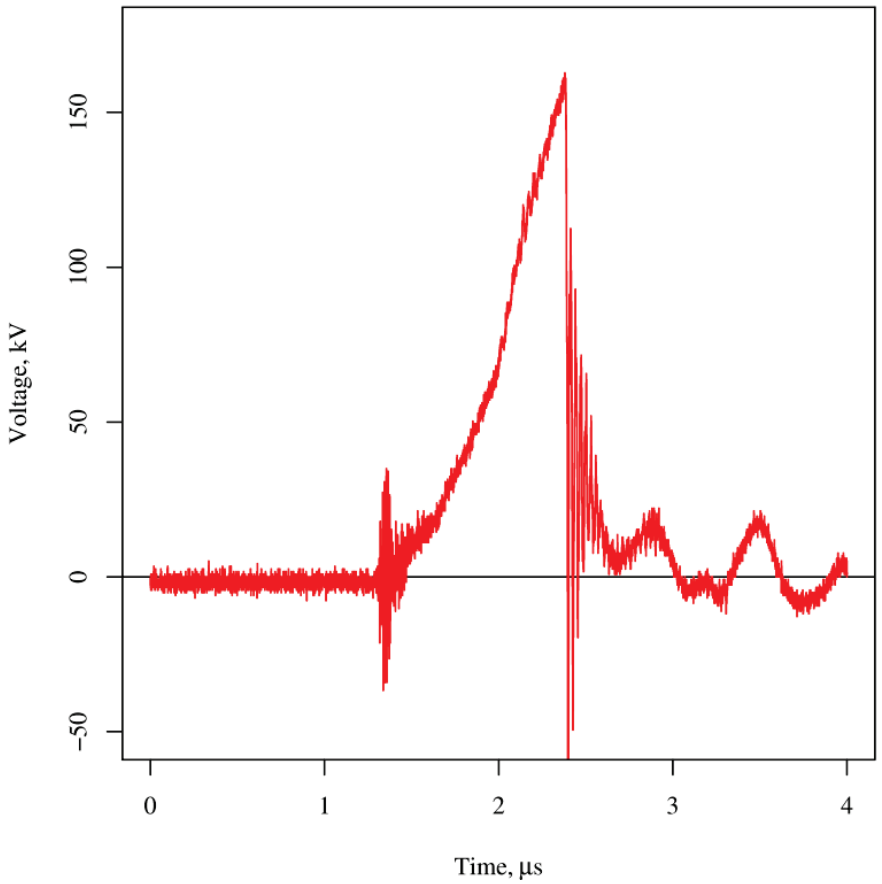

Figure 6.12: A switch voltage waveform illustrating breakdown is pictured here. The voltage rise '1-cos' initiates at 1.41 μs. The switch breaks down 1 μs after initiation at 158.1 kV (63.2 % of peak) with a gap spacing of 1.2 mm.

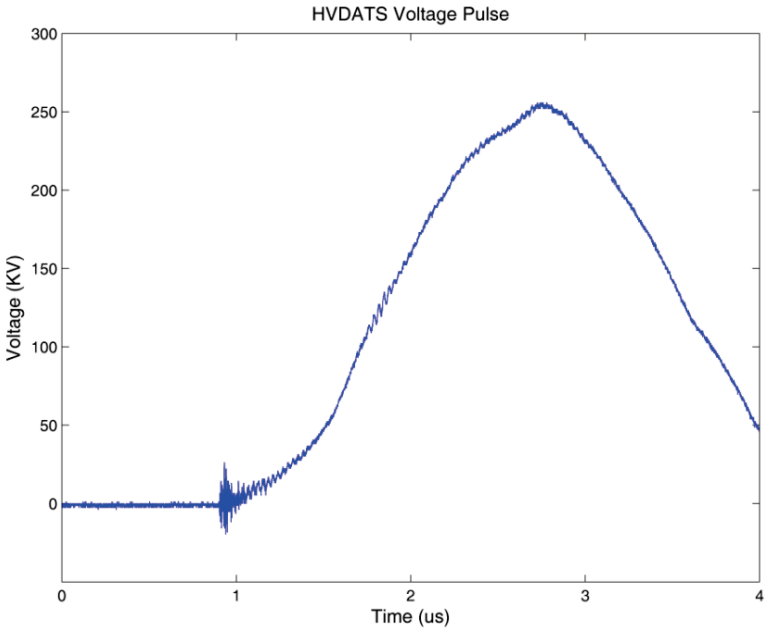

Figure 6.13: The switch voltage waveform without breakdown is shown here. The voltage increases from 0 to 255 KV in 1.6 µs.

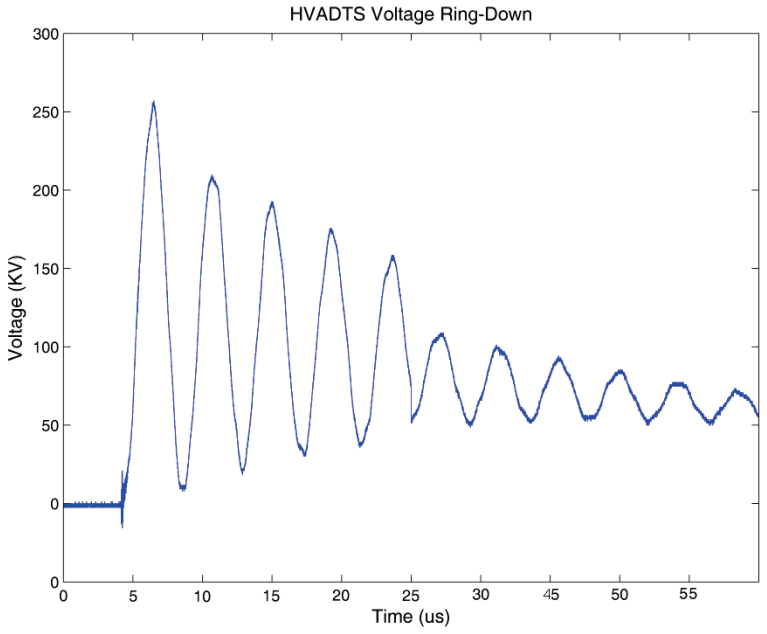

Figure 6.14: The voltage ring without breakdown is shown here. The voltage damps to zero in approximately 60 µs. The voltage rings at approximately 250 KHz.

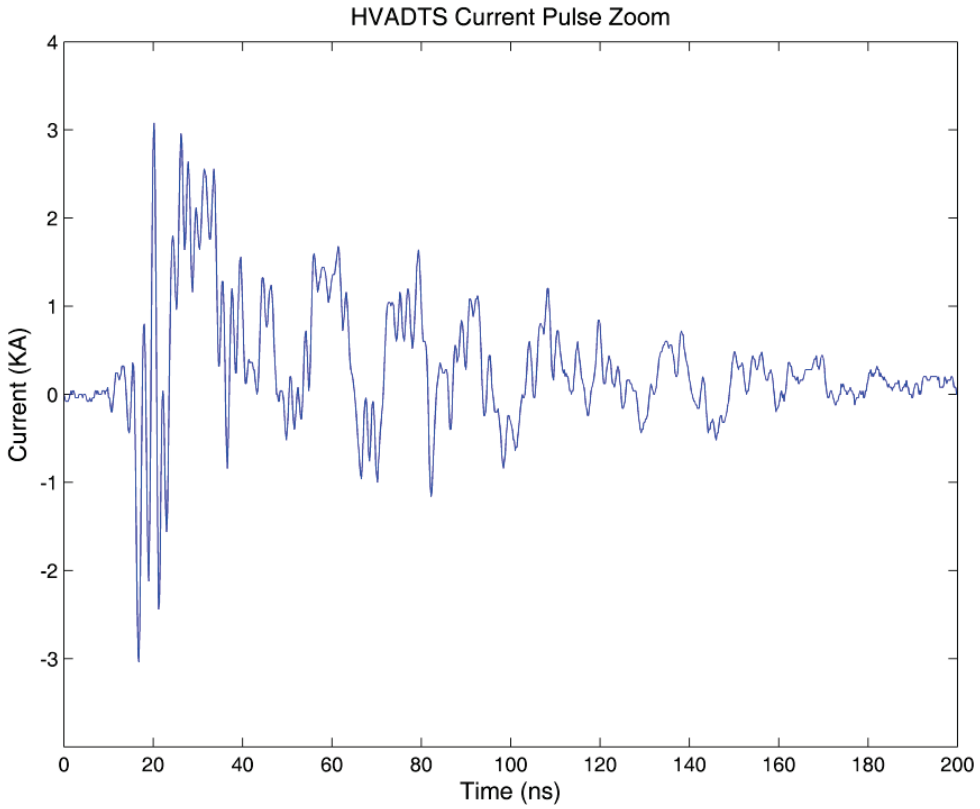

Figure 6.15: The current pulse through the switch after switch closure is shown here. The current peaks at nearly 2 KA.

References

[27] JM Science, Karl-Fischer Coulometric Titrator, 2011, www.jmscience.com.

[28] O. Koreh, K. Torkos, M. Mahara and J. Borossay, "Study of water clusters in insulating oils by fourier transform infrared spectroscopy," *IEEE Transactions on Dielectric Insulation*, Vol. 5, No. 6, 1998.

[29] P. Norgard, R. D. Curry, R. Burdt, G. Anderson, R. Cravey and S.Heidger, "A high pressure flowing oil switch for gigawatt, repetitive applications," *IEEE 15th International Pulse Power Conference,* 2005.

[30] NorthStar High Voltage, PVM-6 Voltage Probe, 2009, www.highvoltageprobes.com.

CHAPTER 7

EXPERIMENTAL RESULTS

The results contained in this section are the result of nearly three years of experimental testing at UMC on the HVADTS system. The goal of the experimental testing is to reduce self-break oil switch jitter. The first section displays the results of the preliminary test cycles. The preliminary tests were completed to establish a baseline on the HVADTS system as well as identify several dielectric oils as candidates for further testing. The second section describes the initial testing on the particle-infused dielectric oils. In the third section the particle-infused oils are further investigated with varying pre-test and inline filter pore sizes and suspension procedures. The fourth section describes a test cycle comparing two oils, Nycodiel PAO and alkylbenzene, at four different pressures and a 1.2 mm gap spacing. The oils are tested with no additives, surfactant only, and surfactant with particles. In section five the gap spacing is widened to 2 mm and Nycodiel PAO and alkylbenzene are tested. Section 6.6 describes testing comparing both pure and particle-infused oil dielectrics. Section seven includes analysis of the conditioning and post-test shots. Each data point is the result of 50 breakdowns. The results suggest three ways to reduce jitter: eliminating water concentration, widening gap spacing, and infusing the oil with high-K particles.

7.1 Initial HVADTS Baseline and Candidate Results

The goal of the first stage of testing is designed to identify candidate fluids that exhibited good performance characteristics and to eliminate those that do not perform as well. In this stage, UMC evaluated a wide range of oil chemistries. The performance of a particular fluid is evaluated by considering both the average electric field strength at breakdown for a sample of breakdowns, and the percent standard deviation (PSD) of the electric field, which we define here

as the ratio of the standard deviation to the mean value of the breakdown electric field for a sample of breakdowns. The PSD is a measure of the system jitter.

The first series of tests were conducted with candidate fluid-dependent gap separations in order to obtain self-breakdown at approximately 80% of the attainable charge voltage. The results of this first cycle of tests are reported in Figures 7.1 and 7.2, showing the mean breakdown electric field and the percent standard deviation (PSD) of the breakdown electric field, respectively. In the tests, "Diala AX" represents a standard transformer oil, and "MIL-PRF-87252" is a poly-α olefin (PAO) based on the dimer of decene. The MIL-PRF-87252C oil is a PAO has been used extensively at UMC as a high pressure switching medium under a previous program in which a pressurized, flowing oil switch was designed and tested [31].

The results of Figures 7.1 and 7.2 indicate several fluids that are candidates for further testing. The standard transformer oil Diala AX, the decene/dodecene PAO blend, and the silahydrocarbon all exhibit PSD < 12%, whereas the ester, the decene PAO and the alkylbenzene has PSD > 12%. The ester has the highest PSD and exhibited the worst performance of any of the oils. Transformer oil (Diala AX) exhibited the lowest standard deviation.

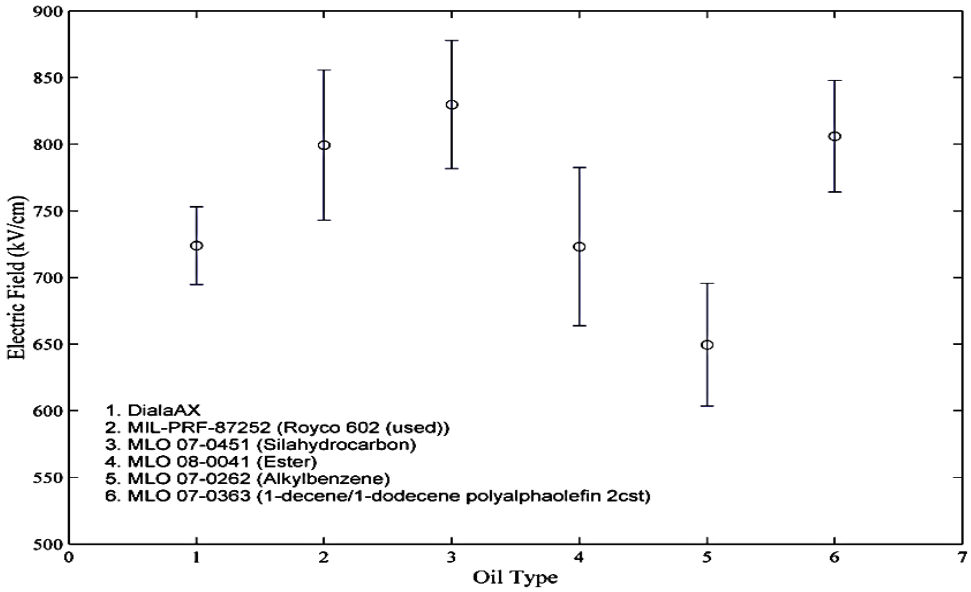

Figure 7.1: The mean electric field at breakdown for the candidate oils in test cycle 1. Error bars represent 1-σ standard deviation. The oil pressure is 1000 psig (6.895 MPa) and variable gap spacing is employed.

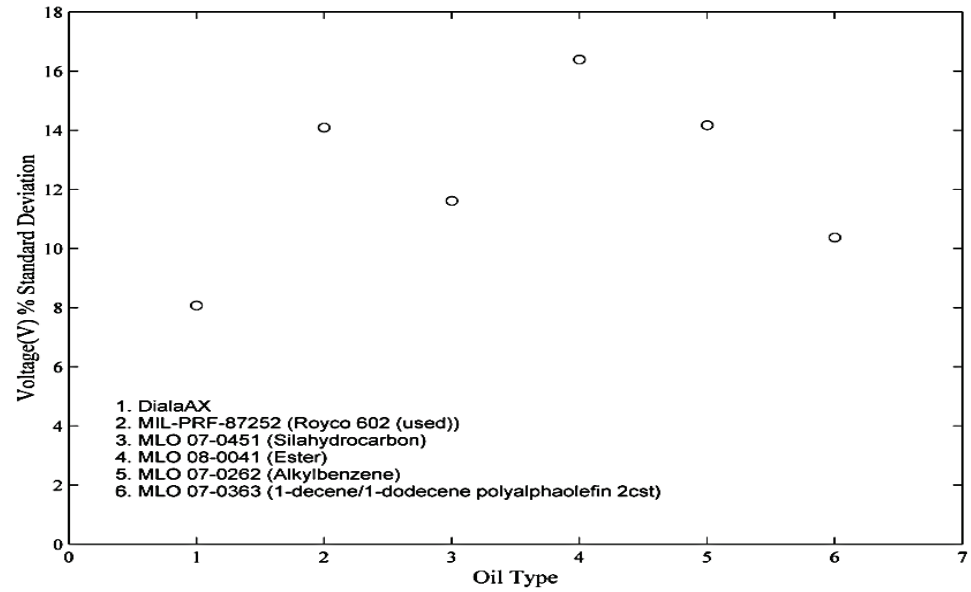

Figure 7.2: The percent standard deviation of the electric field at breakdown for the candidate oils in test cycle 1. The oil pressure is 1000 psig (6.895 MPa) and variable gap spacing is employed.

A second series of tests were conducted to examine the effects of different pressures on the candidate oil samples. In this cycle, the gap separations are maintained a fixed value of 1.6 mm and the oil pressure is stepped through five evenly spaced values ranging from 500 psi (3.45 MPa) to 1500 psig (10.34 MPa). It is important to note that this range of pressures excludes the critical pressure of the candidate fluids, all of which are less than 3.45 MPa. The critical pressure is an important parameter because it specifies, in part, a point in the thermodynamic state of the fluid where spontaneous partitioning from the liquid to the gas states (or vice versa) can occur, and it is believed that this is a necessary precursor to breakdown. In this cycle an additional silicone-based fluid called "DC-200" is included having a much lower viscosity than the silahydrocarbon; DC-200 is a Dow Corning silicone oil (Polydimethly-siloxane) with a viscosity of 20 cSt, compared to > 60 cSt for the silahydrocarbon. In addition to DC-200, an additional blended PAO is used to illustrate the effects of viscosity while maintaining the base chemistry.

The results of test cycle are illustrated in Figures 7.3 and 7.4, showing the mean electric field at breakdown and the PSD of the breakdown voltage. The mean breakdown electric field increases with increasing oil pressure. The PSD, however, appears to be somewhat worse in test cycle 2 when compared to test cycle 1. It is unclear at this point whether the observed differences between test cycle for individual oil types are a result of the gap separation or not. In all cases but one, the PSD in Figure 7.4 increases slightly from 500 to 750 psi, and then begins a gradual decrease as pressure is increased to 1500 psi. The one case in which the PSD does not decrease continuously with increasing pressure is alkylbenzene; the PSD data point at 1500 psi may be an anomalous result, for the trend appears to be in agreement with the other oil types up to 1500 psi.

The transformer oil, the Royco 602, the alkylbenzene, and the 4 cSt PAO blend appear to have very similar breakdown properties. In Figure 7.3, for instance, the transformer oil and the 4 cSt PAO blend are statistically indistinguishable at most pressures, both having nearly the same mean and standard deviation values. The Royco 602 exhibits slightly higher average and standard deviation breakdown electric fields, whereas the alkylbenzene has lower average and standard deviation breakdown electric fields. From a PSD standpoint, these four oils are virtually identical.

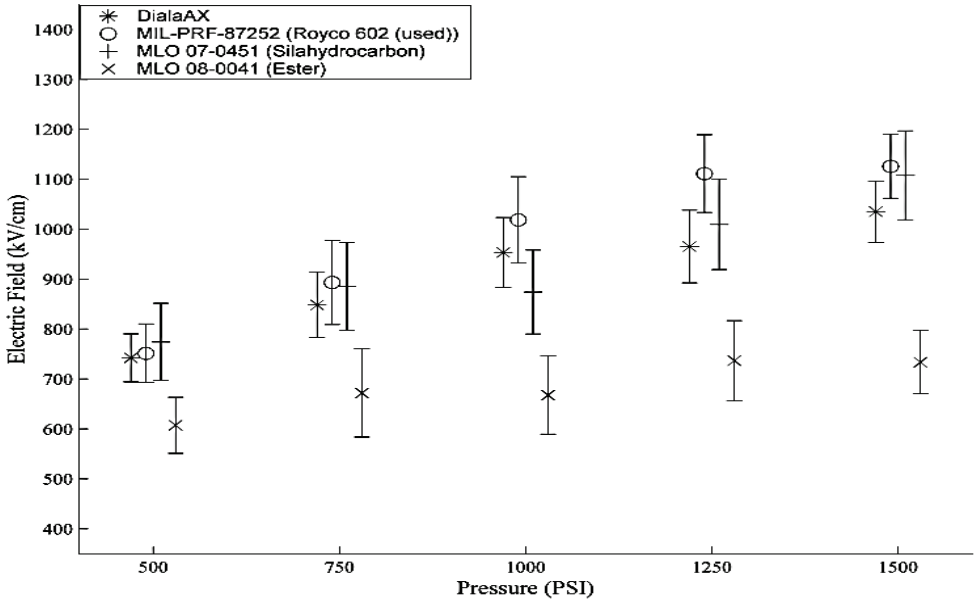

Figure 7.3A: The mean electric field at breakdown for four of the candidate oils in test cycle 2 for several oil pressures. The error bars represent 1-σ standard deviation and a fixed gap spacing of 1.6 mm is employed.

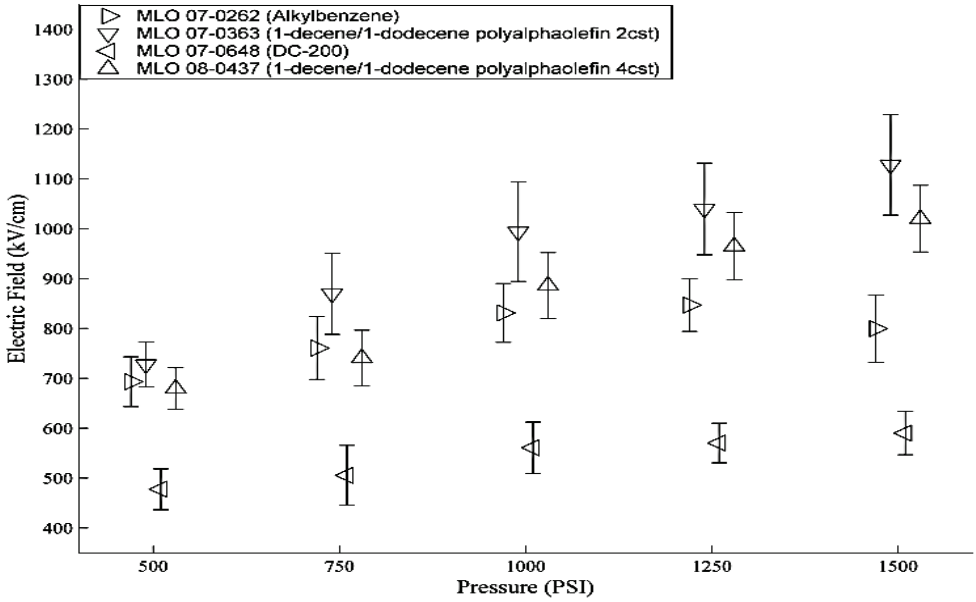

Figure 7.3B: The mean electric field at breakdown for four of the candidate oils in test cycle 2 for several oil pressures. The error bars represent 1-σ standard deviation and a fixed gap spacing of 1.6 mm is employed.

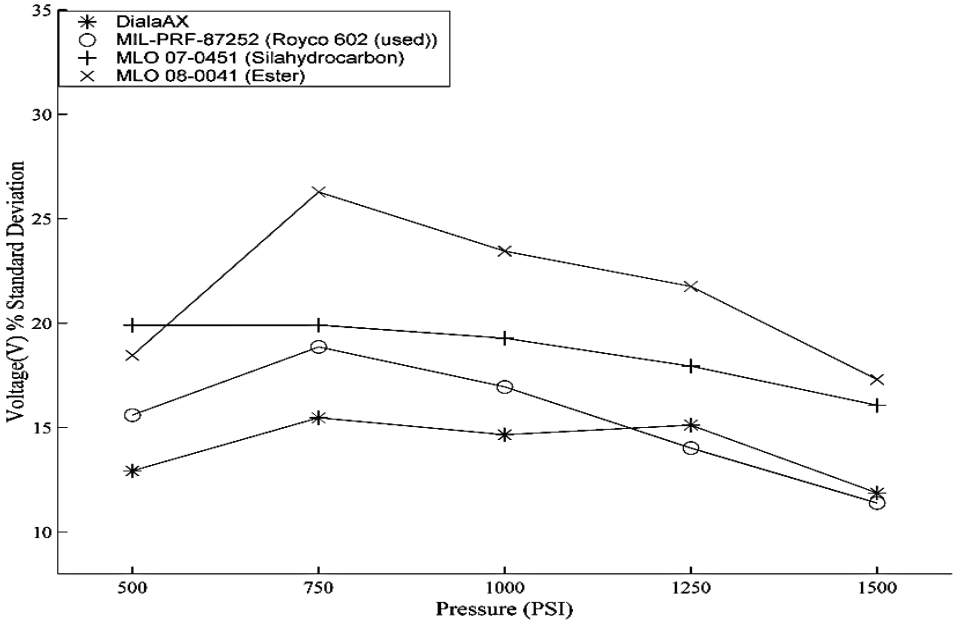

Figure 7.4A: The percent standard deviation of the electric field at breakdown for four of the candidate oils in test cycle 2 for several oil pressures. A fixed gap spacing of 1.6 mm is employed.

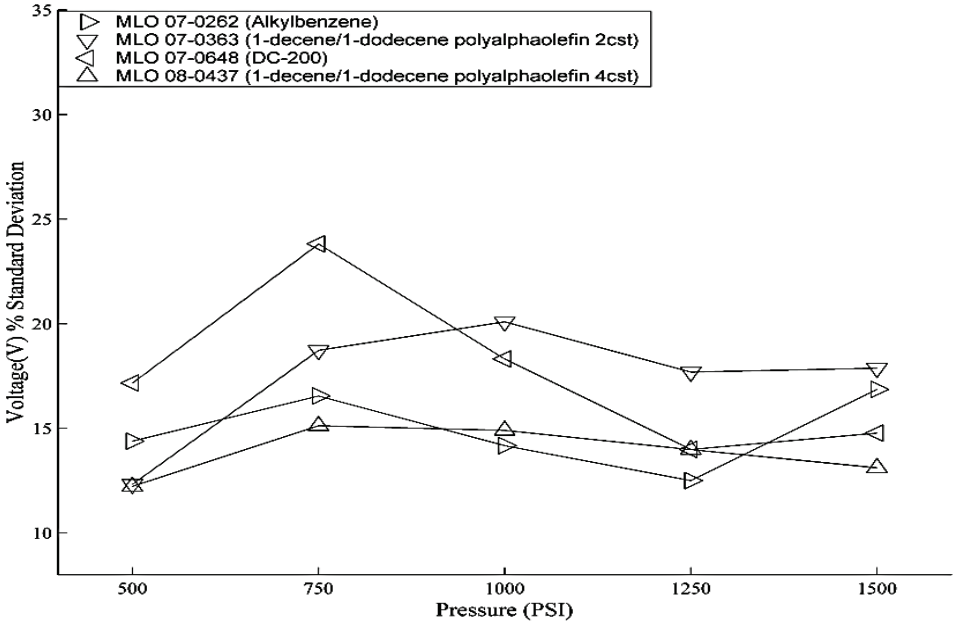

Figure 7.4B: The percent standard deviation of the electric field at breakdown for four of the candidate oils in test cycle 2 for several oil pressures. A fixed gap spacing of 1.6 mm is employed.

7.2 Initial High-K Particle Results

A third test cycle was initiated in which particle BST was added to several of the candidate oils. Figure 7.5 illustrates the PSD values obtained during this test cycle. The addition of BST particles produces a 30% reduction in PSD at 500 psi. In all cases, the PSD rises as the pressure increases from 500 to 750 psi, as is seen in figures 7.3 and 7.4. One of the tests indicates that as pressure increases the PSD of the particle loaded oil actually increases, while another test indicates that the addition of BST actually decreases PSD. Additional testing was required to accommodate the apparent contradiction in results. The Diala AX transformer oil data of figure 7.5 is included in figure 7.6 along with new Diala AX data with and without particle loading. The second test with the particle loaded Diala AX shows a marked decrease in PSD at high pressure. After testing, Batch 6481 of figure 7.5 was found to be contaminated possibly contributing to its poor performance. Filter clogging issues were not resolved at this point in testing, contributing the higher PSD of the particle-infused oils.

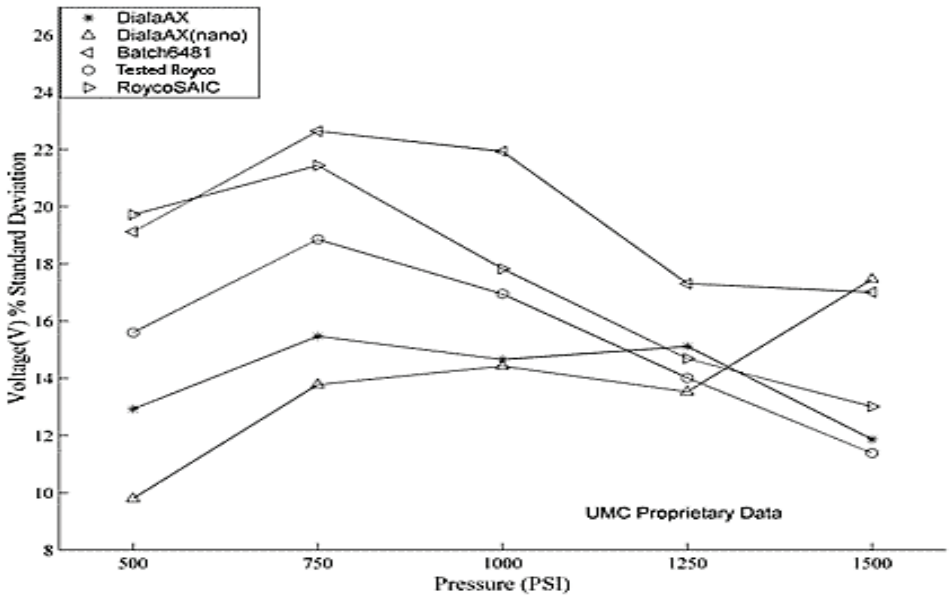

Figure 7.5: The percent standard deviation of the electric field at breakdown for several of the candidate oils in test cycle 3 for several oil pressures. A dispersion of particle BST is added to the transformer oil. Fixed gap spacing of 1.6 mm is employed. "Tested Royco" refers to Royco PAO that is removed from the reservoir of the UMC rep-rate test stand. This "Tested Royco" is subjected to more than one million breakdowns in its lifetime.

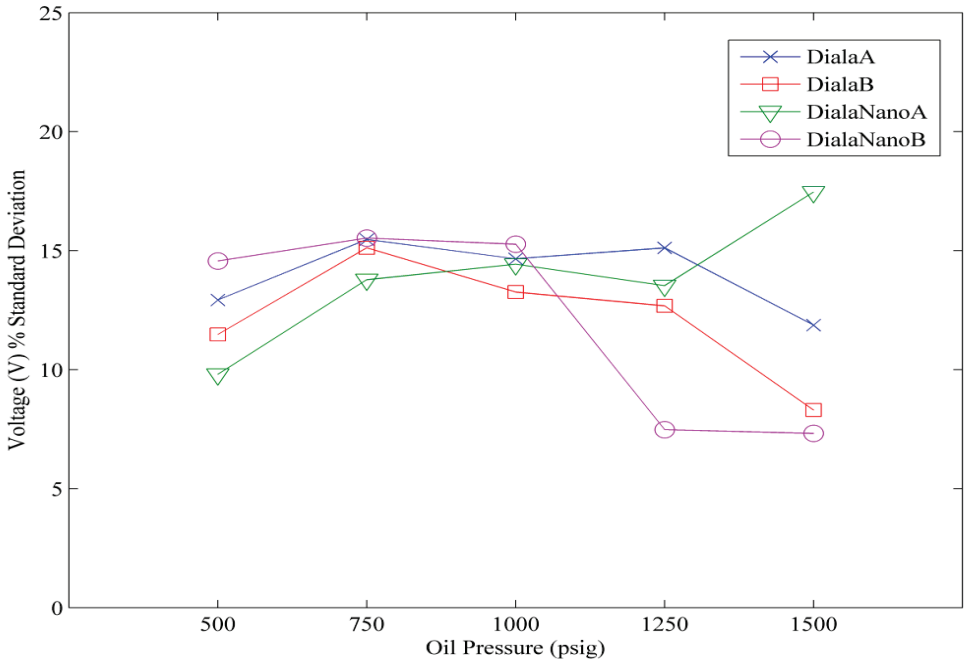

Figure 7.6: Pictured is the percent standard deviation of the electric field at breakdown before and after the addition of particles to two samples of transformer oil in test cycle 3. A fixed gap spacing of 1.6 mm is employed. DialaA and DialaB are the same oils tested in two different runs. The data is more repeatable at lower pressures.

A fourth test cycle was initiated to provide additional insight into the effects of BST particles on the breakdown properties of oil, the results of which are illustrated in Figures 7.7 and 7.8. The candidate oil selected for testing is the Nycodiel, a MIL-PRF-87252 decene-based PAO. A BST particle and a PZT nanopowder are selected as candidate loading materials. The PZT particles are loaded into the PAO to only 1% by weight, whereas BST is loaded into the PAO at concentrations of 0.1, 1.0, and 5.0 % (by weight). The use of lead based PZT is minimized due to health concerns. Lead is found to produce a significant reduction in both the mean breakdown electric field strength and the PSD of the breakdown electric field. In general, increasing the concentration of particles causes reduced average electric field intensity at breakdown. The use of particles of either constituency produces significant reductions in PSD of the electric field intensity at breakdown. At this point in the research, filters were becoming clogged almost immediately rendering the inline filter system ineffective at removing carbon byproducts [32].

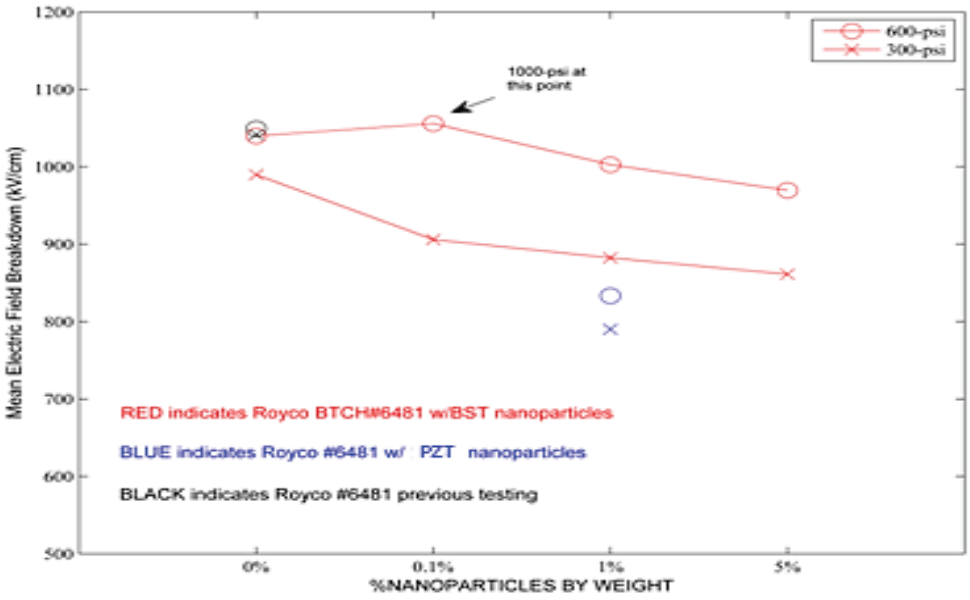

Figure 7.7: The mean electric field at breakdown for the candidate oils in test cycle 4 for several particle types and dispersion concentrations. A fixed gap spacing of 1.6 mm is employed at two oil pressures.

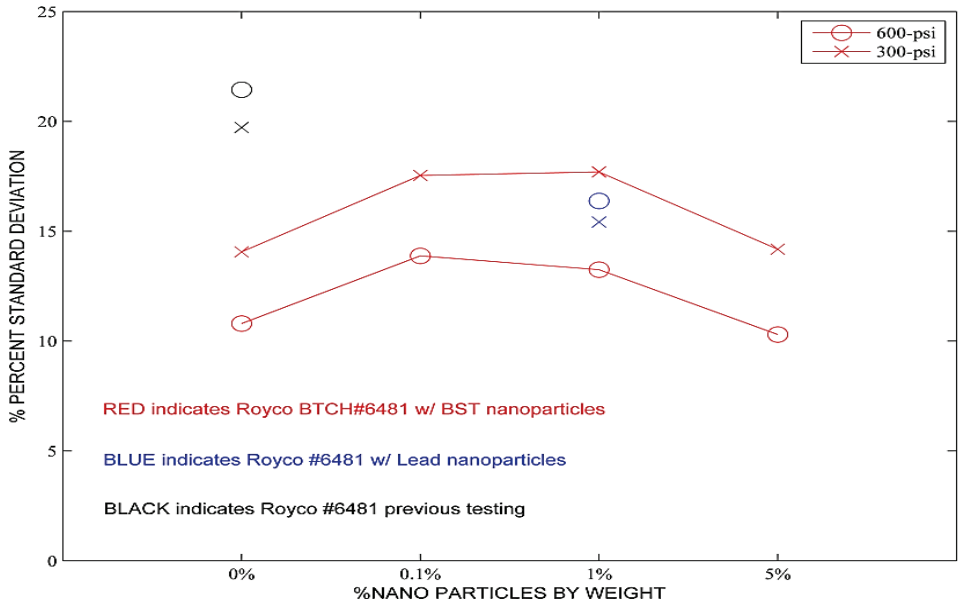

Figure 7.8: The percent standard deviation of the electric field at breakdown for the candidate oils in test cycle 4 for several oil pressures. A fixed gap spacing of 1.6 mm is employed.

7.3 Particle Suspension and Filtration Procedure Refinement

The second stage of the experimental approach taken by UMC is a more extensive evaluation of the effects that particle dispersions have upon the breakdown characteristics of selected oils. During this stage of the research a rigorous experimental design is employed that produces increased confidence in the results. In addition, this stage of the experiment is utilized to augment and refine the particle processing methods to develop a consistent means of loading the candidate oils with specific concentrations of particles through the use of enhanced filtering/dispersion techniques and surfactant chemistry.

The selected oils are preprocessed prior to high voltage testing to introduce various surfactants and particle concentrations, as well as to evaluate some of the qualities of the dielectric such as water concentration. Approximately one liter of oil is pre-filtered through a 0.45 μm nitrocellulose filter to remove macroparticle contaminants. Next, BST and a chemical surfactant are added at various concentrations to different samples of oil. At this point, the BST cannot be considered a nanoparticle due to the naturally occurring agglomeration that develops during the drying process after the BST has been ball-milled. Therefore the oil-surfactant-BST mixture is exposed to high-power ultrasound energy (e.g., sonicated) for a period of time to break the agglomerates into nanometer-sized particles. Though the sonication is effective at breaking down many of the agglomerates, the results are imperfect and a significant concentration of agglomerated microparticles remains.

It is important to remove these larger components from the oil, for they almost immediately saturate the recirculation filter, thus limiting the effectiveness of the filter to remove carbon byproducts. The oil is therefore filtered to remove the larger BST particles. Several different filter pore sizes are employed for the experiments conducted in this cycle, ranging from as large as 5 μm to as little as 200 nm. A vacuum-filtration method was employed to force the particle oil through the filter pores.

The final step taken during pre-processing is to sparge dried nitrogen through the oil at 20 scfh for ten minutes. This process, known as sparging, utilizes mass transfer to remove unbound, dissolved water from the oil. The rate of sparging is set such that the oil appears to be

vigorously boiling. Measurements of dissolved water indicate that the sparging process could rapidly reduce the water content of most oils with 5 or 10 minutes of vigorous sparging [33].

High voltage testing of the selected fluids involves circulating the oil to remove discharge byproducts, primarily carbon, and then pressurizing the oil and applying a continuously increasing voltage to the sample until breakdown occurs. A series of 50 breakdowns at each oil pressure are collected for each of the oil samples tested. Following each test run the switch is removed from the HVADTS system and completely cleaned. The electrode surfaces are repolished using silicon carbide sandpaper (320 grit) until the electrode surface deformations are no longer visible. Immediately prior to high voltage testing, the switch is pressurized and 30 breakdowns are accumulated to condition the electrodes and prevent conditioning drift in the data.

The tests are conducted with pre-filter pore sizes of 5, 1, 0.45, and 0.2 μm, and the inline filter sizes are 5, 1, and 0.45 μm. Again, prior to testing, the oil is sparged to reduce water concentration to less than 100 parts per million (ppm). A set of 100 tests are performed per oil, with 50 tests for each of two oil pressures.

Table 2 provides a summary of the data taken during this test cycle; including external variables (filter sizes & water concentration). The effort is concentrated on the Nycodiel PAO (MIL-PRF-87252) and 1-Hexadecene. The data is organized into three main sections, the first section summarizing breakdown characteristics at relatively low pressure, the second section summarizing breakdown characteristics at higher pressure, and the third section bracketing the high and low pressure characteristics. Several basic trends emerge from the data in Table 2 as the level of BST particles is increased: the mean breakdown voltage decreases and the percent standard deviation decreases. In a few cases, for example “Low Pressure A Hexadecene”, the introduction of particles actually produced an increase in PSD, however this finding runs contrary to the majority of the other results, therefore we believe it may be an anomalous finding. The PSD results are illustrated graphically in figures 7.12 and 7.13 for each of the results summarized in the table.

Figures 7.10 and 7.11 are photographs of the 142 mm diameter 3 μm pore size inline filters used during the test cycles of sections D, E, and F. The filter housing of figure 6.8 is not

purchased until after this test cycle. This test cycle utilizes much lower-capacity pancake filters. However, the filter pores of figures 7.10 and 7.11 appear the same as the pancake filters after testing. Higher jitter values result from tests when the filter became clogged. The results of the test cycle suggest that the pre-filter size of 3 μm and inline filter size of 3 μm produces the lowest jitter values. **The results also suggest that lower jitter values can be attributed to the particle-infused oils with the lowest water concentrations.** Future test cycles suggest there is a strong correlation between water concentration and jitter in the particle-infused oils.

In later test cycles, a drying procedure is implemented to determine the actual particle concentrations remaining in the particle-infused oil after filtration. This drying method is then utilized in all subsequent tests.

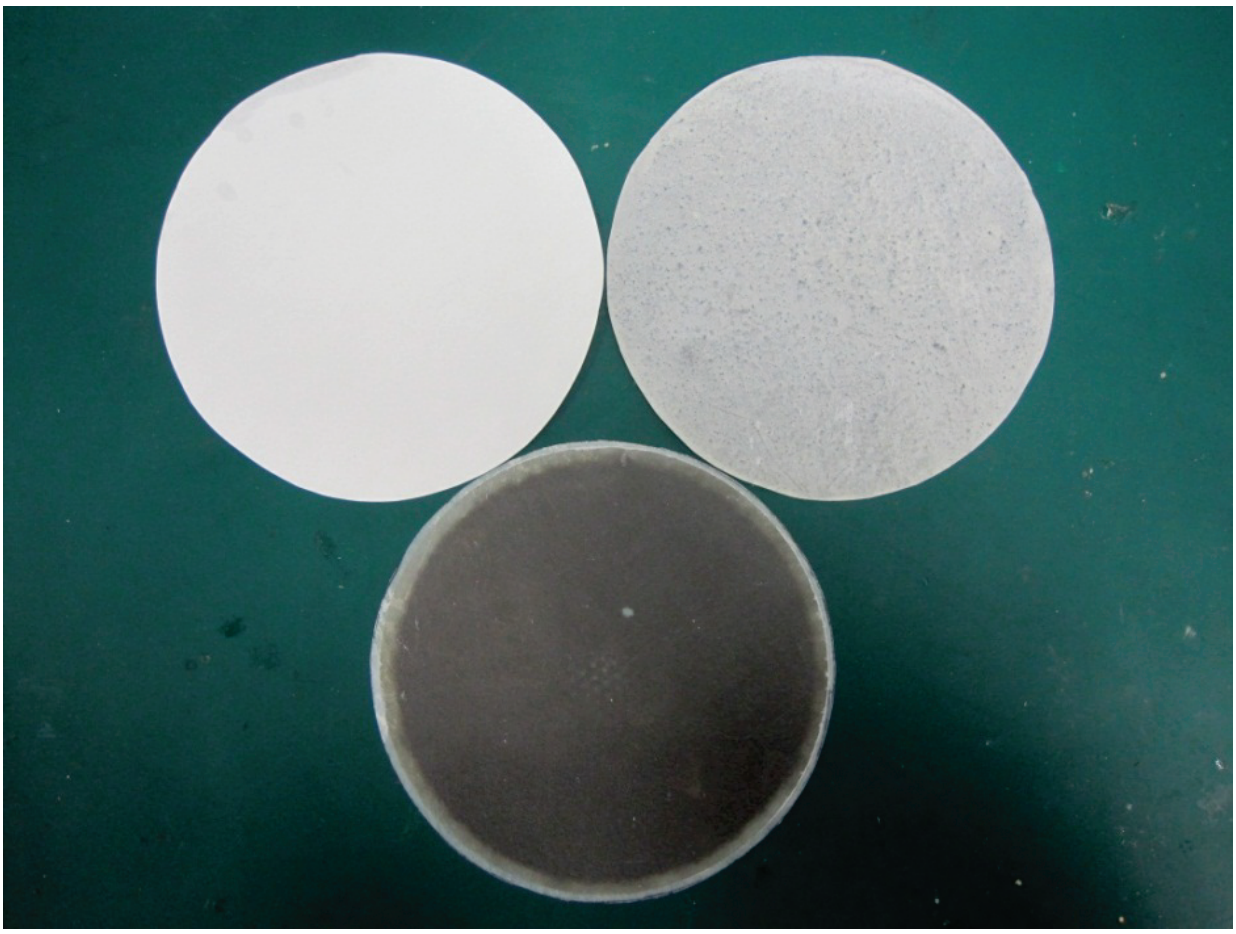

Figure 7.9: Three 142 mm filters are pictured: the filter at the upper left is fresh, the filter at the bottom is used with oil without a particle concentration and the filter at the upper right is used with particle-infused oil.

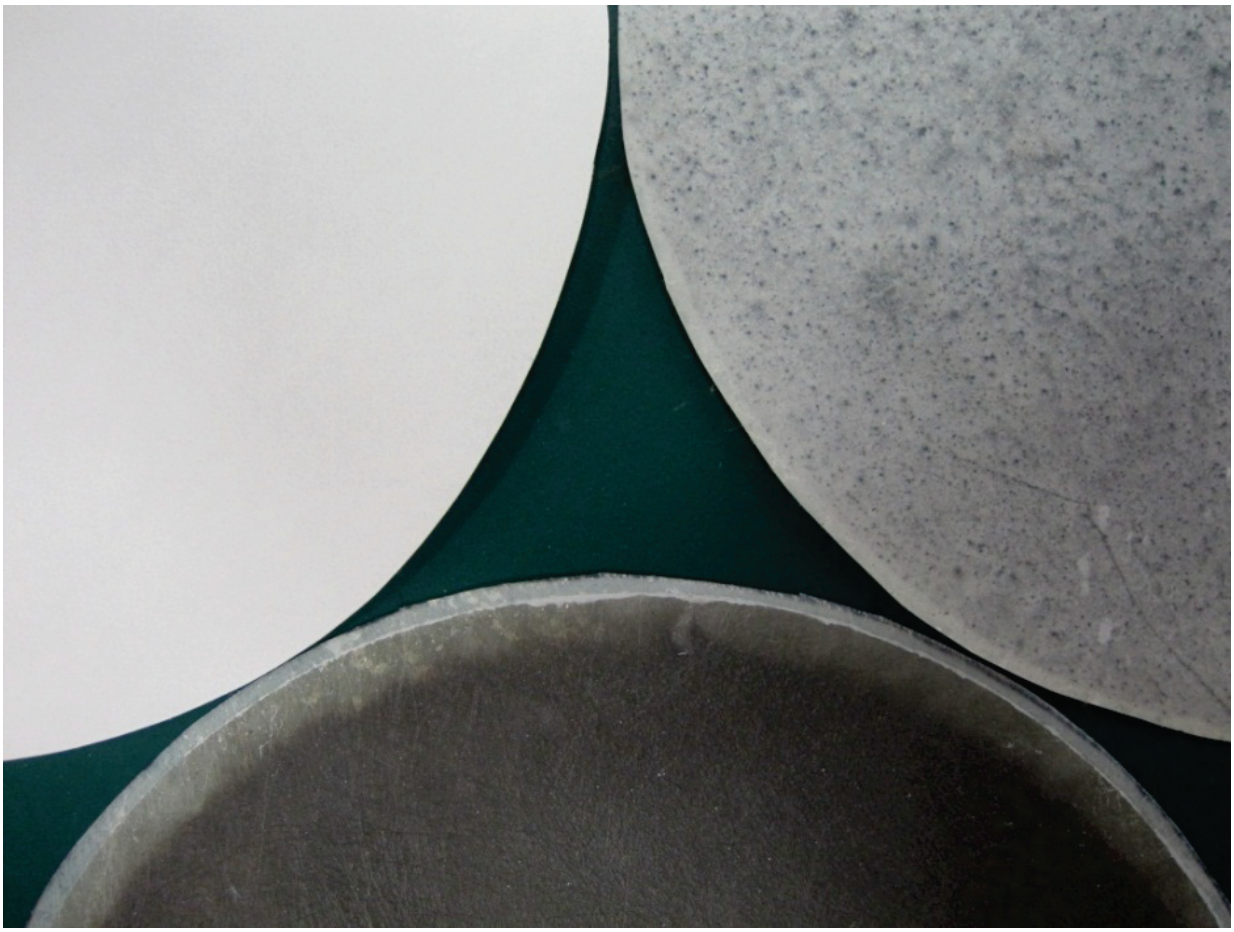

Figure 7.10: A macro photograph of the filters indicates a strong carbon presence on both the used filters with and without a particle suspension. Test cycle 5 utilized 50 mm filters, the 142 mm filters are only used in the final test cycles.

Table 2. Experimental results for test cycle 5 of Nycodiel PAO and Hexadecene with concentrations of BST particles and surfactant.

Oil Name	**Mean Breakdown Voltage (kV)**		**Percent Standard Deviation (PSD)**		**Pre-Filter Size**	**Inline Filter Size**	**Clogged?**	**Water (ppm)**
LOWER PRESSURE	**300-psi**	**600-psi**	**300-psi**	**600-psi**				
Pure Hexadecene	177	188.4	14.88%	11.03%	None	1-um	no	X
Hexadecene 5% BST 1% Surfactant *	176.4	186	17.28%	14.53%	none	5-um	yes	X
Hexadecene 5% BST 1% Surfactant	163.2	173.8	**9.57%**	**9.93%**	1-um	1-um	yes	X
Pure Hexadecene	207.84	201.35	12.31%	12.74%	3-um	3-um	no	30
Hexadecene 5% BST 1% Surfactant	173.22	190.46	17.71%	**9.56%**	3-um	3-um	no	52
AlkylBenzene 5% BST 1% Surfactant	162.54	201.57	23.25%	11.33%	3-um	3-um	no	54
Pure Nyco **	176.7	185.5	13.36%	13.55%	none	1-um	no	22
Nyco 5% BST 1% Surfactant	162.2	180.4	13.30%	**7.61%**	3-um	3-um	no	58
Nyco 5% BST 1% Surfactant	155.2	173.4	13.05%	**9.80%**	1-um	1-um	yes	43
HIGHER PRESSURE	**600-psi**	**1000-psi**	**600-psi**	**1000-psi**				
Pure Nyco	146	164.8	16.97%	14.05%	0.2-um	.45-um	yes	133***
Pure Nyco ****	183.7	196.7	14.68%	10.25%	0.2-um	3-um	no	23
Nyco 5% BST 1% Surfactant	162.5	172.2	13.40%	10.24%	.45- um	3-um	no	56
Nyco 5% BST 1% Surfactant	176.8	187.6	14.21%	11.10%	1-um	3-um	no	64
Nyco 5% BST 1% Surfactant	185.3	195.5	**8.61%**	**7.01%**	3-um	3-um	no	45
Pure Hexadecene	199.06	203.36	15.39%	13.76%	3-um	3-um	no	69
Hexadecene 5% BST 1% Surfactant	192.42	206.39	14.52%	**9.58%**	3-um	3-um	no	35

LOW AND HIGH PRESSURE	**300-psi**	**1000-psi**	**300-psi**	**1000-psi**				
Pure Nyco *****	166.55	190.32	21.61%	16.78%	3-um	5-um	no	32
Pure Nyco	171.82	192.59	22.24%	18.77%	3-um	5-um	no	19
Pure Nyco 5% BST 1% Surfactant	173.99	206.35	19.37%	**8.81%**	3-um	5-um	no	89
* All percentages are by weight								
** Nyco conforms to MIL-PRF-87252								
*** This sample is contaminated by water saturated DialaAX transformer oil before testing								
**** This is the contaminated sample resparged and retested								
***** Insulator Punch Through								

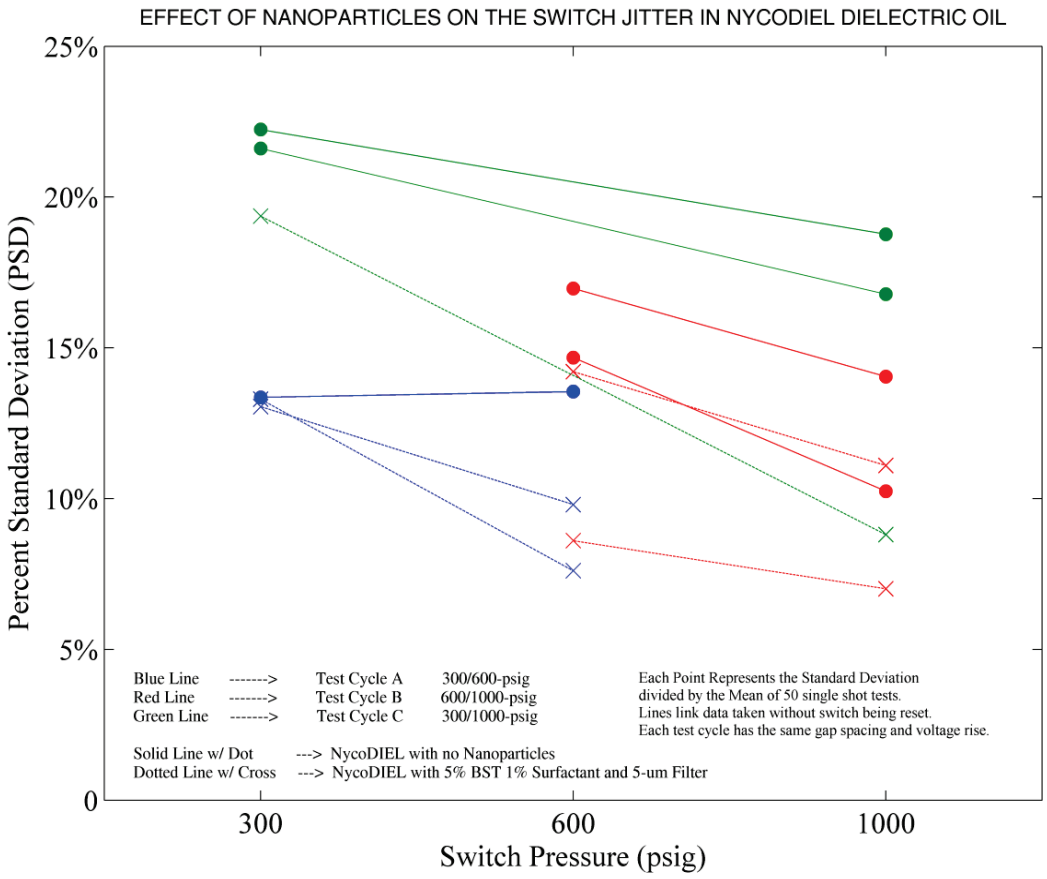

Figure 7.11: The percent standard deviation of the breakdown voltage is shown at different pressures for Nycodiel with (x) and without (o) BST particles and surfactant. The colors indicate the pressure runs summarized in Table 2.

The introduction of particle BST into a commercially available PAO conforming to a military standard for insulating oils has unequivocally reduced the percent standard deviation of the voltage at which breakdown occurs by several percent. These findings suggest that the BST particles, the surfactant, or a combination of the particles and surfactant are acting to reduce the breakdown variability. The localized enhancement effect coupled with an increased bound-charge storage capacity of the BST particles may be assisting the electro-thermal energy conversion process near the electrode. On the other hand, the surfactant chemistry may be introducing ionic compounds that can strongly influence the surface chemistry at the anode and cathode. The next section studies the effects of the surfactant upon the breakdown properties so that this effect, if it exists, may be optimized for a given system.

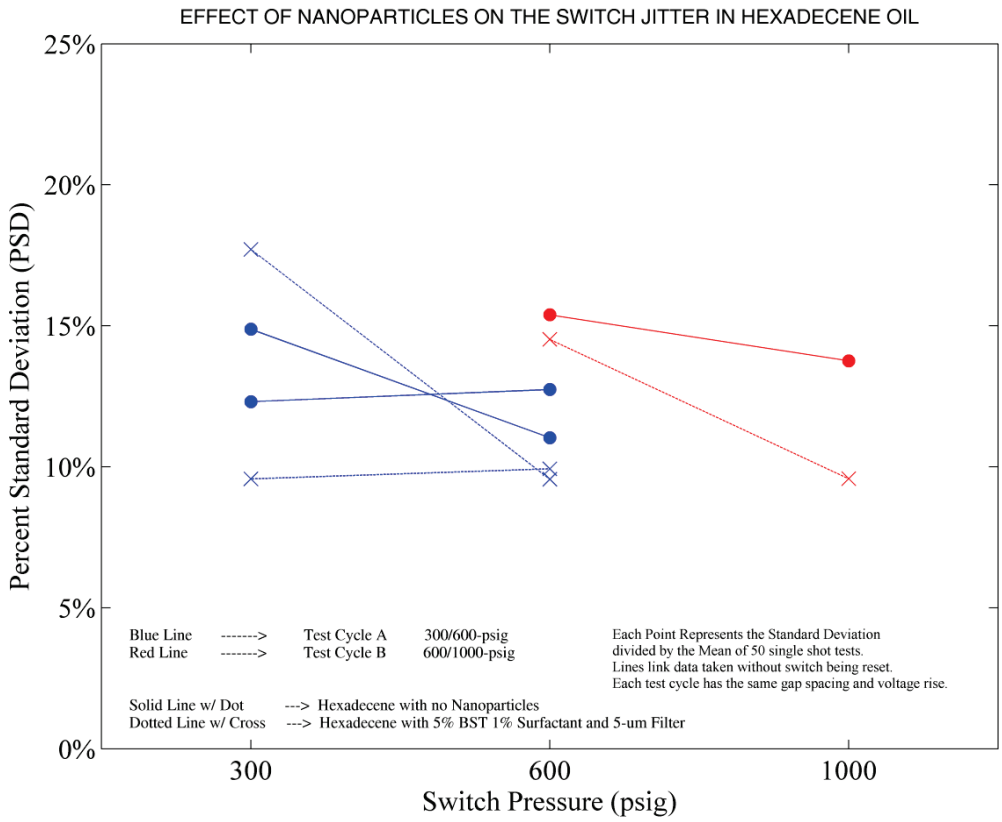

Figure 7.12: The percent standard deviation of the breakdown voltage is shown at different pressures of 1-Hexadecene with (x) and without (o) BST particles and surfactant. The colors indicate the pressure run summarized in Table 2.

To determine if the apparent jitter reduction in PAO oil could be found in other oils, particles were added to generic 1-Hexadecene. The 1-Hexadecene is then tested for breakdown jitter on the HVADTS system with the same setup as the Nycodiel PAO. The results of figure 7.13 indicate that at super-critical pressures the particle-infused 1-Hexadecene exhibits reduced jitter. However, the jitter reduction is not as pronounced as it is with the Nycodiel. At 600 psig and 1000 psig the particle-infused 1-Hexadecene out-performed the control group by several percent. The high jitter value of the particle-infused oil at 300 psig can possibly be attributed to a clogged filter generating an unacceptably high concentration of carbon byproducts.

One factor that is minimized, but not controlled, is the total dissolved water in the sample oils. Water concentration, as mentioned previously, is a significant factor in establishing a well-defined breakdown voltage. The particles/surfactant introduce a significant concentration of free water to the oils, possibly contributing to jitter performance.

7.4 Results of Varied Electrode Surfaces at 1.2 mm Gap Spacing

This section investigates the contribution of the surfactant and the contribution of particles to the reduction of jitter seen in the previous test cycles. The gap spacing is reduced to 1.2 mm to increase the ratio of field protrusion height to the total gap spacing. It is thought that a smaller gap spacing may increase the influence that field enhancements on the electrode surface have on breakdown jitter. This is suggested by gap-narrowing effect seen in the simulations.

The effect of rough and smooth electrode surfaces is also tested in this cycle. Photographs of the two surfaces are shown in figure 5.1. The smooth electrode surface is generated by a figure-8 polishing procedure with 1200 grit sandpaper and the rough electrode surface is generated by a sandblaster. After a testing sequence, the smooth electrode is sanded by hand to eliminate any macroscopic field enhancement before being inserted back into the switch. Any carbon residue generated by the discharges is removed with acetone prior to testing. The electrodes have a one inch diameter and are constructed of 17-4PH stainless steel that has been precipitation hardened to C38 Rockwell hardness.

Rep-rate oil switches are typically paired with a high pressure and high flow rate oil circulation systems. The collapsing arc channel following a breakdown event produces hydrogen bubble byproducts [44]. These byproducts influence subsequent breakdown performance and must be removed from the electrode gap. Flowing oil at high pressure has been shown to reduce jitter by suppressing the magnitude of the bubble oscillation period and increasing the rate of bubble absorption [46]. During this test cycle the oil is tested at 0, 300, 600, and 1000 psig at a static flow to mimic and optimize the high-pressure conditions found in a rep-rate switch. Between shots, the oil is circulated through a 3 μm filter to remove the carbon byproducts.

Nycodiel PAO and alkylbenzene are the two base oils employed. The three oil configurations utilized are pure oil, oil with 1% surfactant by weight, and oil with 5% BST and 1% surfactant by weight. It is not possible to test the BST without the surfactant, as the BST quickly drops out of the oil without the application of a surfactant. The oil is prepared with the sonication and filtering techniques described in chapter 3. The surfactant utilized with the Nycodiel PAO is PB-184 developed by Chemax Inc. The PB-184 is a POE Olyel phosphate or Poly(oxy-1, 2-ethanediyl), alpha-9-octadecenyl-omega-hydroxy-(2)-phosphate. The surfactant utilized with the

Alkylate 225 alkylbenzene is Biosoft S-101 developed by Stepan Co. Biosoft S-101 is a Alkylbenzenesulfonic acid or Alkyl(C10-16)benzenesulfonic acid with 2% alkylbenzene + 1.3% sulfuric acid [34, 35].

It is demonstrated through electrostatic simulation that high-K particles increase the fields on the surface of the electrodes. It is thought that the interactions between the field enhancements on the surface of the electrode, particles near the surface of the electrode, and particles in the bulk of the oil contribute to the apparent jitter-reduction. This research investigates this possible theory.

Additional data is recorded and listed in table 3 for all the remaining tests in this dissertation. The 30 conditioning shots taken at 300 psig before the base tests and the 100 post shots taken at 50 psig after the completion of the base tests are recorded and listed in table 3. The particle concentrations (by weight) acquired from the drying method as well as water concentration measurements are included in table 3 as well.

Also new to the remaining tests, a second breakdown is initiated following the first breakdown at a 1 Hz frequency. No oil recirculation or filtration is attempted between the two shots. The mean breakdown voltage and PSD of the second shot provides useful information regarding the effect the breakdown byproducts generated by the first shot has on any subsequent discharges. All of the even number figures in the rest of the dissertation refer to the data from the first shot and all odd numbered figures correspond to their second shot counterparts.

These results will show that there is a significant interaction between pressure, water concentration, gap spacing and particle concentration on the self-break jitter of the oils tested.

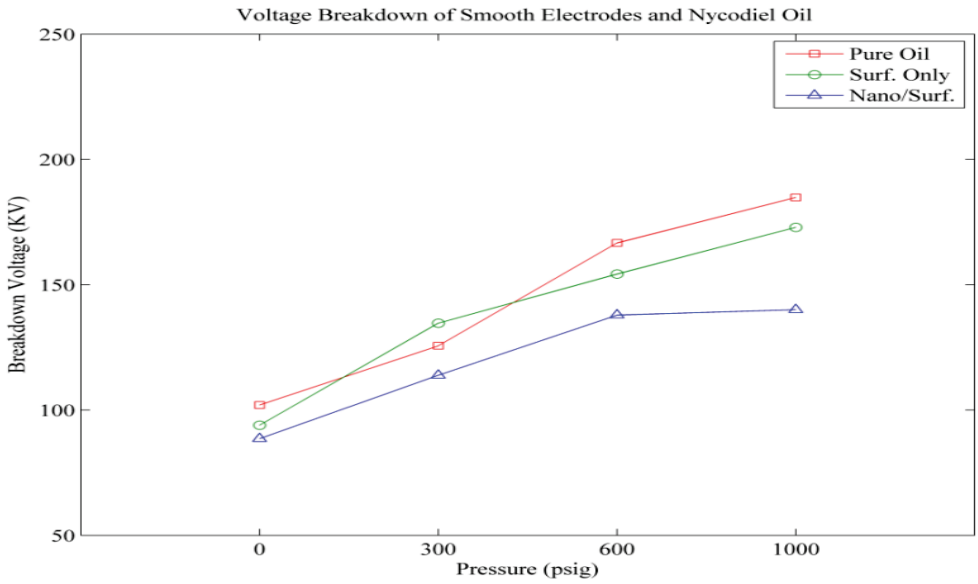

Figure 7.13: The first shot mean voltage breakdown with smooth electrodes and Nycodiel oil results indicate an increasing breakdown voltage with increasing oil pressure. The oil with a surfactant and particle suspension has a slightly lower breakdown voltage.

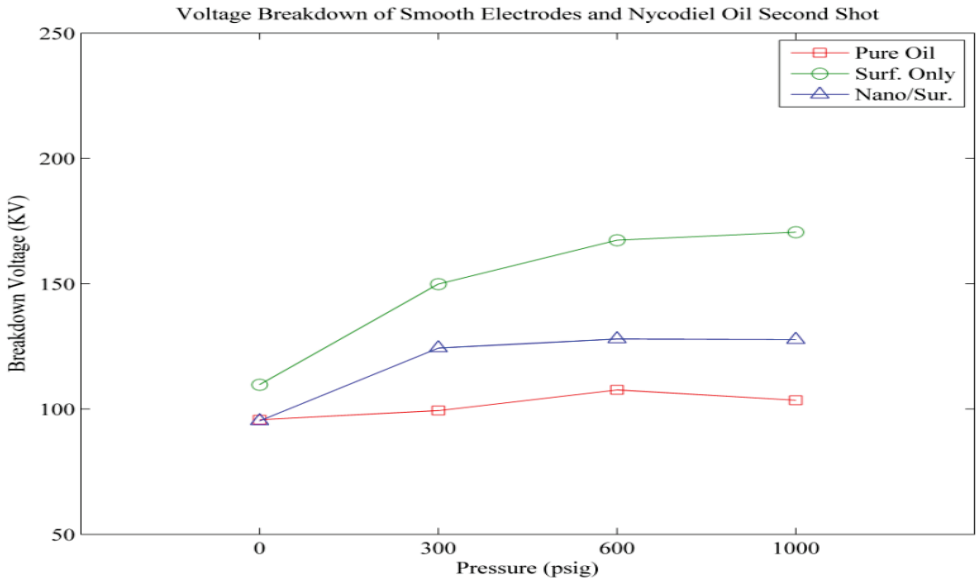

Figure 7.14: The second shot mean voltage breakdown with smooth electrodes and Nycodiel oil results indicate an increasing breakdown voltage with increasing oil pressure between 0 and 300 psig. The increase of the mean breakdown voltage after 300 psig is not as apparent compared to the results of the first shot. The pure oil demonstrates the lowest mean breakdown voltage.

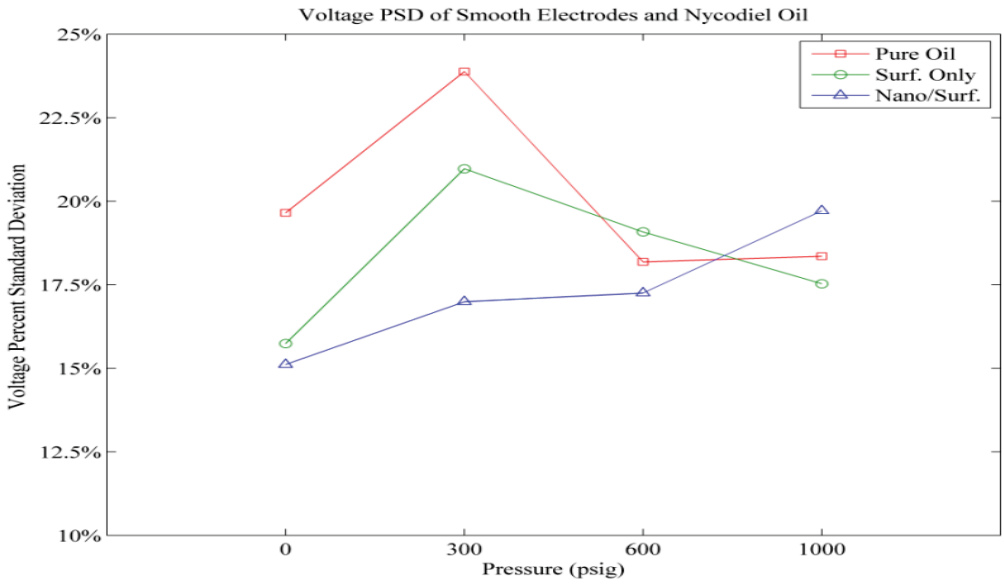

Figure 7.15: The first shot percent standard deviation (jitter) with smooth electrodes and Nycodiel oil results indicate a lower jitter associated with the oil with a surfactant and particle suspension at the lower pressures. At 1000 psig the oil with surfactant only has the lowest jitter.

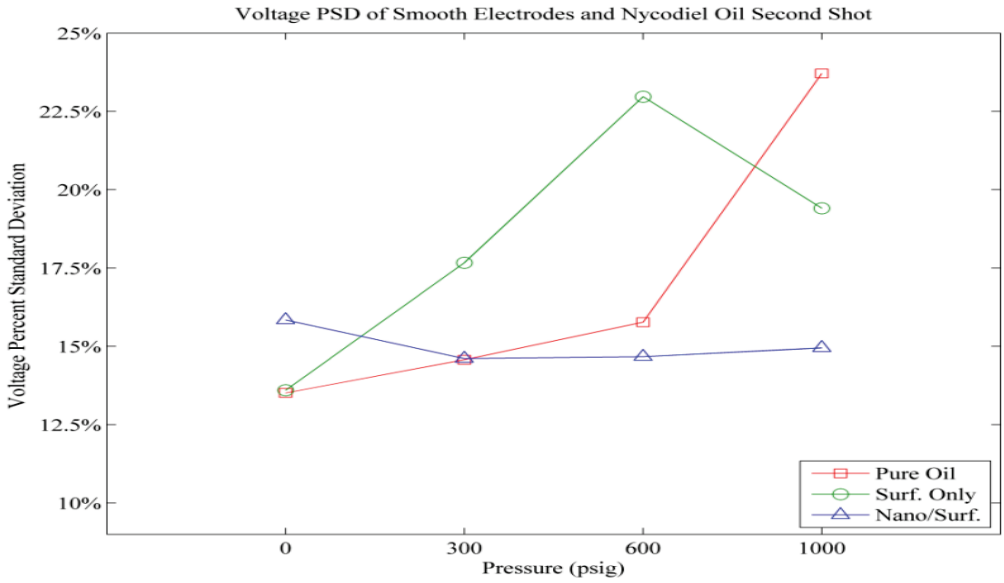

Figure 7.16: The second shot percent standard deviation (jitter) with smooth electrodes and Nycodiel oil results indicate a lower jitter associated with the oil with a surfactant and particle suspension at pressures higher than 300 psig. The surfactant only oil demonstrates high jitter at pressures greater than 0 psig. The pure oil demonstrates high jitter at 1000 psig.

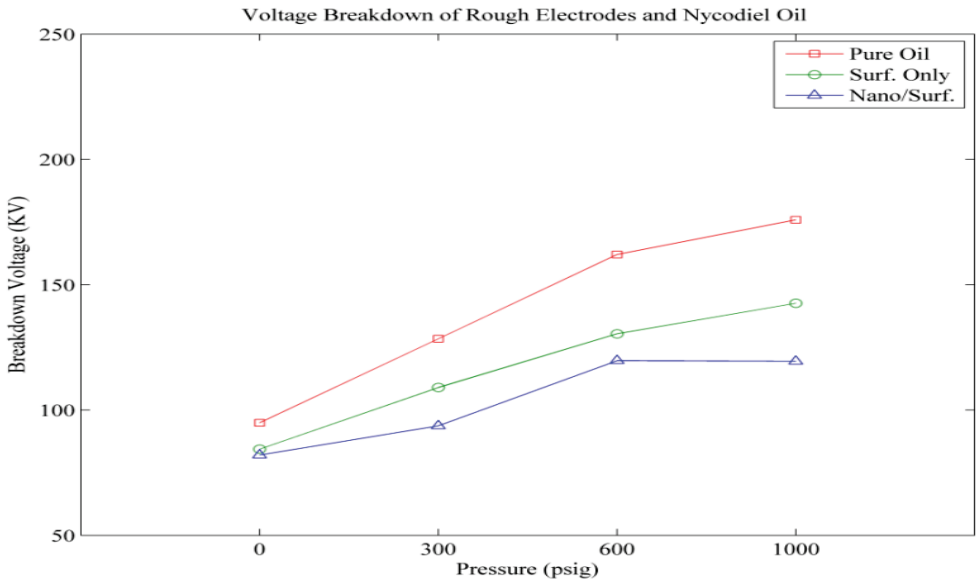

Figure 7.17: The first shot mean voltage breakdown with rough electrodes and Nycodiel oil results indicate an increasing breakdown voltage with increasing oil pressure. The oil with a surfactant and particle suspension has a slightly lower breakdown voltage.

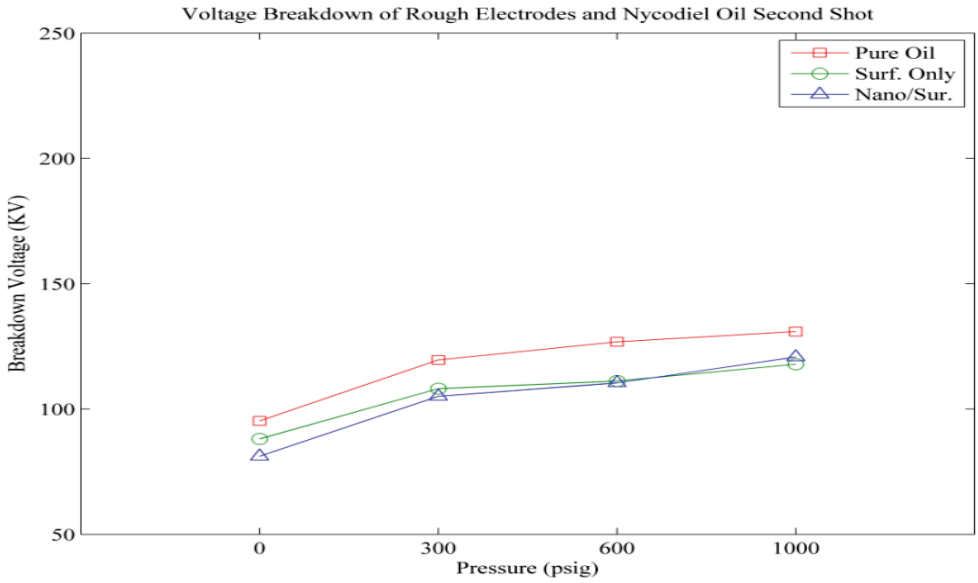

Figure 7.18: The second shot mean voltage breakdown with rough electrodes and Nycodiel oil results indicate an increasing breakdown voltage with increasing oil pressure between 0 and 300 psig. The increase of the mean breakdown voltage after 300 psig is not as apparent compared to the results of the first shot. The pure oil demonstrates the highest mean breakdown voltage.

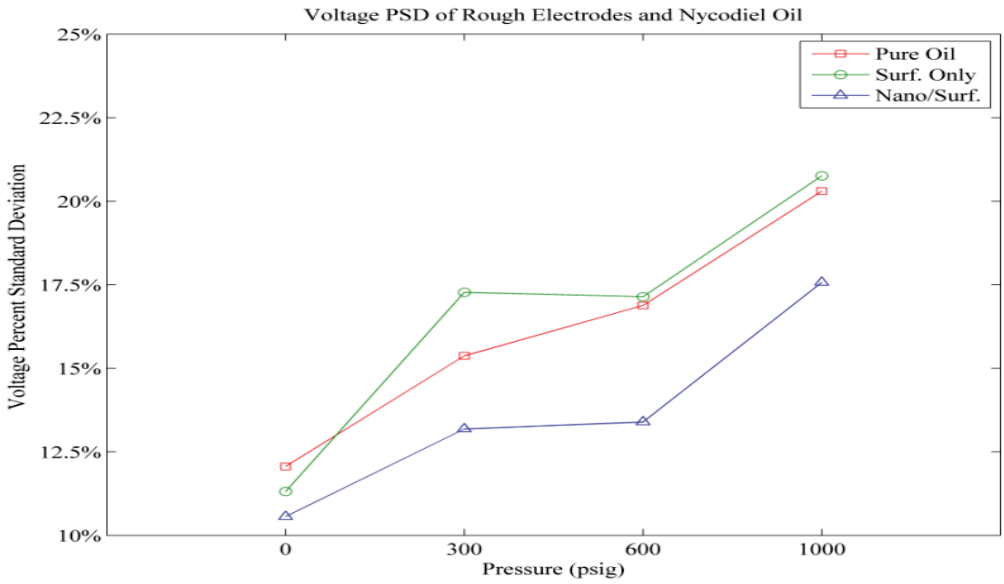

Figure 7.19: The first shot percent standard deviation (jitter) with rough electrodes and Nycodiel oil results indicate a lower jitter associated with the oil with a surfactant and particle suspension at all pressures. The oil with a surfactant and particle suspension has the most significant jitter improvement at 600 psig.

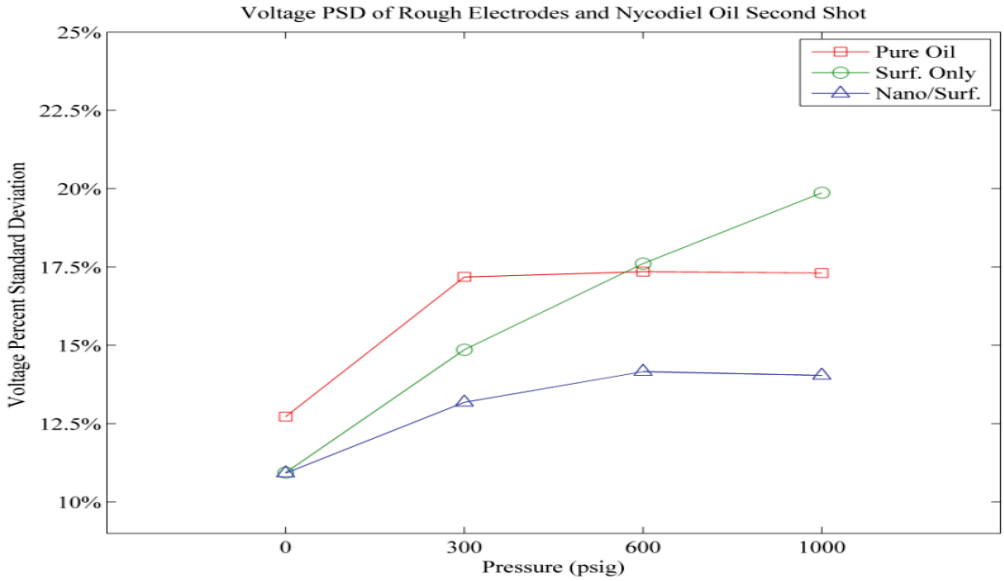

Figure 7.20: The second shot percent standard deviation (jitter) with rough electrodes and Nycodiel oil results indicate a lower jitter associated with the oil with a surfactant and particle suspension at all pressures. The surfactant only oil demonstrates high jitter at 1000 psig. The pure oil demonstrates high average jitter across at all pressures.

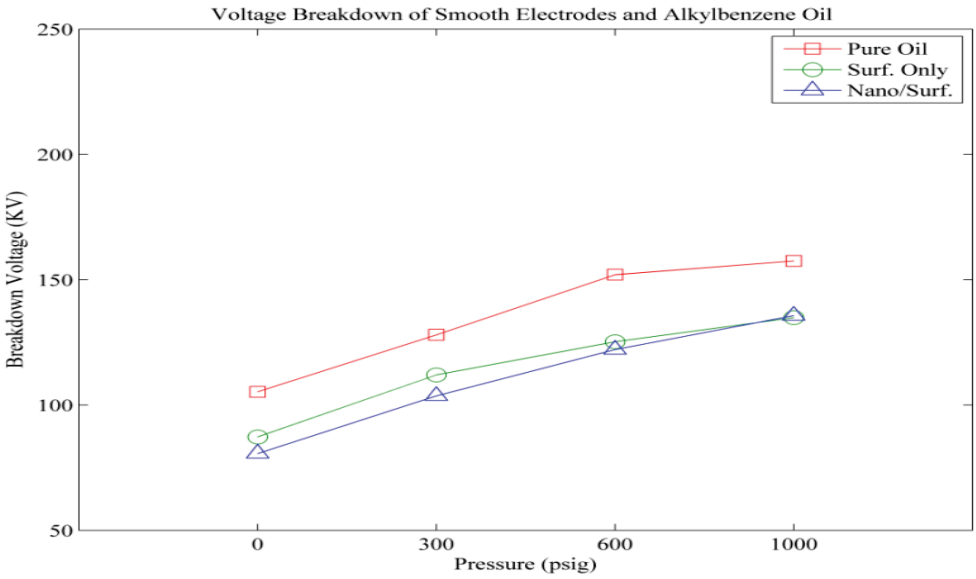

Figure 7.21: The first shot mean voltage breakdown with smooth electrodes and alkylbenzene oil results indicate an increasing breakdown voltage with increasing oil pressure. The oil with a surfactant and particle suspension has a slightly lower breakdown voltage.

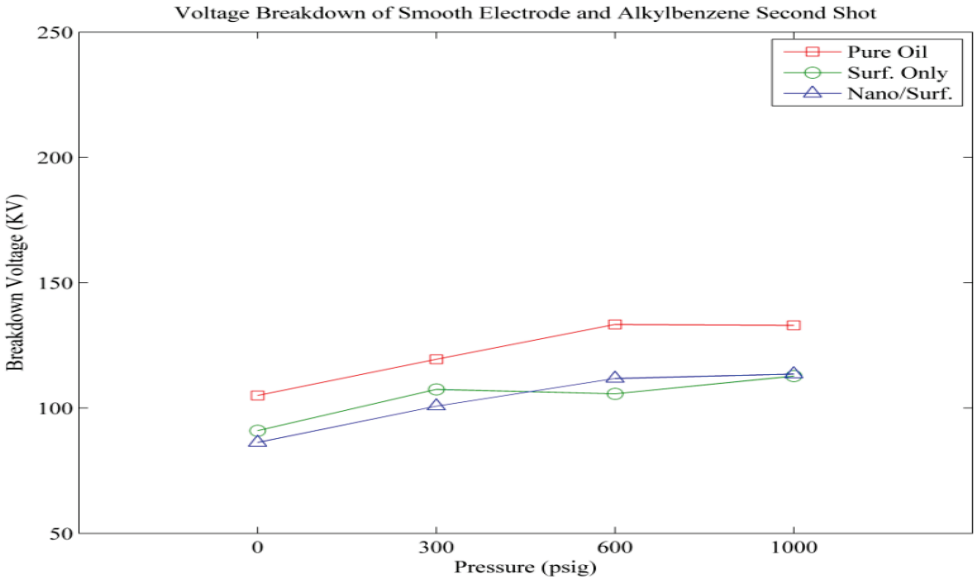

Figure 7.22: The second shot mean voltage breakdown with smooth electrodes and alkylbenzene oil results indicate a slightly increasing breakdown voltage with increasing oil pressure. The increase of the mean breakdown voltage after 600 psig is not as apparent compared to the results of the first shot. The pure oil demonstrates the highest mean breakdown voltage.

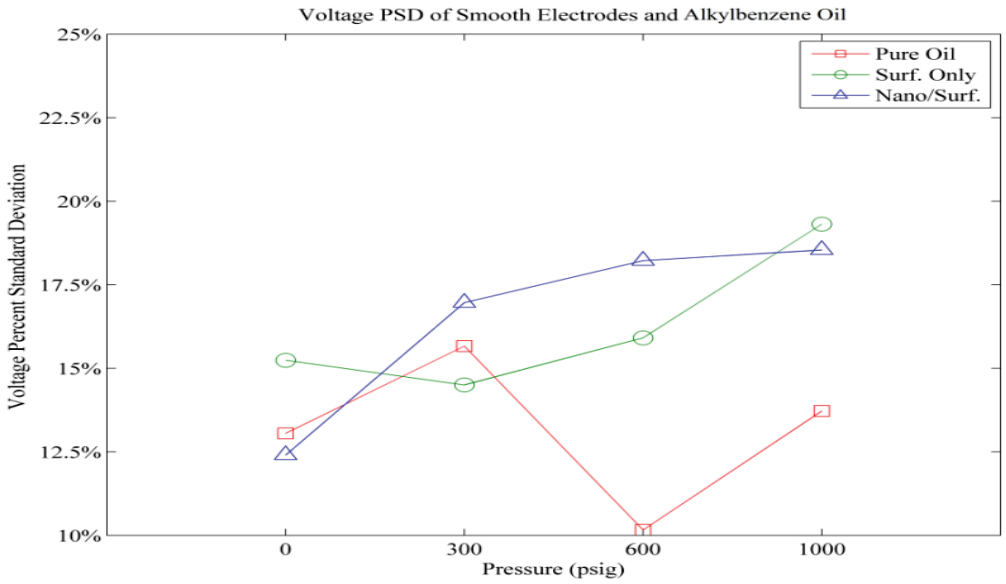

Figure 7.23: The first shot percent standard deviation (jitter) with smooth electrodes and alkylbenzene oil results indicate a lower jitter associated with the oil with a surfactant and particle suspension at 0 psig. At 600 and 1000 psig the pure oil demonstrates significantly lower jitter.

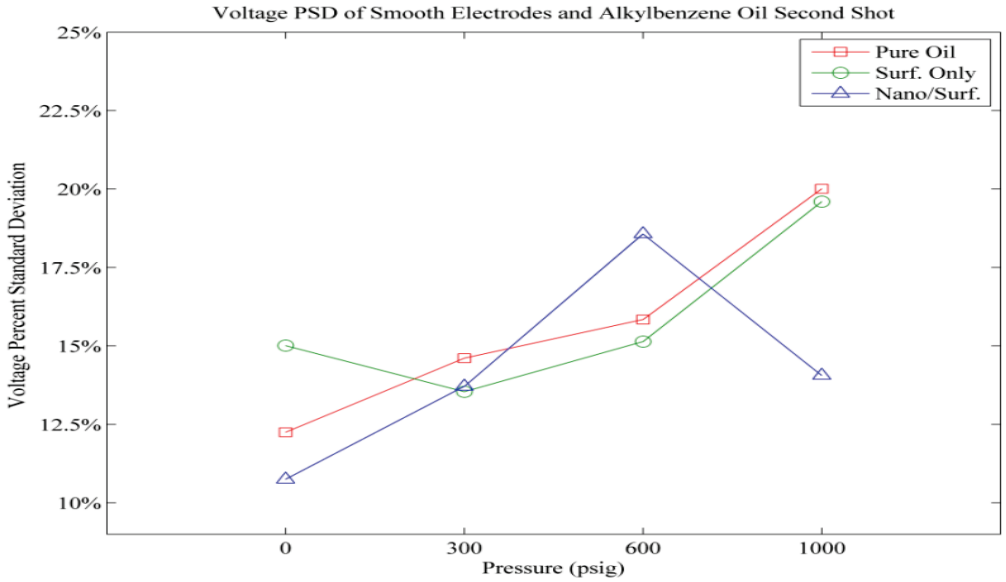

Figure 7.24: The second shot percent standard deviation (jitter) with smooth electrodes and alkylbenzene oil results indicate a lower jitter associated with the oil with a surfactant and particle suspension at pressures of 0 and 1000 psig. The pure oil and surfactant only oil demonstrate similar jitter at all pressures.

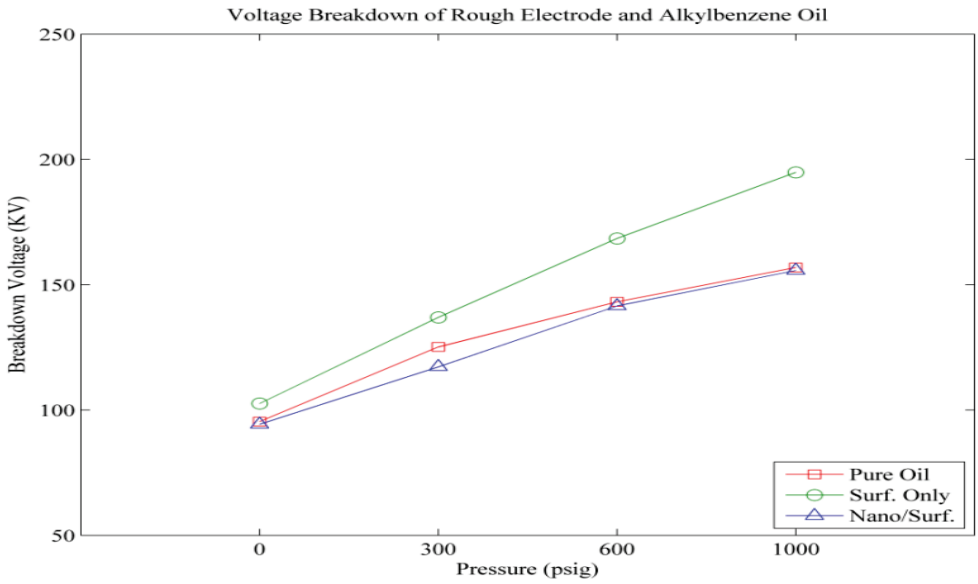

Figure 7.25: The first shot mean voltage breakdown with rough electrodes and alkylbenzene oil results indicate an increasing breakdown voltage with increasing oil pressure. The pure oil and the oil with a surfactant and particle suspension has a similar breakdown trend.

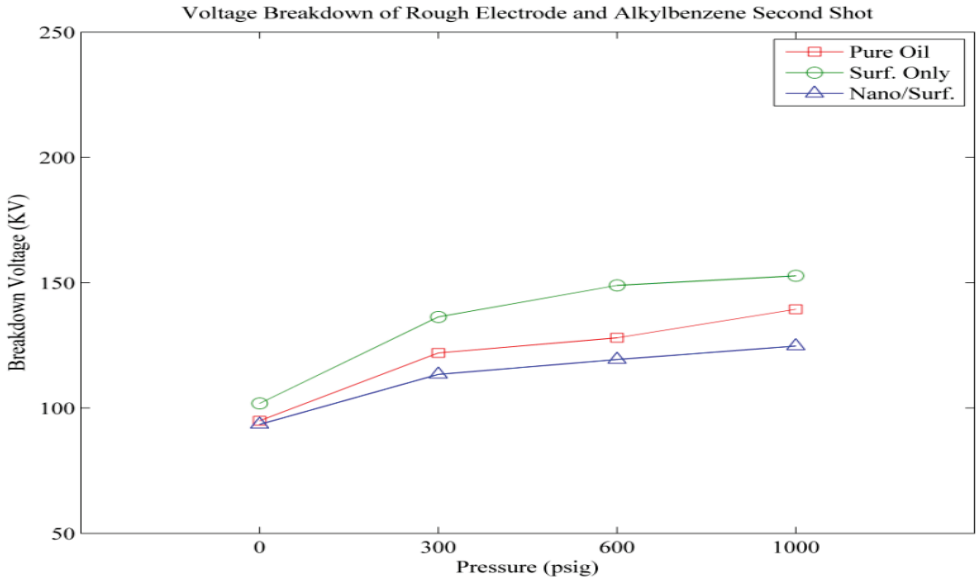

Figure 7.26: The second shot mean voltage breakdown with rough electrodes and alkylbenzene oil results indicate a slightly increasing breakdown voltage with increasing oil pressure. The surfactant only oil demonstrates the highest mean breakdown voltage.

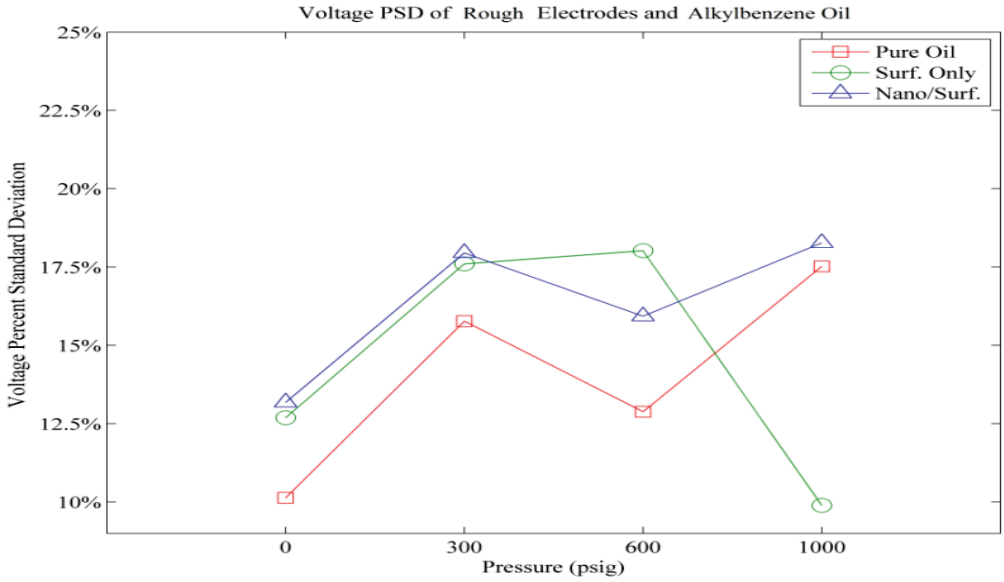

Figure 7.27: The first shot percent standard deviation (jitter) with rough electrodes and alkylbenzene oil results indicate a lower jitter associated with the pure oil at the lower pressures. The surfactant only oil demonstrates the lowest jitter at 1000 psig.

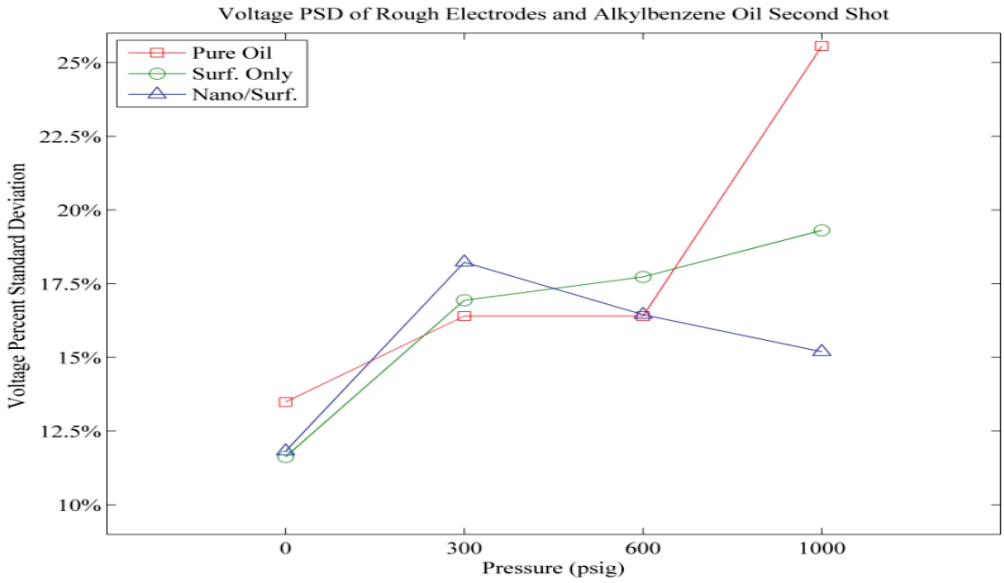

Figure 7.28: The second shot percent standard deviation (jitter) with rough electrodes and alkylbenzene oil results indicate a similar jitter trend for the three oils, except for the pure oil at 1000 psig which demonstrates significantly higher jitter at 1000 psig. The surfactant and particle oil demonstrates the lowest jitter at 1000 psig.

The results from figures 7.14 through 7.29 indicate that utilizing rough electrodes reduces the switch jitter and mean breakdown voltage in nearly every case. The rough electrode surface also generates better trends in the breakdown behavior. Comparing the results of figures 7.16 and 7.20 and figures 7.24 to 7.28, it is apparent that the rough electrode surface produces more consistent jitter values. The experimental, simulation and optical profilometer data all suggest that a smooth electrode surface produces higher rates of jitter than a rough electrode surface. On a smooth electrode surface, a breakdown event can occur on either a smooth or deformed section of the electrode. If the breakdown occurs on a smooth section, the electrons require a higher voltage to emit due to limited enhancement in that area. If the breakdown occurs on a rough section of the smooth electrode, the electrons would not require as much voltage to emit due to field enhancement; and the breakdown can occur at a lower voltage. This combination of high and low breakdowns over a 100-shot test cycle on a smooth surface produces higher jitter.

On a rough electrode surface no smooth surfaces exist, so there is negligible probability that a breakdown will initiate on a smooth surface. As such, the breakdown must initiate on an enhancement. This theory is supported by the experimental data which indicates a lower mean breakdown and jitter for rough electrodes compared to smooth electrodes. This is possibly the reason we are seeing lower jitter when utilizing the rough electrodes.

The differences between the first and second shot are quite apparent. The mean breakdown voltage at 0 psig is similar between the first and second shot, but at pressures greater than 0 psig the breakdown voltages of the first shot are much higher. The jitter is typically worse on the second shot, except in some cases with the particle-infused oils at all pressures and all the oils at higher pressures. It is possible that the particles could be acting to hide the carbon byproducts, in effect diminishing their effect on breakdown jitter [36].

The jitter-reducing effect of the particles is apparent in the Nycodiel PAO and less evident in the alyklbenzene. Table 3 suggests that the surfactant increases the water concentration of the oils by nearly 10x compared to the pure oils. The pure Nycodiel and alkylbenzene has water concentrations of 18.5 and 46.7 μg/mL, respectively; while the particle-infused Nycodiel and alyklbenzene has water concentrations of 99.99 and 453.31 μg/mL, respectively. The extremely high water concentrations in the particle-infused alkylbenzene may have influenced the PSD of the tests.

7.5 Results of a Rough Electrode Surfaces and 2.0 mm Gap Spacing

In this test cycle the gap spacing is expanded to 2 mm to test the effect of a widened gap-spacing on breakdown jitter. The lowest overall jitter attained is 5.01% with a pure alkylbenzene, a rough electrode surface, a gap spacing of 2 mm, a water concentration of 65.88 µg/mL and a pressure of 200 psig. Interestingly, the second highest overall jitter of 5.39% is the second shot of this same configuration. The lowest jitter for the particle-infused alkylbenzene is 8.22% during the same cycle at 200 psig, however the water content is found to be 421.38 µg/mL.

The lowest jitter attained with the Nycodiel PAO is 7.62% with a particle concentration of 1.9%, a rough electrode surface, a gap spacing of 2 mm and a pressure of 100 psig. Unfortunately, the titrator was offline so the water concentration is unknown. However, previous results indicate that the water concentration would have been between 100 and 150 µg/mL. This is further evidence of the need to maintain low water concentrations throughout switch testing.

The 2 mm test utilizes pressures of 0, 100, 200 and 300 psig. Higher pressures cannot be tested because of the voltage limitations of the HVADTS system. All of the 2 mm data is attained with rough electrode surfaces. The particle-infused Nycodiel demonstrates much lower jitter than the pure Nycodiel. The particle-infused Nycodiel with 1.5% surfactant did not perform as well as the particle-infused Nycodiel, possibly due to the higher water concentration associated with the higher percentage of surfactant.

It is obvious from these results that widening the gap spacing to 2 mm significantly decreases the breakdown jitter. As the gap spacing is widened, the ratio of the height of the electrode surface deformation to the overall gap spacing decreases possibly decreasing the impact that the field enhancement has on breakdown jitter.

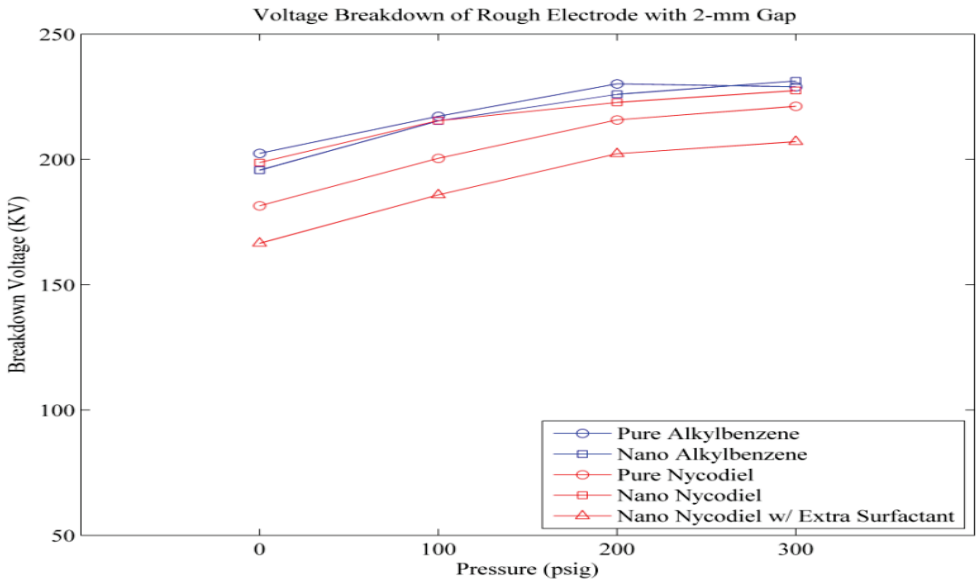

Figure 7.29: The first shot mean voltage breakdown with rough electrodes and two oils at the 2 mm gap spacing results indicate an increasing breakdown voltage with increasing pressure. The Nycodiel pure oil and Nycodiel with particles and extra surfactant demonstrates a lower breakdown voltage.

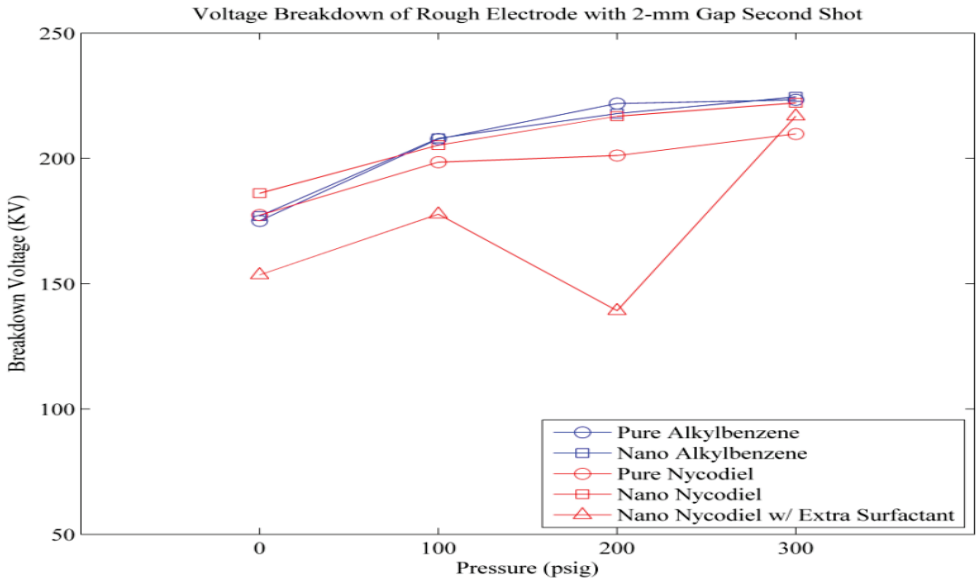

Figure 7.30: The second shot mean voltage breakdown with rough electrodes and two oils at the 2 mm gap spacing results indicate an increasing breakdown voltage with increasing pressure. The Nycodiel oil with particles and extra surfactant demonstrates the lowest breakdown voltages, especially at 200 psig.

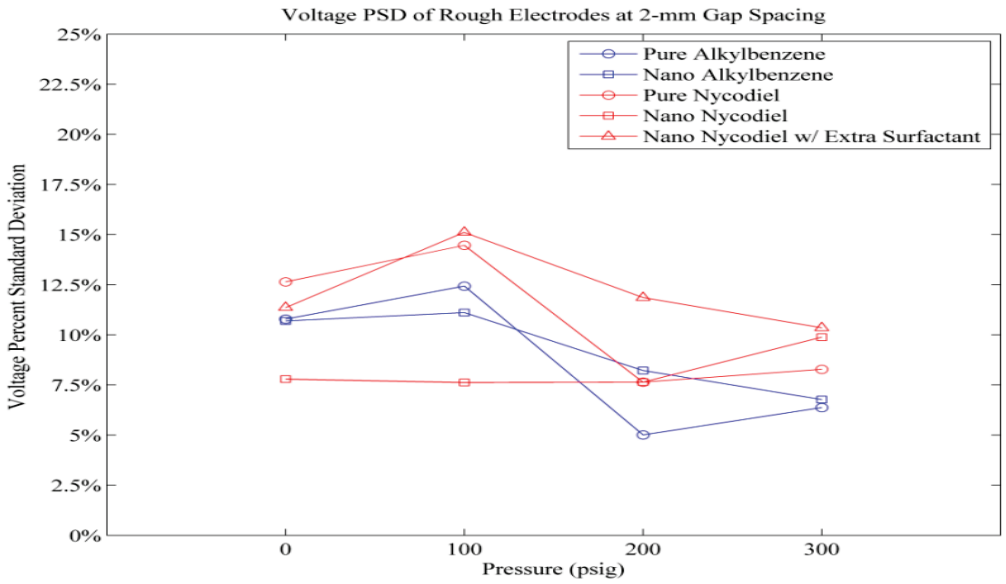

Figure 7.31: The first shot percent standard deviation (jitter) with rough electrodes and two oils at the 2 mm gap spacing results indicate lower jitter by the Nycodiel oil with particles and surfactant at all pressures. The alkylbenzene pure oil demonstrates slightly lower jitter at higher pressures. The Nycodiel oil with particles and extra surfactant demonstrates the highest jitter performance.

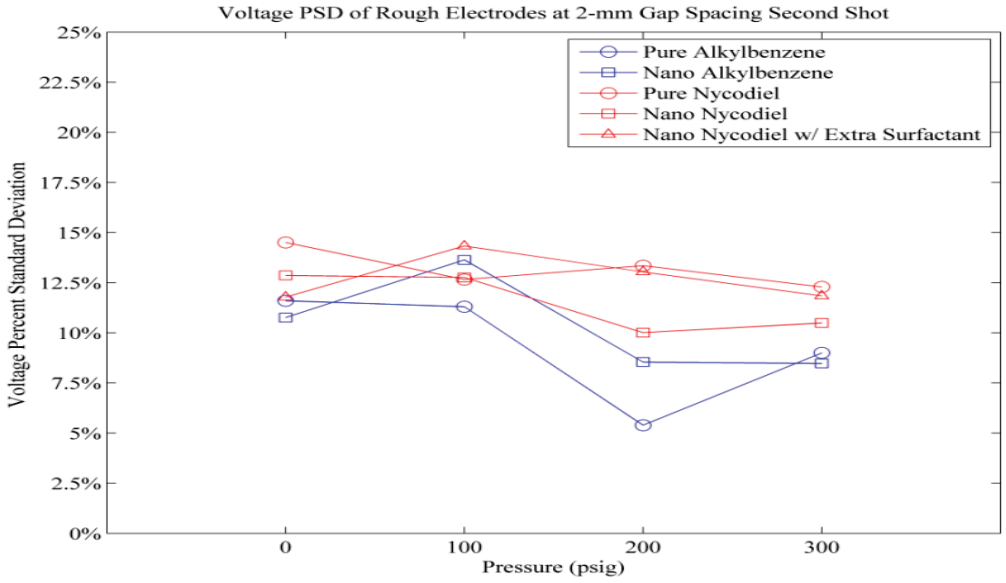

Figure 7.32: The second shot percent standard deviation (jitter) with rough electrodes and two oils at the 2 mm gap spacing results indicate similar jitter performance with all the Nycodiel oils with the Nycodiel oil with particles and surfactant demonstrating slightly lower jitter. The pure alkylbenzene oil demonstrates lower jitter than the alkylbenzene oil with particles and surfactant.

7.6 Results of additional Testing with 1.6 mm Gap Spacing

The University of Missouri – Columbia has been working over the past couple of years sponsored by a research grant. The goal of the venture is to develop, test and commercialize an oil-based dielectric switching medium. The METSS Corporation is well-known for their skill and expertise in developing oils, greases and lubricants for various hydraulic and lubricant applications and has provided many of the oils.

The test cycles utilize a gap spacing of 1.6 mm and rough electrode surfaces. The oils provided by METTS, the DF oils, are not sparged with dry nitrogen prior to testing. A new surfactant called Atlox 4914 is provided by the METSS Corporation. The particle-infused Nycodiel incorporating the Atlox has fair jitter performance when sparged prior to testing, however the high viscosity of the surfactant makes it difficult to filter effectively. The particles quickly clog the filter. When the filter was taken apart the particles were found "caked" onto the filter. The Pb-184 has a much lower viscosity than the Atlox 4914 and does not clog the filter.

The oils demonstrate nearly identical mean breakdown voltages across all pressure with the exception of the Nyco w/ BST & Atlox 4914 (2). The reason for this discrepancy is unknown as a water concentration measurement was not possible due to the titrator being offline. The second shot mean breakdown values are nearly identical for all the oils across all pressures.

The particle-infused oils tend to produce lower jitter values during the test cycle than the other oils. The best performing oil is Nyco w/ BST & Pb-184 (2) (Resparged). Special care is taken to remove as much water as possible from the Nyco w/ BST & Pb-184 (2) (Resparged) oil as well as from the HVADTS oil reconditioning circuit The oil is sparged with dry nitrogen for 120 minutes at 20 scfh and the HVADTS oil reconditioning circuit is sparged with dry nitrogen at 90 scfh for 10 minutes. The results indicate low jitter at all pressures as well as the lowest water concentration achieved in a particle-infused oil post-test of 61.72 µg/mL. Developing a system to maintain even lower water concentrations during operation will further reduce the self-break jitter.

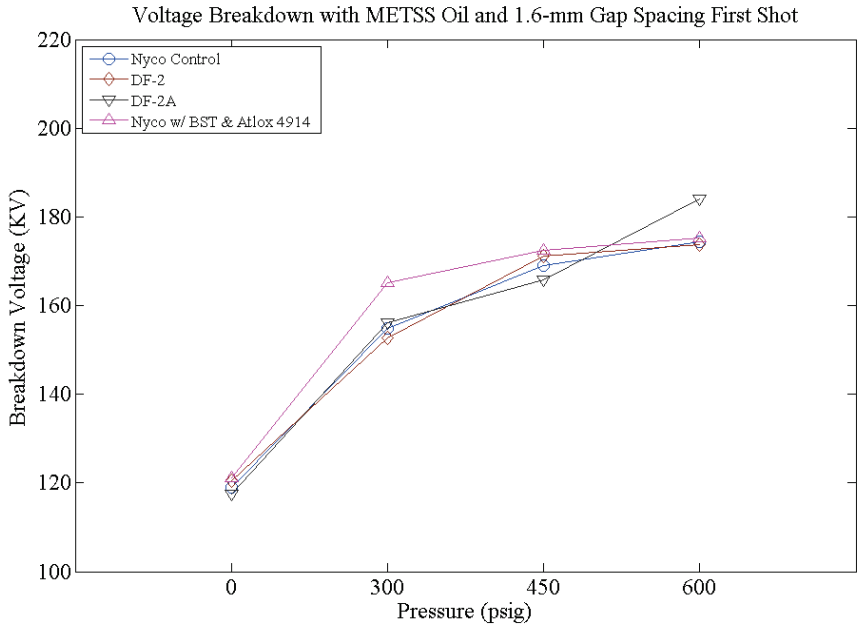

Figure 7.33A: The first shot mean breakdown voltage with rough electrodes results indicate higher breakdown voltages with increasing pressure. The Nyco w/ BST & Atlox 4914 (2) demonstrates a slightly lower breakdown voltage than the other oils.

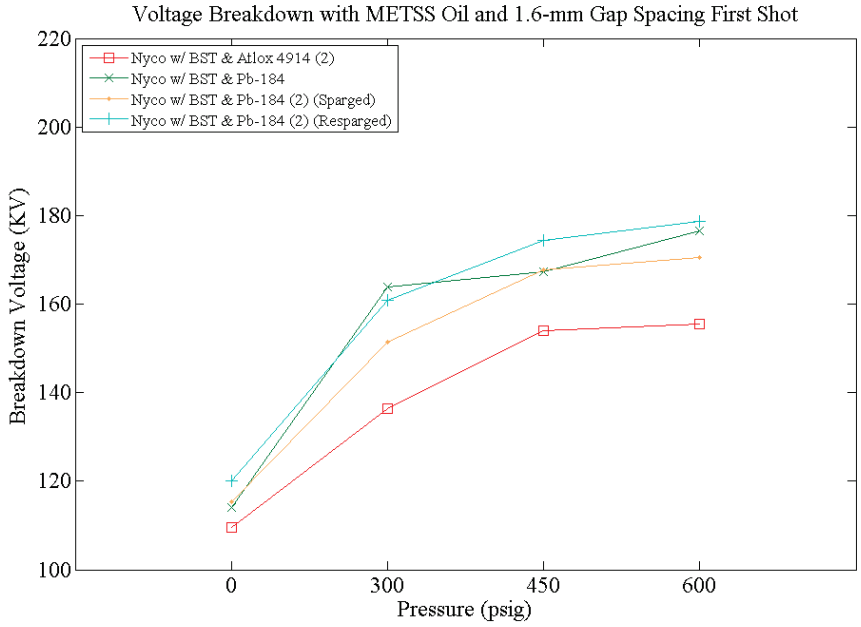

Figure 7.33B: The first shot mean breakdown voltage with rough electrodes results indicate higher breakdown voltages with increasing pressure. The Nyco w/ BST & Atlox 4914 (2) demonstrates a slightly lower breakdown voltage than the other oils.

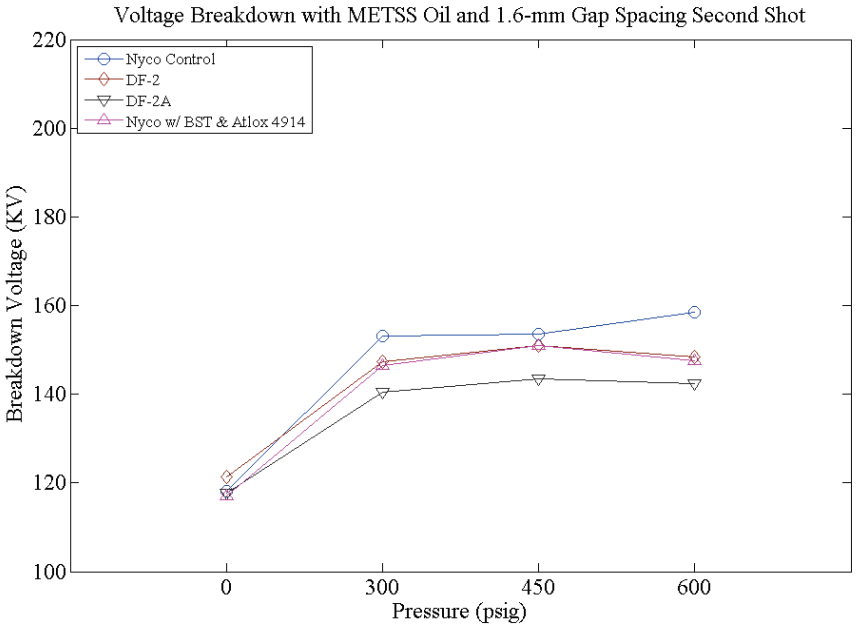

Figure 7.34A: The second shot mean breakdown voltage with rough electrodes results indicate an increasing breakdown voltage with increasing oil pressure between 0 and 300 psig. There is no apparent increase in breakdown voltage after 300 psig.

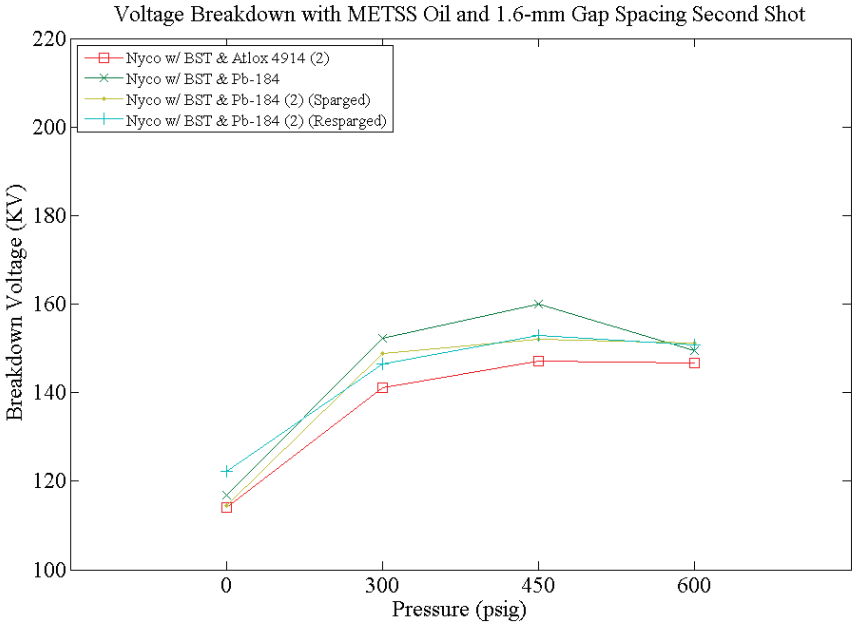

Figure 7.34B: The second shot mean breakdown voltage with rough electrodes results indicate an increasing breakdown voltage with increasing oil pressure between 0 and 300 psig. There is no apparent increase in breakdown voltage after 300 psig.

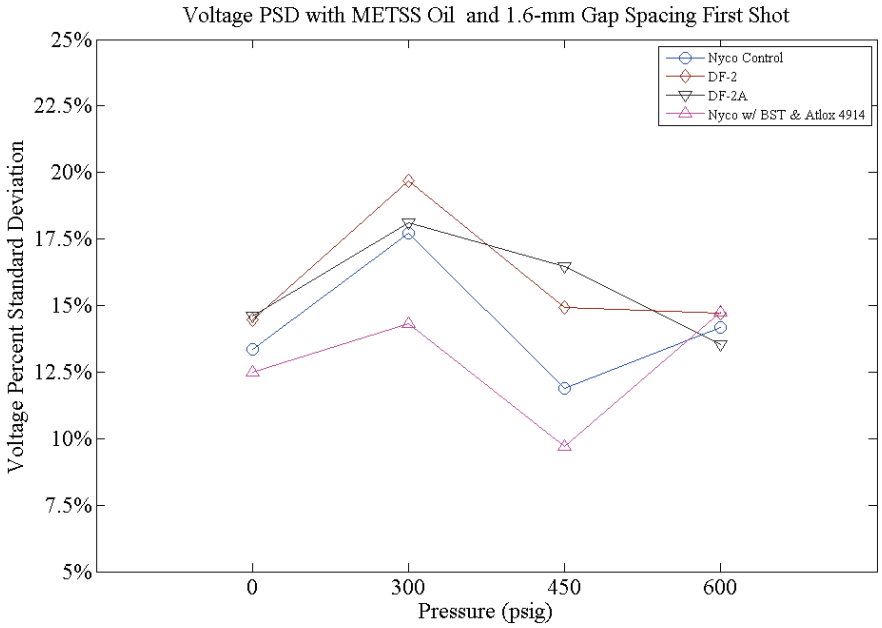

Figure 7.35A: The first shot percent standard deviation (jitter) with rough electrodes and METSS oil results indicate that the oils with particles and surfactant demonstrate the lowest jitter. In particular, the Nyco w/ BST & Pb-184 (2) (Resparged) and Nyco w/ BST & Atlox 4914 demonstrate low jitter values.

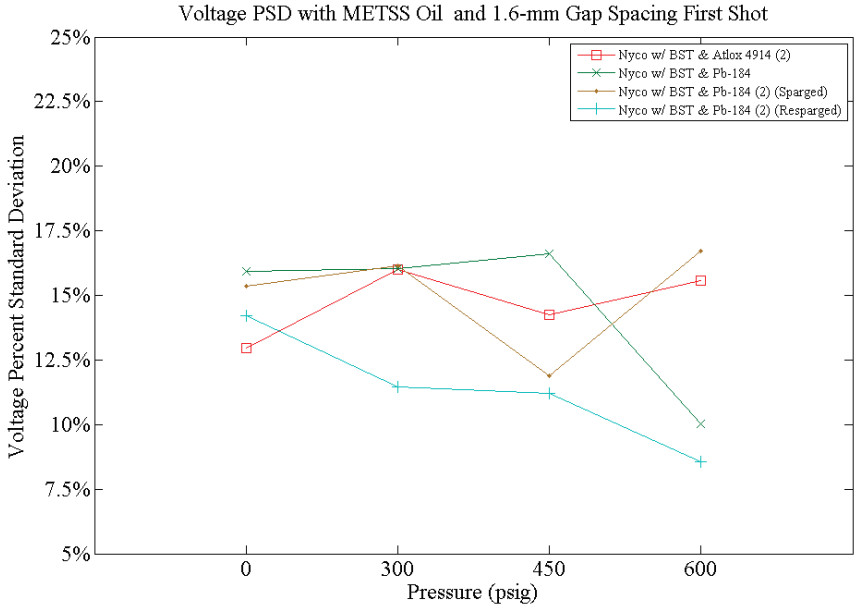

Figure 7.35B: The first shot percent standard deviation (jitter) with rough electrodes and METSS oil results indicate that the oils with particles and surfactant demonstrate the lowest jitter. In particular, the Nyco w/ BST & Pb-184 (2) (Resparged) and Nyco w/ BST & Atlox 4914 demonstrate low jitter values.

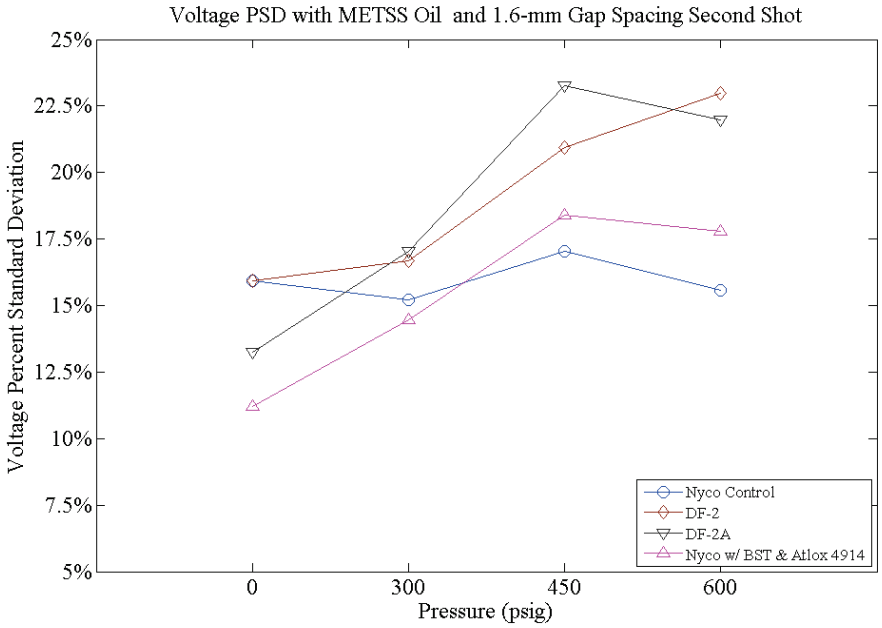

Figure 7.36A: The second shot percent standard deviation (jitter) with rough electrodes and METSS oil results indicate increasing jitter with increasing pressure. The Nyco Control and Nyco w/ BST & Pb-184 demonstrate the most stable jitter behavior across the pressures.

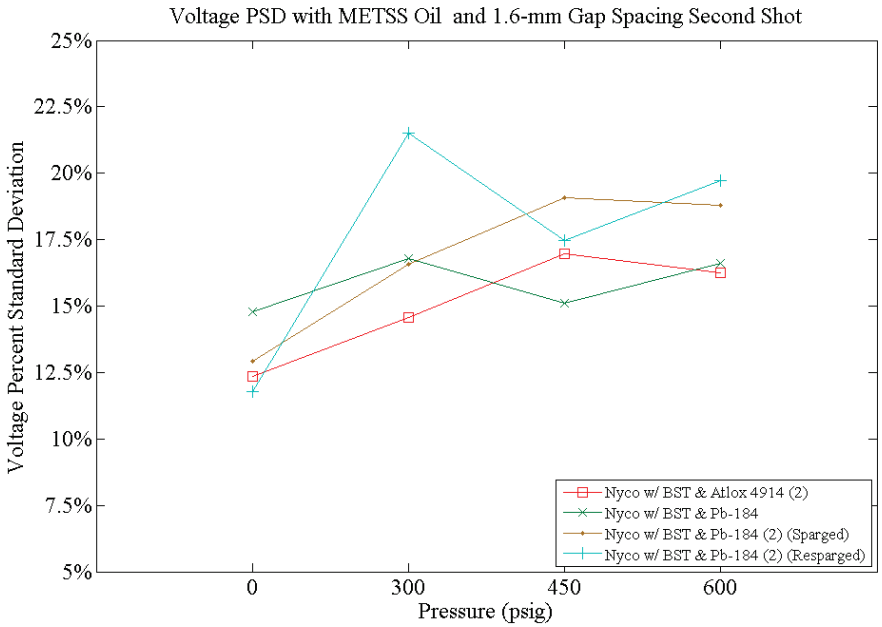

Figure 7.36B: The second shot percent standard deviation (jitter) with rough electrodes and METSS oil results indicate increasing jitter with increasing pressure. The Nyco Control and Nyco w/ BST & Pb-184 demonstrate the most stable jitter behavior across the pressures.

7.7 Conditioning and Post-Shot Data

Table 3 lists the mean breakdown voltage and PSD (jitter) of the conditioning and post-test breakdowns. The conditioning procedure consists of 30 breakdowns at 300 psig taken at 1 Hz prior to actual testing. There is no filtering between shots. The conditioning process allows development of ionic and deformation processes on the electrode surface prior to the actual tests to prevent conditioning drift in the data. Averaging across the mean breakdown and PSD values of the conditioning shots with regard to gap spacing gives the following values: 117.27 KV and 15.27% at 1.2 mm gap spacing, 139.7 KV and 15.25% at 1.6 mm gap spacing and 207 KV and 10.21% at 2.0 mm gap spacing. It is clear that the mean breakdown increases with increasing gap spacing with jitter decreasing between gap spacing of 1.6 and 2.0 mm. The particle-infused oils tend to produce the lower jitter values in most cases. The lowest jitter values of 5.8 and 8.6% are observed in the particle-infused oils at 2.0 mm gap spacing.

The post-test procedure consists of 100 breakdowns at 50 psig taken at 1 Hz after actual testing. There is no filtering between shots. Averaging across the mean breakdown and PSD values of the post-test shots with regard to gap spacing gives the following values: 132.15 KV and 11.49% at 1.6 mm gap spacing and 187.73 KV and 12.62% at 2.0 mm gap spacing. There is no post-test data for the 1.2 mm gaps spacing. The results from table 1 suggest that there is negligible difference in PSD and breakdown between the pure oils and the particle-infused oils. The high carbon concentration could possibly be acting to mitigate the jitter-reducing effect of the particles. This is further evidence of the importance of carbon filtration between shots.

Table 3. Additional Oil Data					Conditioning Data		Post Data							
					30 shots 300 psig		100 shots 50 psig		Water Conc. (µg/mL)			Particle Concentration %		
Oil	Additives	Gap (mm)	Electrode	Filter (µm)	Mean (KV)	PSD (%)	Mean (KV)	PSD (%)	PreSparge	PreTest	PostTest	Pretest	PostTest	Sparge Time (min)
DF-3	X	1.6	Smooth	1	X	X	X	X	X	X	X	X	X	X
DF-9	X	1.6	Smooth	1	X	X	X	X	X	41.65	X	X	X	X
DF-14	X	1.6	Smooth	1	X	X	X	X	X	17.39	X	X	X	X
DF-16	X	1.6	Smooth	1	X	X	X	X	X	22.78	X	X	X	X
DF-1	X	1.6	Smooth	1	X	X	X	X	X	X	X	X	X	X
NycoDiel	X	1.6	Rough	1	139.79	9.91	131.16	10.52	X	X	X	X	X	X
DF-2	X	1.6	Rough	1	137.89	14.63	125.47	12.43	X	X	X	X	X	X
DF-2A	X	1.6	Rough	1	136.04	15.49	128.98	12.8	X	X	X	X	X	X
NycoDiel	5% BST 1% Atlox 4914	1.6	Rough	3	142.29	13.99	126.04	10.81	X	X	X	1.01	0.4	X
NycoDiel	5% BST 1% Atlox 4914	1.6	Rough	3	150.78	15.87	131.48	11.61	X	X	X	3.6	2.6	X
NycoDiel	5% BST 1% PB-184	1.6	Rough	3	141.66	19.82	128.55	10.66	X	208.88	218.23	2.2	1.9	X
NycoDiel	5% BST 1% PB-184	1.6	Rough	3	131.37	12.6	157.96	12.35	167.17	39.67	136.89	2.3	2.1	50
NycoDiel	5% BST 1% PB-184	1.6	Rough	3	137.77	19.69	127.57	10.77	125.05	45	61.72	0.93	0.84	120
ABeAA	Alkylbenzene	1.2	Smooth	3	114.74	15.18	X	X	43.78	6.63	53.01	X	X	X
ABeBA	Alkylbenzene	1.2	Rough	3	114.86	15.78	X	X	32.22	3.83	46.67	X	X	X
ABeAB	Alkylbenzene w/ 1% Biosoft	1.2	Smooth	3	104.86	14.29	X	X	294.56	186.52	291.87	X	X	30
ABeBB	Alkylbenzene w/ 1% Biosoft	1.2	Rough	3	117.93	18.13	X	X	415.57	216.11	451.91	X	X	30
ABeCA	Alkylbenzene w/ 1% Biosoft 5% BST	1.2	Smooth	3	121.51	17.35	X	X	785.81	150.72	394.27	2.08	1.75	30
ABeCB	Alkylbenzene	1.2	Rough	3	120.54	11.57	X	X	1096.17	157.68	453.31	1.34	1.04	30

	w/ 1% Biosoft 5% BST													
NycoAA (Fail)	NycoDiel	1.2	Smooth	3	X	X	X	X	X	X	X	X	X	X
NycoAA	NycoDiel	1.2	Smooth	3	110.85	10.92	X	X	10.85	5.24	18.5	X	X	X
NycoBA	NycoDiel	1.2	Rough	3	97.17	21.5	X	X	9.78	3.72	23.42	X	X	X
NycoAB	NycoDiel w/ 1% Pb184	1.2	Smooth	3	143.84	19.43	X	X	81.9	5.46	102	X	X	40
NycoBB	NycoDiel w/ 1% Pb184	1.2	Rough	3	108.91	16.56	X	X	69.96	7.15	156.4	X	X	30
NycoCA	NycoDiel w/ 1% Pb184 5% BST	1.2	Smooth	3	138.2	11.24	X	X	89.18	13.51	95.31	0.75	X	20
NycoCB	NycoDiel w/ 1% Pb184 5% BST	1.2	Rough	3	113.08	14.28	X	X	96.42	11.9	99.09	X	0.47	20
	2mm Data: pressures at 0 100 200 300													
ABeDA	Alkylbenzene	2	Rough	3	213.81	9.25	194.13	10.68	52.68	24.2	65.88	X	X	30
ABeDB	Alkylbenzene w/ 1% Biosoft 5% BST	2	Rough	3	225.24	5.8	197.37	15.04	375.39	99.51	421.38	1.34	1.27	30
NycoDA	NycoDiel	2	Rough	3	205.53	13.2	187.21	12.74	39.07	24.2	65.88	X	X	30
Nyco2DB	NycoDiel w/ 1% PB-184 5% BST	2	Rough	3	221.82	8.6	200.29	11.46	X	X	X	X	1.9	30
NycoDB	NycoDiel w/ 2% PB-184 5% BST	2	Rough	3	172.04	14.21	159.68	13.18	137.77	43	X	X	2.2	30

References

[31] R. Curry, K. MacDonald, J. Leckbee and P. Norgard, "Development of high power, high pressure, rep- rate, liquid dielectric switches," *14th International Pulsed Power Conference,* 2003.

[32] C. Yeckel, R. Curry and P. Norgard, "Pulsed breakdown characterization of oil dielectrics for high-power switching applications," *28th International Power Modulator Conference*, 2008.

[33] M.L. Horry, G.L. Donovan, J.E. Potter, and D.D. Bloomquist, "Z-Facility dielectric oil cleanup," *12th International Pulsed Power Conference*, Monterey CA, 1999.

[34] Chemax Corporation, Pb-184 Surfactant, MSDS, 2011.

[35] Stephan Corporation, Biosoft-S101, MSDS, 2011.

[36] M. Krins, H. Borsi and E. Gokenbach, "Influence of carbon particles on the breakdown voltage of transformer oil," *International Conference on Conduction and Breakdown in Dielectric Liquids*, Rome, Italy, July 15 - 19, 1996.

[37] METSS Corporation, 2011.

CHAPTER 8

CONCLUDING REMARKS

8.1 DISCUSSION

After several years of working to reduce the self-break jitter of oil switches it is apparent that there is no simple solution. There are many factors and interactions that must be considered when investigating methods to reduce jitter. My research indicates that four variables may be more significant: particle concentration, water concentration, gap spacing, and electrode surface roughness. The data suggests that the lowest switch jitter could be attained in a rep-rate flowing-oil system if a particle-infused PAO oil dielectric with a particle concentration greater than 1% flows freely through a 3 μm filter at a large (>2 mm) gap spacing with rough electrodes and a water concentration less than 10 μg/mL.

Widening the gap spacing beyond 2 mm would require an overhaul of the switch system to accommodate a higher voltage pulse. A gap space of 4 mm would require a pulse of nearly 500 KV. Developing a particle-infused oil dielectric that generates no sedimentation would require a more sophisticated technique to fragment the particles into smaller agglomerations. Maintaining a water concentration of less than 10 μg/mL during switch operation would require a water removal system installed as part of the reconditioning system. A rough electrode surface would automatically be generated by the breakdown arcs; however, as the shot count increases the filter pore size must decrease to prevent accumulation of carbon byproducts. There is a necessary trade-off between the high-k particle size and carbon accumulation.

Other aspects of the switch, such as electrode materials, rate of voltage rise and oil temperature were not investigated. A series of breakdowns on an electrode material other than stainless steel may generate a different electrode surface profile than the current profile resulting

in dissimilar breakdown behavior. However, if a series of breakdowns generate a similar surface profile as seen on our electrodes, the difference in breakdown behavior would be negligible. Other researchers have indicated breakdown jitter decreases with increasing rate of voltage rise. It is quite probable that their findings would translate to our system. As the rate of rise of the electric field increases, the average breakdown strength increases. Several additional references are available regarding breakdown in oil [38-44].

The viscosity of an oil dielectric is proportional to its temperature. The lower viscosity oil, or oil at a higher temperature, would phase partition to a vapor/gas at a higher rate producing lower breakdown jitter. Not much is known regarding the temperature effect on oils in pulsed conditions; however, there have been some publications in the 60 Hz breakdown regime [38, 39].

The effect of pressure on breakdown jitter, though thoroughly investigated, is still highly unknown. From the results, the lowest jitter value is typically observed at 0 psig; however this is not always the case. Despite the rigorous treatment of pressure as a testing variable, it is necessary to continue testing at different pressures. The hydrostatic pressure on a liquid has long been known to affect its average breakdown electric field strength [40]. This is a result of the increase in electrical energy that must be supplied to the liquid to overcome the mechanical energy of the applied hydrostatic pressure. The phenomenon accounts for the shape of the relationship between average breakdown strength and hydrostatic pressure, however it is not clear if this particular phenomenon plays any role in the establishment of breakdown jitter. On the other hand, the increased pressure may result in a 'pressure broadening' effect, in which the increased number of collisions due to the increased pressure results in a spreading of the energy [41]. This broadening effect may be partially responsible for the breakdown jitter.

The lowest jitter attained with the Nycodiel PAO is 7.62% with a particle concentration of 1.9%, a rough electrode surface, a gap spacing of 2 mm and a pressure of 100 psig. Unfortunately, the titrator was offline so the water concentration is unknown. However, previous results indicate that the water concentration would have been between 100 and 150 μg/mL. Reducing this water concentration to less than 10 μg/mL would no doubt improve results.

The lowest overall jitter attained is 5.01% with a pure alkylbenzene, a rough electrode surface, a gap spacing of 2 mm, a water concentration of 65.88 μg/mL and a pressure of 200

psig. Interestingly, the second highest overall jitter of 5.39% is the second shot of this same configuration. The lowest jitter for the particle-infused alkylbenzene is 8.22% during the same cycle at 200 psig, however the water content is found to be 421.38 μg/mL. A system to reduce water levels in the particle-infused oils to less than 10 μg/mL during switch operation is vital to mitigating switch jitter.

8.2 Summary and Proposed Future Work

The tests conducted demonstrate statistically significant data that clearly indicates the capacity of suspensions of particle BST to improve the relative variation in breakdown electric field of insulating oil. Specifically, concentrations of BST particles of up to 5% (by weight) have been shown to decrease the PSD of the breakdown electric field by several percent, producing a PSD of as low as 7% of the mean breakdown electric field strength. We are the first to demonstrate the efficacy of using BST particles to reduce switching jitter.

Our team has developed a sound methodology for incorporating particles into insulating oils. Utilizing high-voltage laboratory tests, several surfactants have been identified by the chemistry laboratory. The ongoing research into surfactant chemistry as well as enhanced methods of sonication may be brought to bear on the planned future studies of particle suspensions for increased dielectric quality.

Several research directions have been proposed to further reduce the self-break jitter of an oil switch. Widening the electrode gap spacing, enhancing the suspension characteristics of the particle-infused oil, maintaining low water concentration levels throughout switch operation and utilizing a rep-rate flowing oil test stand for experiments have been suggested as future thrusts for the current program.

References

[38] A. Nosseir, S. El-Debeiky, I. Hashad and H. A-Bary, "Effect of temperature on the breakdown probability of liquid dielectrics," *IEEE Transactions on Electrical Insulation*, Vol. EI-15, No. 6, December,1990.

[39] C. Yeckel, R. Curry and P. Norgard, "A comparison of the AC breakdown strength of new and used poly-α olefin coolant*", IEEE Transactions on Dielectric Electrical Insulation*, Vol. 14, pp. 820-824, August, 2007.

[40] K. C. Kao and J. B. Higham, "The effects of hydrostatic pressure, temperature, and voltage duration on the electric strengths of hyocarbon liquids," *Journal of the Electrochemical Society*, vol. 108(6), pp. 522–528, June 1961.

[41] N. Hodgson and H. Weber, Laser Resonators and Beam Propagation: Fundamentals, Advanced Concepts and Applications. New York, NY: Springer Science+Business Media, Inc., 2nd ed., 2005.

[42] H. Sueda and K. Kao, "Pre-breakdown phenomenon in high-viscosity dielectric liquids," *IEEE Transactions on Electrical Insulation*, Vol. EI-17, No.3, June, 1982.

[43] R. Romanets, V. Bolshakov, B. Dikarev and G. Karasev, "Electrophysical characteristics and testing of dielectric liquids," *ICDL*, Roma, Italy, 1996.

[44] P. Watson, W. Chadband and W. Mak, "Bubble growth following a localized electrical discharge and its relationship to the breakdown of triggered spark gaps in liquids," *IEEE Transactions on Dielectric Insulation*, EI-20, No. 2, 1985.

[45] J. Maksiejewski, "The breakdown process of a liquid trigatron," *IEEE Transactions on Dielectric Insulation*, Vol. 23, No. 2, 1988.

[46] S. Milton and A. Prosperetti, "Bubble dynamics and cavitation," *Annual Review of Fluid Mechanics*, Vol. 9, pp. 145-185, 1977.

[47] V. Shinet and M. Patel, "An evaluation of the gassing tendency under electrothermal stress of some dielectric liquids," *Journal of Lubrication Science*, Vol. 15, Iss. 3, 1998.

[48] F. Carraz, P. Rain and R. Tobazeon, "Particle initiated breakdown in a quasi-uniform field in transformer oil," *IEEE Transactions on Dielectrics and Electrical Insulation*, Dec. 1995.

Appendix

1A) Sample A: Nycodiel w/ 2.0% BST Concentration: New Oil

Size Distribution: Intensity

Size Distribution Report by Intensity
v2.0

Malvern

Sample Details

Sample Name: A Average
SOP Name: mansettings.nano
General Notes: UNIVERSITY OF MISSOURI
Nycodiel PAO Oil
DJ Particle Technology Labs PTL ID: 85544

File Name:	23236.dts	**Dispersant Name:**	Hexane
Record Number:	7	**Dispersant RI:**	1.375
Material RI:	1.59	**Viscosity (cP):**	0.2940
Material Absorbtion:	0.01	**Measurement Date and Time:**	Tuesday, September 06, 201...

System

Temperature (°C):	25.0	**Duration Used (s):**	70
Count Rate (kcps):	209.0	**Measurement Position (mm):**	4.65
Cell Description:	Glass cuvette with square aper...	**Attenuator:**	6

Results

			Diam. (nm)	% Intensity	Width (nm)
Z-Average (d.nm):	233.8	**Peak 1:**	239.3	100.0	77.88
PdI:	0.209	**Peak 2:**	0.000	0.0	0.000
Intercept:	0.917	**Peak 3:**	0.000	0.0	0.000

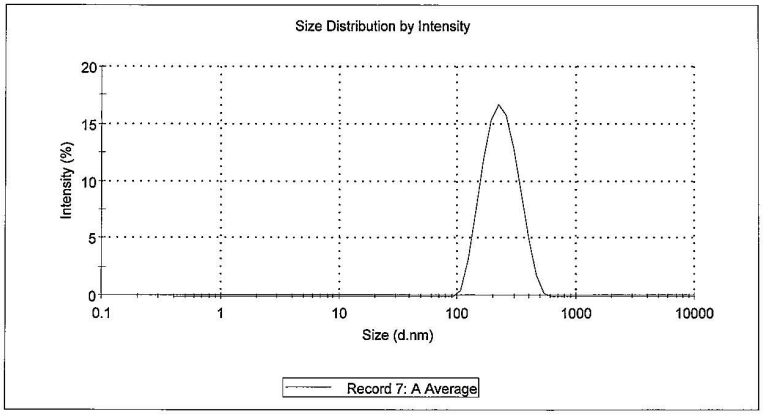

Malvern Instruments Ltd
www.malvern.com

Zetasizer Ver. 6.20
Serial Number : MAL500684

File name: 23236
Record Number: 7
06 Sep 2011 12:05:55 PM

1B) Sample A: Nycodiel w/ 2.0% BST Concentration: New Oil

Size Statistics: Intensity

Size Statistics Report by Intensity
v2.0

Malvern

Sample Details

Sample Name:	A Average
File Name:	23236.dts
SOP Name:	mansettings.nano
Measurement Date and Time:	Tuesday, September 06, 2011 9:47:34 AM

Z-Average (nm):	233.84	**Derived Count Rate (kcps):**	72611.8663920...
Standard Deviation:	0	**Standard Deviation:**	0
%Std Deviation:	0	**%Std Deviation:**	0
Variance:	0	**Variance:**	0

Size d.nm	Mean Intensity %	Std Dev Intensity %	Size d.nm	Mean Intensity %	Std Dev Intensity %	Size d.nm	Mean Intensity %	Std Dev Intensity %	Size d.nm	Mean Intensity %	Std Dev Intensity %
0.4000	0.0		5.615	0.0		78.82	0.0		1106	0.0	
0.4632	0.0		6.503	0.0		91.28	0.0		1281	0.0	
0.5365	0.0		7.531	0.0		105.7	0.5		1484	0.0	
0.6213	0.0		8.721	0.0		122.4	3.2		1718	0.0	
0.7195	0.0		10.10	0.0		141.8	7.5		1990	0.0	
0.8332	0.0		11.70	0.0		164.2	12.0		2305	0.0	
0.9649	0.0		13.54	0.0		190.1	15.4		2669	0.0	
1.117	0.0		15.69	0.0		220.2	16.7		3091	0.0	
1.294	0.0		18.17	0.0		255.0	15.8		3580	0.0	
1.499	0.0		21.04	0.0		295.3	12.9		4145	0.0	
1.736	0.0		24.36	0.0		342.0	8.9		4801	0.0	
2.010	0.0		28.21	0.0		396.1	4.9		5560	0.0	
2.328	0.0		32.67	0.0		458.7	1.9		6439	0.0	
2.696	0.0		37.84	0.0		531.2	0.3		7456	0.0	
3.122	0.0		43.82	0.0		615.1	0.0		8635	0.0	
3.615	0.0		50.75	0.0		712.4	0.0		1.000e4	0.0	
4.187	0.0		58.77	0.0		825.0	0.0				
4.849	0.0		68.06	0.0		955.4	0.0				

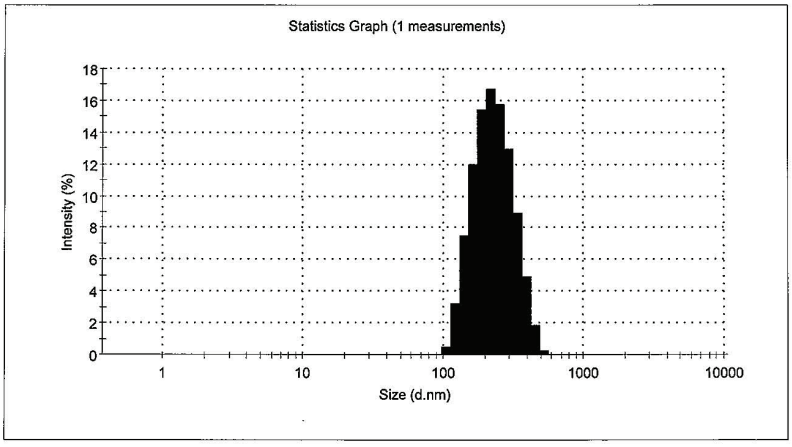

1C) Sample A: Nycodiel w/ 2.0% BST Concentration: New Oil
Size Distribution: Volume

Size Distribution Report by Volume
v2.0

Malvern

Sample Details

Sample Name: A Average
SOP Name: mansettings.nano
General Notes: UNIVERSITY OF MISSOURI
Nycodiel PAO Oil
DJ Particle Technology Labs PTL ID: 85544

File Name:	23236.dts	**Dispersant Name:**	Hexane
Record Number:	7	**Dispersant RI:**	1.375
Material RI:	1.59	**Viscosity (cP):**	0.2940
Material Absorbtion:	0.01	**Measurement Date and Time:**	Tuesday, September 06, 201...

System

Temperature (°C):	25.0	**Duration Used (s):**	70
Count Rate (kcps):	209.0	**Measurement Position (mm):**	4.65
Cell Description:	Glass cuvette with square ape...	**Attenuator:**	6

Results

			Diam. (nm)	% Volume	Width (nm)
Z-Average (d.nm):	233.8	**Peak 1:**	248.2	100.0	88.27
PdI:	0.209	**Peak 2:**	0.000	0.0	0.000
Intercept:	0.917	**Peak 3:**	0.000	0.0	0.000

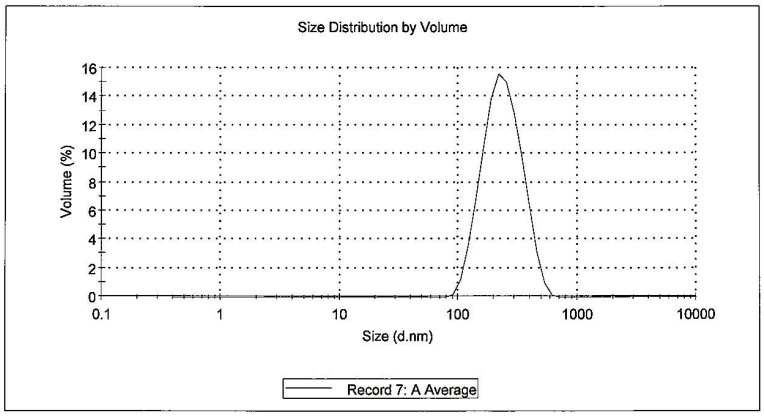

1D) Sample A: Nycodiel w/ 2.0% BST Concentration: New Oil
Size Statistics: Volume

Size Statistics Report by Volume
v2.0

Malvern

Sample Details

Sample Name:	A Average
File Name:	23236.dts
SOP Name:	mansettings.nano
Measurement Date and Time:	Tuesday, September 06, 2011 9:47:34 AM

Z-Average (nm):	233.84	**Derived Count Rate (kcps):**	72611.8663920...
Standard Deviation (nm):	0	**Standard Deviation (kcps):**	0
%Std Deviation:	0	**%Std Deviation:**	0
Variance:	0	**Variance:**	0

Size d.nm	Mean Volume %	Std Dev Volume %	Size d.nm	Mean Volume %	Std Dev Volume %	Size d.nm	Mean Volume %	Std Dev Volume %	Size d.nm	Mean Volume %	Std Dev Volume %
0.4000	0.0		5.615	0.0		78.82	0.0		1106	0.0	
0.4632	0.0		6.503	0.0		91.28	0.2		1281	0.0	
0.5365	0.0		7.531	0.0		105.7	1.3		1484	0.0	
0.6213	0.0		8.721	0.0		122.4	3.7		1718	0.0	
0.7195	0.0		10.10	0.0		141.8	6.9		1990	0.0	
0.8332	0.0		11.70	0.0		164.2	10.5		2305	0.0	
0.9649	0.0		13.54	0.0		190.1	13.9		2669	0.0	
1.117	0.0		15.69	0.0		220.2	15.6		3091	0.0	
1.294	0.0		18.17	0.0		255.0	15.0		3580	0.0	
1.499	0.0		21.04	0.0		295.3	12.8		4145	0.0	
1.736	0.0		24.36	0.0		342.0	9.8		4801	0.0	
2.010	0.0		28.21	0.0		396.1	6.3		5560	0.0	
2.328	0.0		32.67	0.0		458.7	3.1		6439	0.0	
2.696	0.0		37.84	0.0		531.2	0.9		7456	0.0	
3.122	0.0		43.82	0.0		615.1	0.1		8635	0.0	
3.615	0.0		50.75	0.0		712.4	0.0		1.000e4	0.0	
4.187	0.0		58.77	0.0		825.0	0.0				
4.849	0.0		68.06	0.0		955.4	0.0				

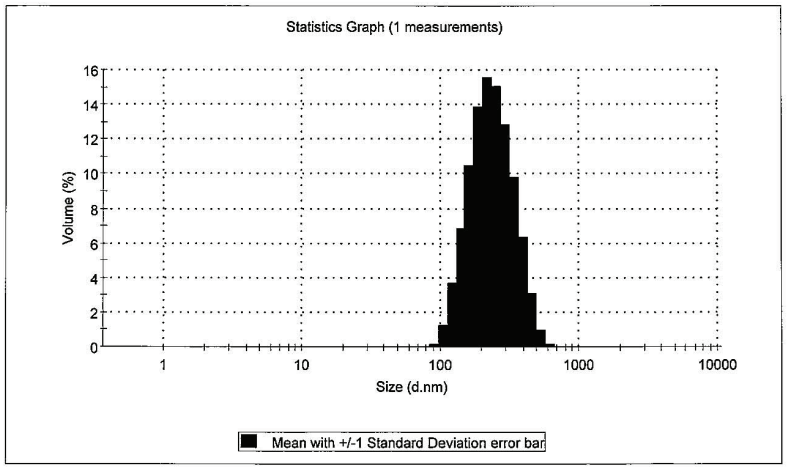

2A) Sample B: Alkylbenzene w/ 2.0% BST Concentration: New Oil
Size Distribution: Intensity

Size Distribution Report by Intensity

v2.0

Malvern

Sample Details

Sample Name: B Average
SOP Name: mansettings.nano
General Notes: UNIVERSITY OF MISSOURI
Alkylbenzene Lab
DJ Particle Technology Labs PTL ID: 85545

File Name:	23236.dts	**Dispersant Name:**	Hexane
Record Number:	37	**Dispersant RI:**	1.375
Material RI:	1.59	**Viscosity (cP):**	0.2940
Material Absorbtion:	0.01	**Measurement Date and Time:**	Wednesday, September 07, ...

System

Temperature (°C):	25.0	**Duration Used (s):**	60
Count Rate (kcps):	417.6	**Measurement Position (mm):**	4.65
Cell Description:	Glass cuvette with square aper...	**Attenuator:**	7

Results

			Diam. (nm)	% Intensity	Width (nm)
Z-Average (d.nm):	304.3	**Peak 1:**	240.3	100.0	52.01
PdI:	0.226	**Peak 2:**	0.000	0.0	0.000
Intercept:	0.885	**Peak 3:**	0.000	0.0	0.000

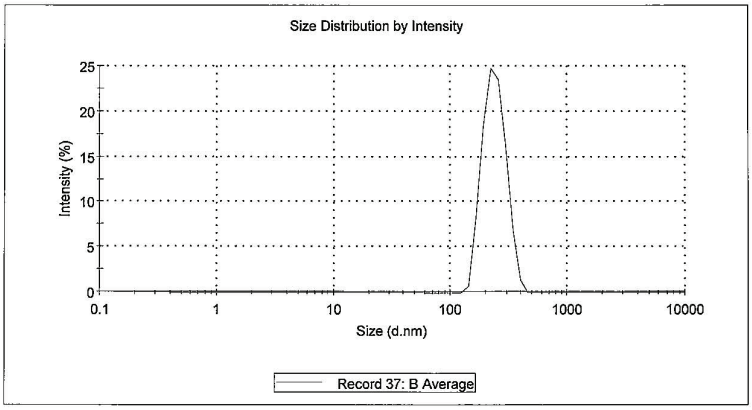

2B) Sample B: Alkylbenzene w/ 2.0% BST Concentration: New Oil
Size Statistics: Intensity

Size Statistics Report by Intensity

v2.0

Malvern

Sample Details

Sample Name:	B Average
File Name:	23236.dts
SOP Name:	mansettings.nano
Measurement Date and Time:	Wednesday, September 07, 2011 9:02:39 AM

Z-Average (nm):	304.285	**Derived Count Rate (kcps):**	43306.8443109...
Standard Deviation:	0	**Standard Deviation:**	0
%Std Deviation:	0	**%Std Deviation:**	0
Variance:	0	**Variance:**	0

Size d.nm	Mean Intensity %	Std Dev Intensity %	Size d.nm	Mean Intensity %	Std Dev Intensity %	Size d.nm	Mean Intensity %	Std Dev Intensity %	Size d.nm	Mean Intensity %	Std Dev Intensity %
0.4000	0.0		5.615	0.0		78.82	0.0		1106	0.0	
0.4632	0.0		6.503	0.0		91.28	0.0		1281	0.0	
0.5365	0.0		7.531	0.0		105.7	0.0		1484	0.0	
0.6213	0.0		8.721	0.0		122.4	0.0		1718	0.0	
0.7195	0.0		10.10	0.0		141.8	0.7		1990	0.0	
0.8332	0.0		11.70	0.0		164.2	8.4		2305	0.0	
0.9649	0.0		13.54	0.0		190.1	18.5		2669	0.0	
1.117	0.0		15.69	0.0		220.2	24.8		3091	0.0	
1.294	0.0		18.17	0.0		255.0	23.5		3580	0.0	
1.499	0.0		21.04	0.0		295.3	15.9		4145	0.0	
1.736	0.0		24.36	0.0		342.0	6.8		4801	0.0	
2.010	0.0		28.21	0.0		396.1	1.4		5560	0.0	
2.328	0.0		32.67	0.0		458.7	0.0		6439	0.0	
2.696	0.0		37.84	0.0		531.2	0.0		7456	0.0	
3.122	0.0		43.82	0.0		615.1	0.0		8635	0.0	
3.615	0.0		50.75	0.0		712.4	0.0		1.000e4	0.0	
4.187	0.0		58.77	0.0		825.0	0.0				
4.849	0.0		68.06	0.0		955.4	0.0				

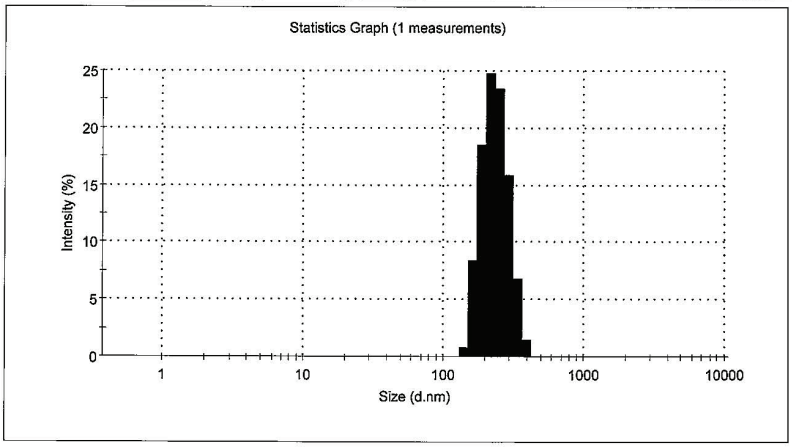

2C) Sample B: Alkylbenzene w/ 2.0% BST Concentration: New Oil
Size Distribution: Volume

Size Distribution Report by Volume

v2.0

Malvern

Sample Details

Sample Name:	B Average
SOP Name:	mansettings.nano
General Notes:	UNIVERSITY OF MISSOURI Alkylbenzene Lab DJ Particle Technology Labs PTL ID: 85545

File Name:	23236.dts	**Dispersant Name:**	Hexane
Record Number:	37	**Dispersant RI:**	1.375
Material RI:	1.59	**Viscosity (cP):**	0.2940
Material Absorbtion:	0.01	**Measurement Date and Time:**	Wednesday, September 07, ...

System

Temperature (°C):	25.0	**Duration Used (s):**	60
Count Rate (kcps):	417.6	**Measurement Position (mm):**	4.65
Cell Description:	Glass cuvette with square ape...	**Attenuator:**	7

Results

			Diam. (nm)	% Volume	Width (nm)
Z-Average (d.nm):	304.3	**Peak 1:**	244.7	100.0	59.45
PdI:	0.226	**Peak 2:**	0.000	0.0	0.000
Intercept:	0.885	**Peak 3:**	0.000	0.0	0.000

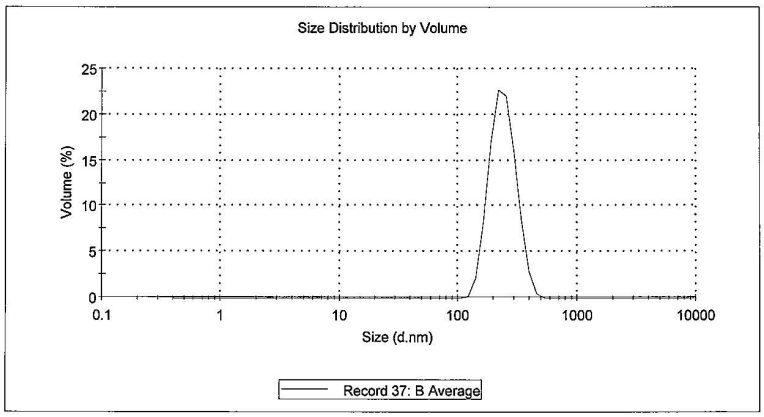

2D) Sample B: Alkylbenzene w/ 2.0% BST Concentration: New Oil
Size Statistics: Volume

Size Statistics Report by Volume
v2.0

Malvern

Sample Details

Sample Name: B Average
File Name: 23236.dts
SOP Name: mansettings.nano
Measurement Date and Time: Wednesday, September 07, 2011 9:02:39 AM

Z-Average (nm):	304.285	**Derived Count Rate (kcps):**	43306.8443109...
Standard Deviation (nm):	0	**Standard Deviation (kcps):**	0
%Std Deviation:	0	**%Std Deviation:**	0
Variance:	0	**Variance:**	0

Size d.nm	Mean Volume %	Std Dev Volume %	Size d.nm	Mean Volume %	Std Dev Volume %	Size d.nm	Mean Volume %	Std Dev Volume %	Size d.nm	Mean Volume %	Std Dev Volume %
0.4000	0.0		5.615	0.0		78.82	0.0		1106	0.0	
0.4632	0.0		6.503	0.0		91.28	0.0		1281	0.0	
0.5365	0.0		7.531	0.0		105.7	0.0		1484	0.0	
0.6213	0.0		8.721	0.0		122.4	0.2		1718	0.0	
0.7195	0.0		10.10	0.0		141.8	2.2		1990	0.0	
0.8332	0.0		11.70	0.0		164.2	8.3		2305	0.0	
0.9649	0.0		13.54	0.0		190.1	16.9		2669	0.0	
1.117	0.0		15.69	0.0		220.2	22.6		3091	0.0	
1.294	0.0		18.17	0.0		255.0	22.0		3580	0.0	
1.499	0.0		21.04	0.0		295.3	16.0		4145	0.0	
1.736	0.0		24.36	0.0		342.0	8.4		4801	0.0	
2.010	0.0		28.21	0.0		396.1	2.9		5560	0.0	
2.328	0.0		32.67	0.0		458.7	0.5		6439	0.0	
2.696	0.0		37.84	0.0		531.2	0.0		7456	0.0	
3.122	0.0		43.82	0.0		615.1	0.0		8635	0.0	
3.615	0.0		50.75	0.0		712.4	0.0		1.000e4	0.0	
4.187	0.0		58.77	0.0		825.0	0.0				
4.849	0.0		68.06	0.0		955.4	0.0				

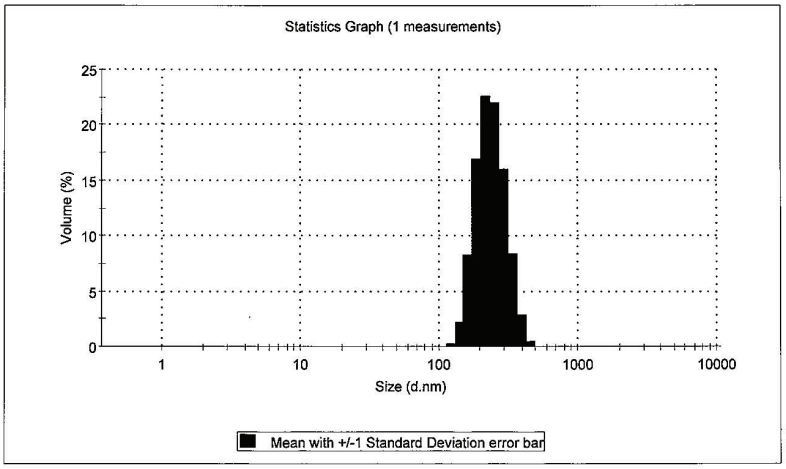

3A) Sample C: NycoDiel w/ 1.0% BST Concentration: New Oil
Size Distribution: Intensity

Size Distribution Report by Intensity
v2.0

Malvern

Sample Details

Sample Name: C Average
SOP Name: mansettings.nano
General Notes: UNIVERSITY OF MISSOURI
Nycodiel PAO Oil
DJ Particle Technology Labs PTL ID: 85546

File Name:	23236.dts	**Dispersant Name:**	Hexane
Record Number:	31	**Dispersant RI:**	1.375
Material RI:	1.59	**Viscosity (cP):**	0.2940
Material Absorbtion:	0.01	**Measurement Date and Time:**	Wednesday, September 07, ...

System

Temperature (°C):	25.0	**Duration Used (s):**	60
Count Rate (kcps):	264.1	**Measurement Position (mm):**	1.25
Cell Description:	Glass cuvette with square aper...	**Attenuator:**	5

Results

			Diam. (nm)	% Intensity	Width (nm)
Z-Average (d.nm):	484.3	**Peak 1:**	442.9	99.8	120.4
PdI:	0.260	**Peak 2:**	5553	0.2	69.08
Intercept:	0.825	**Peak 3:**	0.000	0.0	0.000

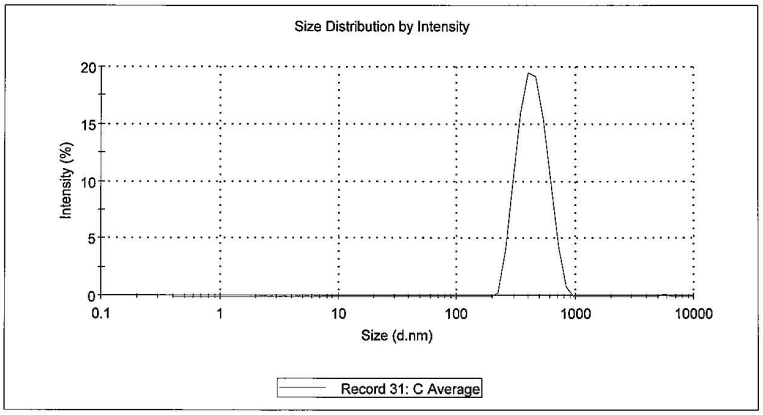

3B) Sample C: NycoDiel w/ 1.0% BST Concentration: New Oil

Size Statistics: Intensity

Size Statistics Report by Intensity
v2.0

Malvern

Sample Details

Sample Name:	C Average
File Name:	23236.dts
SOP Name:	mansettings.nano
Measurement Date and Time:	Wednesday, September 07, 2011 8:39:29 AM

Z-Average (nm):	484.2553	**Derived Count Rate (kcps):**	238661.024648...
Standard Deviation:	0	**Standard Deviation:**	0
%Std Deviation:	0	**%Std Deviation:**	0
Variance:	0	**Variance:**	0

Size d.nm	Mean Intensity %	Std Dev Intensity %	Size d.nm	Mean Intensity %	Std Dev Intensity %	Size d.nm	Mean Intensity %	Std Dev Intensity %	Size d.nm	Mean Intensity %	Std Dev Intensity %
0.4000	0.0		5.615	0.0		78.82	0.0		1106	0.0	
0.4632	0.0		6.503	0.0		91.28	0.0		1281	0.0	
0.5365	0.0		7.531	0.0		105.7	0.0		1484	0.0	
0.6213	0.0		8.721	0.0		122.4	0.0		1718	0.0	
0.7195	0.0		10.10	0.0		141.8	0.0		1990	0.0	
0.8332	0.0		11.70	0.0		164.2	0.0		2305	0.0	
0.9649	0.0		13.54	0.0		190.1	0.0		2669	0.0	
1.117	0.0		15.69	0.0		220.2	0.3		3091	0.0	
1.294	0.0		18.17	0.0		255.0	4.0		3580	0.0	
1.499	0.0		21.04	0.0		295.3	10.1		4145	0.0	
1.736	0.0		24.36	0.0		342.0	16.1		4801	0.0	
2.010	0.0		28.21	0.0		396.1	19.5		5560	0.2	
2.328	0.0		32.67	0.0		458.7	19.2		6439	0.0	
2.696	0.0		37.84	0.0		531.2	15.5		7456	0.0	
3.122	0.0		43.82	0.0		615.1	9.8		8635	0.0	
3.615	0.0		50.75	0.0		712.4	4.3		1.000e4	0.0	
4.187	0.0		58.77	0.0		825.0	0.9				
4.849	0.0		68.06	0.0		955.4	0.0				

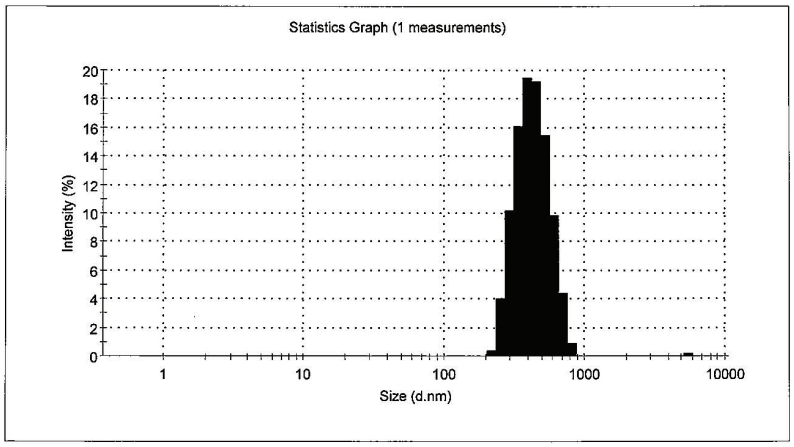

3C) Sample C: NycoDiel w/ 1.0% BST Concentration: New Oil
Size Distribution: Volume

Size Distribution Report by Volume
v2.0

Malvern

Sample Details

Sample Name:	C Average
SOP Name:	mansettings.nano
General Notes:	UNIVERSITY OF MISSOURI Nycodiel PAO Oil DJ Particle Technology Labs PTL ID: 85546

File Name:	23236.dts	**Dispersant Name:**	Hexane
Record Number:	31	**Dispersant RI:**	1.375
Material RI:	1.59	**Viscosity (cP):**	0.2940
Material Absorbtion:	0.01	**Measurement Date and Time:**	Wednesday, September 07, ...

System

Temperature (°C):	25.0	**Duration Used (s):**	60
Count Rate (kcps):	264.1	**Measurement Position (mm):**	1.25
Cell Description:	Glass cuvette with square ape...	**Attenuator:**	5

Results

			Diam. (nm)	% Volume	Width (nm)
Z-Average (d.nm):	484.3	**Peak 1:**	492.5	99.6	147.5
PdI:	0.260	**Peak 2:**	5585	0.4	582.3
Intercept:	0.825	**Peak 3:**	0.000	0.0	0.000

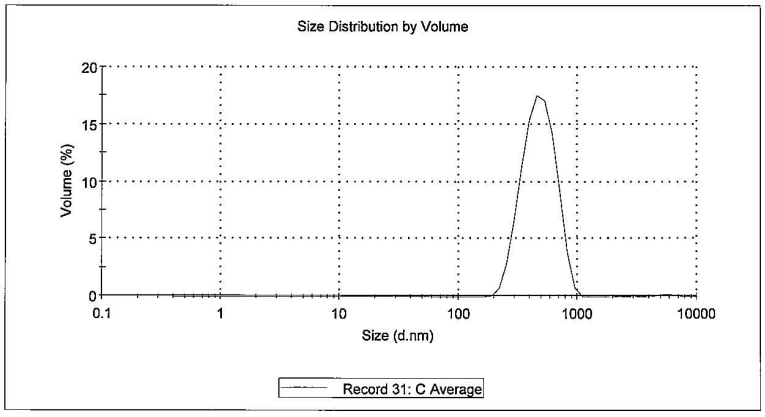

3D) Sample C: NycoDiel w/ 1.0% BST Concentration: New Oil
Size Statistics: Volume

Size Statistics Report by Volume
v2.0

Malvern

Sample Details

Sample Name:	C Average
File Name:	23236.dts
SOP Name:	mansettings.nano
Measurement Date and Time:	Wednesday, September 07, 2011 8:39:29 AM

Z-Average (nm):	484.2553	**Derived Count Rate (kcps):**	238661.024648...
Standard Deviation (nm):	0	**Standard Deviation (kcps):**	0
%Std Deviation:	0	**%Std Deviation:**	0
Variance:	0	**Variance:**	0

Size d.nm	Mean Volume %	Std Dev Volume %	Size d.nm	Mean Volume %	Std Dev Volume %	Size d.nm	Mean Volume %	Std Dev Volume %	Size d.nm	Mean Volume %	Std Dev Volume %
0.4000	0.0		5.615	0.0		78.82	0.0		1106	0.0	
0.4632	0.0		6.503	0.0		91.28	0.0		1281	0.0	
0.5365	0.0		7.531	0.0		105.7	0.0		1484	0.0	
0.6213	0.0		8.721	0.0		122.4	0.0		1718	0.0	
0.7195	0.0		10.10	0.0		141.8	0.0		1990	0.0	
0.8332	0.0		11.70	0.0		164.2	0.0		2305	0.0	
0.9649	0.0		13.54	0.0		190.1	0.0		2669	0.0	
1.117	0.0		15.69	0.0		220.2	0.7		3091	0.0	
1.294	0.0		18.17	0.0		255.0	2.9		3580	0.0	
1.499	0.0		21.04	0.0		295.3	6.7		4145	0.0	
1.736	0.0		24.36	0.0		342.0	11.3		4801	0.1	
2.010	0.0		28.21	0.0		396.1	15.4		5560	0.2	
2.328	0.0		32.67	0.0		458.7	17.5		6439	0.1	
2.696	0.0		37.84	0.0		531.2	17.1		7456	0.0	
3.122	0.0		43.82	0.0		615.1	14.2		8635	0.0	
3.615	0.0		50.75	0.0		712.4	9.2		1.000e4	0.0	
4.187	0.0		58.77	0.0		825.0	3.8				
4.849	0.0		68.06	0.0		955.4	0.7				

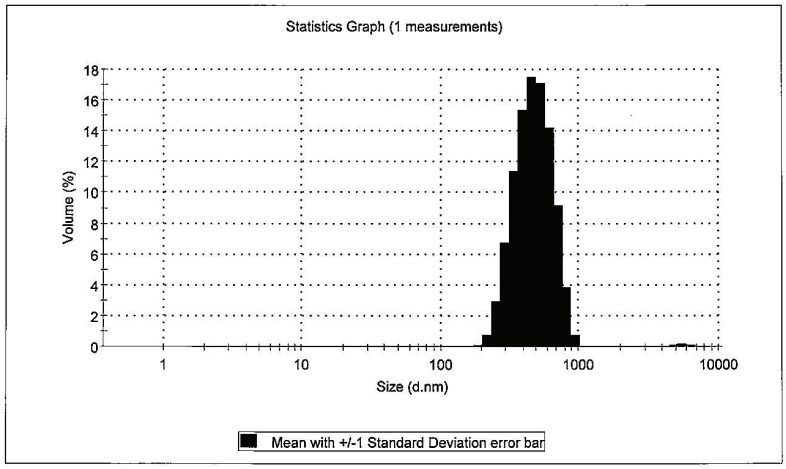

4A) Sample D: NycoDiel w/ 2.0% BST Concentration: Used Oil
Size Distribution: Intensity

Size Distribution Report by Intensity
v2.0

Malvern

Sample Details

Sample Name:	D Average
SOP Name:	mansettings.nano
General Notes:	UNIVERSITY OF MISSOURI Nycodiel PAO Oil DJ Particle Technology Labs PTL ID: 85547

File Name:	23236.dts	**Dispersant Name:**	Hexane
Record Number:	25	**Dispersant RI:**	1.375
Material RI:	1.59	**Viscosity (cP):**	0.2940
Material Absorbtion:	0.01	**Measurement Date and Time:**	Tuesday, September 06, 201...

System

Temperature (°C):	25.0	**Duration Used (s):**	70
Count Rate (kcps):	170.8	**Measurement Position (mm):**	4.65
Cell Description:	Glass cuvette with square aper...	**Attenuator:**	6

Results

			Diam. (nm)	% Intensity	Width (nm)
Z-Average (d.nm):	283.9	**Peak 1:**	289.3	100.0	78.19
PdI:	0.191	**Peak 2:**	0.000	0.0	0.000
Intercept:	0.912	**Peak 3:**	0.000	0.0	0.000

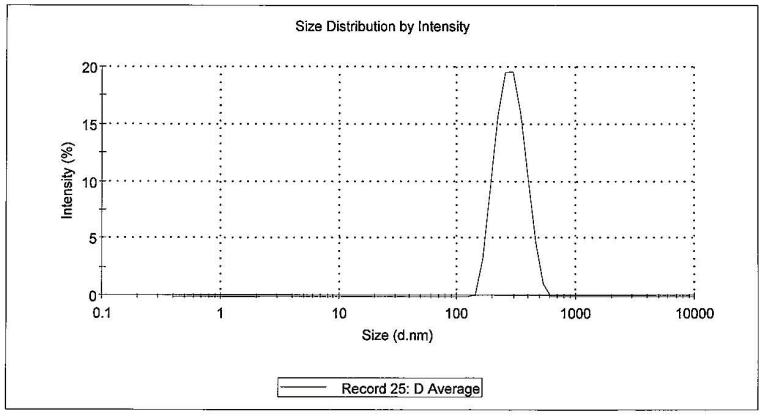

4B) Sample D: NycoDiel w/ 2.0% BST Concentration: Used Oil
Size Statistics: Intensity

Size Statistics Report by Intensity
v2.0

Malvern

Sample Details

Sample Name:	D Average
File Name:	23236.dts
SOP Name:	mansettings.nano
Measurement Date and Time:	Tuesday, September 06, 2011 12:02:30 PM

Z-Average (nm):	283.9059	**Derived Count Rate (kcps):**	59333.5918416...
Standard Deviation:	0	**Standard Deviation:**	0
%Std Deviation:	0	**%Std Deviation:**	0
Variance:	0	**Variance:**	0

Size d.nm	Mean Intensity %	Std Dev Intensity %	Size d.nm	Mean Intensity %	Std Dev Intensity %	Size d.nm	Mean Intensity %	Std Dev Intensity %	Size d.nm	Mean Intensity %	Std Dev Intensity %
0.4000	0.0		5.615	0.0		78.82	0.0		1106	0.0	
0.4632	0.0		6.503	0.0		91.28	0.0		1281	0.0	
0.5365	0.0		7.531	0.0		105.7	0.0		1484	0.0	
0.6213	0.0		8.721	0.0		122.4	0.0		1718	0.0	
0.7195	0.0		10.10	0.0		141.8	0.2		1990	0.0	
0.8332	0.0		11.70	0.0		164.2	3.4		2305	0.0	
0.9649	0.0		13.54	0.0		190.1	9.4		2669	0.0	
1.117	0.0		15.69	0.0		220.2	15.7		3091	0.0	
1.294	0.0		18.17	0.0		255.0	19.5		3580	0.0	
1.499	0.0		21.04	0.0		295.3	19.6		4145	0.0	
1.736	0.0		24.36	0.0		342.0	16.0		4801	0.0	
2.010	0.0		28.21	0.0		396.1	10.4		5560	0.0	
2.328	0.0		32.67	0.0		458.7	4.8		6439	0.0	
2.696	0.0		37.84	0.0		531.2	1.1		7456	0.0	
3.122	0.0		43.82	0.0		615.1	0.0		8635	0.0	
3.615	0.0		50.75	0.0		712.4	0.0		1.000e4	0.0	
4.187	0.0		58.77	0.0		825.0	0.0				
4.849	0.0		68.06	0.0		955.4	0.0				

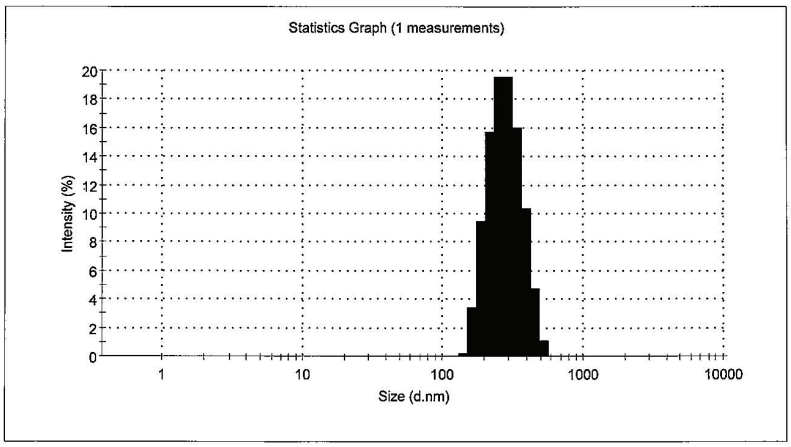

4C) Sample D: NycoDiel w/ 2.0% BST Concentration: Used Oil
Size Distribution: Volume

Size Distribution Report by Volume
v2.0

Malvern

Sample Details

Sample Name: D Average
SOP Name: mansettings.nano
General Notes: UNIVERSITY OF MISSOURI
Nycodiel PAO Oil
DJ Particle Technology Labs PTL ID: 85547

File Name:	23236.dts	**Dispersant Name:**	Hexane
Record Number:	25	**Dispersant RI:**	1.375
Material RI:	1.59	**Viscosity (cP):**	0.2940
Material Absorbtion:	0.01	**Measurement Date and Time:**	Tuesday, September 06, 201...

System

Temperature (°C):	25.0	**Duration Used (s):**	70
Count Rate (kcps):	170.8	**Measurement Position (mm):**	4.65
Cell Description:	Glass cuvette with square ape...	**Attenuator:**	6

Results

			Diam. (nm)	% Volume	Width (nm)
Z-Average (d.nm):	283.9	**Peak 1:**	302.1	100.0	89.92
PdI:	0.191	**Peak 2:**	0.000	0.0	0.000
Intercept:	0.912	**Peak 3:**	0.000	0.0	0.000

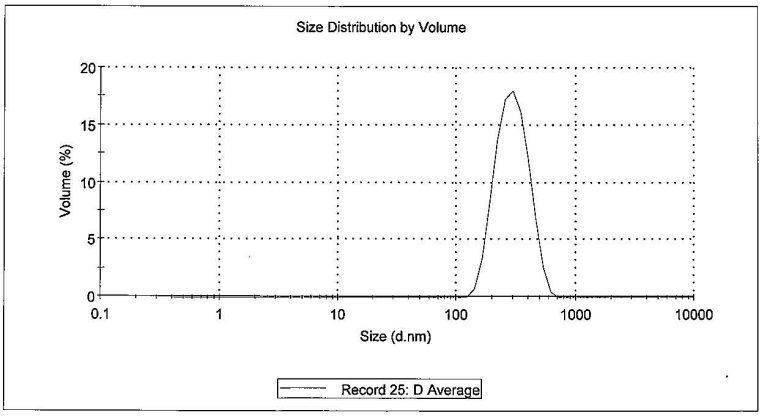

4D) Sample D: NycoDiel w/ 2.0% BST Concentration: Used Oil
Size Statistics: Volume

Size Statistics Report by Volume
v2.0

Malvern

Sample Details

Sample Name:	D Average
File Name:	23236.dts
SOP Name:	mansettings.nano
Measurement Date and Time:	Tuesday, September 06, 2011 12:02:30 PM

Z-Average (nm):	283.9059	**Derived Count Rate (kcps):**	59333.5918416...
Standard Deviation (nm):	0	**Standard Deviation (kcps):**	0
%Std Deviation:	0	**%Std Deviation:**	0
Variance:	0	**Variance:**	0

Size d.nm	Mean Volume %	Std Dev Volume %	Size d.nm	Mean Volume %	Std Dev Volume %	Size d.nm	Mean Volume %	Std Dev Volume %	Size d.nm	Mean Volume %	Std Dev Volume %
0.4000	0.0		5.615	0.0		78.82	0.0		1106	0.0	
0.4632	0.0		6.503	0.0		91.28	0.0		1281	0.0	
0.5365	0.0		7.531	0.0		105.7	0.0		1484	0.0	
0.6213	0.0		8.721	0.0		122.4	0.0		1718	0.0	
0.7195	0.0		10.10	0.0		141.8	0.7		1990	0.0	
0.8332	0.0		11.70	0.0		164.2	3.5		2305	0.0	
0.9649	0.0		13.54	0.0		190.1	8.4		2669	0.0	
1.117	0.0		15.69	0.0		220.2	13.8		3091	0.0	
1.294	0.0		18.17	0.0		255.0	17.2		3580	0.0	
1.499	0.0		21.04	0.0		295.3	18.0		4145	0.0	
1.736	0.0		24.36	0.0		342.0	16.2		4801	0.0	
2.010	0.0		28.21	0.0		396.1	12.1		5560	0.0	
2.328	0.0		32.67	0.0		458.7	6.9		6439	0.0	
2.696	0.0		37.84	0.0		531.2	2.6		7456	0.0	
3.122	0.0		43.82	0.0		615.1	0.5		8635	0.0	
3.615	0.0		50.75	0.0		712.4	0.0		1.000e4	0.0	
4.187	0.0		58.77	0.0		825.0	0.0				
4.849	0.0		68.06	0.0		955.4	0.0				

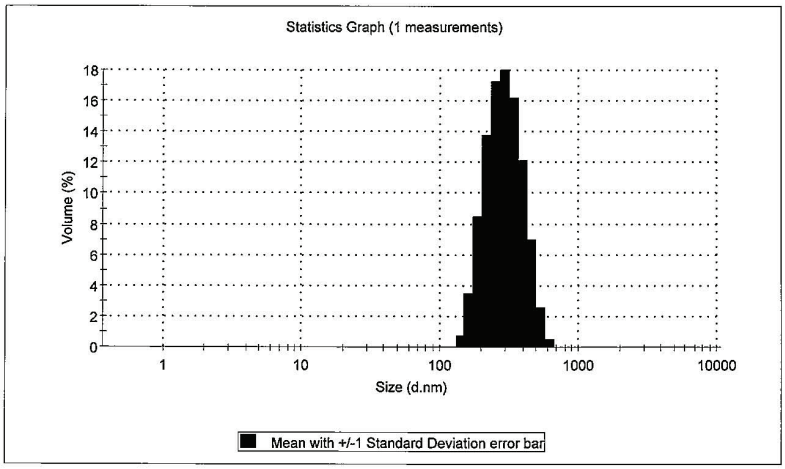

VITA

Christopher Anthony Yeckel was born to Calvin and Jacquelyn Yeckel on June 22, 1983 in St. Louis, MO. The oldest of three male siblings, Chris attributes much of his character to his two younger brothers Greg and Jeff. Chris was an overactive and average student in his youth who liked to play sports and excelled in gymnastics. Chris joined the Boy Scouts and achieved the rank of Eagle Scout; along the way he developed a deep respect for nature. It was not until his junior year at the University of Missouri – Columbia that mathematics finally clicked and Chris began his affair with physics and electricity. Pulsed power became the focal point of his interest and still is today. Chris has worked with very large and very small pulsed power systems under his advisor Dr. Randy Curry at the Center for Physical and Power Electronics throughout his career. At the time of this writing Chris currently works at Stangenes Industries doing everything from brainstorming to full production of electronic systems for an assortment of high and low power civilian and military applications. Chris is happily married to his best friend Amy and currently resides in Northern California enjoying life.